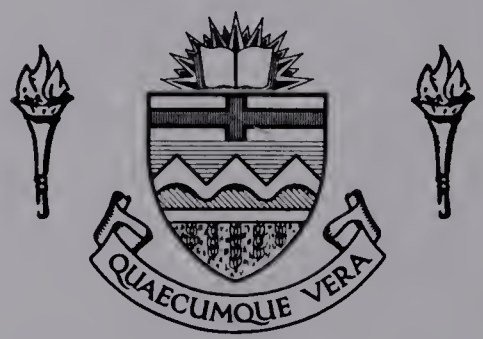

The University of Alberta
Printing Department
Edmonton, Alberta

THE UNIVERSITY OF ALBERTA

RELEASE FORM

NAME OF AUTHOR Michael John PERLYNN

TITLE OF THESIS Web Slenderness Limits for Compact Beam-Columns

DEGREE FOR WHICH THESIS WAS PRESENTED M.Sc.

YEAR THIS DEGREE GRANTED 1974

Permission is hereby granted to THE UNIVERSITY OF ALBERTA LIBRARY to reproduce single copies of this thesis and to lend or sell such copies for private, scholarly or scientific research purposes only.

The author reserves other publication rights, and neither the thesis nor extensive extracts from it may be printed or otherwise reproduced without the author's written permission.

Dated August 2

THE UNIVERSITY OF ALBERTA

WEB SLENDERNESS LIMITS FOR COMPACT BEAM-COLUMNS

by

© MICHAEL JOHN PERLYNN

A THESIS

SUBMITTED TO THE FACULTY OF GRADUATE STUDIES AND RESEARCH

IN PARTIAL FULFILMENT OF THE REQUIREMENTS

FOR THE DEGREE OF MASTER OF SCIENCE

DEPARTMENT OF CIVIL ENGINEERING

EDMONTON, ALBERTA

FALL, 1974

THE UNIVERSITY OF ALBERTA

FACULTY OF GRADUATE STUDIES AND RESEARCH

The undersigned certify that they have read, and recommend to the Faculty of Graduate Studies and Research for acceptance, a thesis entitled WEB SLENDERNESS LIMITS FOR COMPACT BEAM-COLUMNS submitted by MICHAEL JOHN PERLYNN in partial fulfilment of the requirements for the degree of Master of Science.

Date: Aug. 26, 1977

ABSTRACT

This investigation was established in an attempt to determine more rational web slenderness limitations for compact beam-columns. The present limits, as set forth by the Canadian Standards Association Standard S16-1969, do not distinguish between member cross-sections that may be non-compact, compact, or suitable for plastic design. The present web slenderness limitations have been established on the assumption that member cross-sections may be required to deform plastically. This results in limits that are too conservative for compact beam-columns.

The results of nine compact beam-column tests, along with test results from three other investigations conducted on beams and columns, are presented. This study, utilizing the combined results, shows that the limiting web slenderness ratios for compact beam-columns can safely be increased above the present values.

ACKNOWLEDGEMENTS

This investigation was made possible by a grant provided by the Canadian Steel Industries Construction Council.

The author wishes to express his sincere appreciation to Dr. G.L. Kulak under whose direction the work was performed and whose advice and continuing guidance were most valuable.

Gratefully acknowledged are the comments and criticisms of Professors J. Longworth, D.W. Murray and J.S. Kennedy, who served on the examining committee.

The contributions of Mr. N.M. Holtz and members of the laboratory staff in carrying out the testing program, and Mrs. Barbara Gallaiford, who typed the thesis, are also gratefully acknowledged.

TABLE OF CONTENTS

LIST OF TABLES

LIST OF FIGURES

CHAPTER I

INTRODUCTION

1.1 General

Members subjected to axial forces and bending are classified as either non-compact, compact, or suitable for plastic design. The classification of a member is determined by its performance upon reaching its ultimate combination of axial load and moment. The flange and web slenderness limits outlined in the Canadian Standards Association Standard S16[1] were established to ensure that non-compact sections could just reach the yield moment, compact sections could just reach the plastic moment (M_{pc}, plastic moment reduced for axial load) and a section suitable for plastic design could both reach the plastic moment and undergo sufficient rotation to redistribute the moments (Figure 1.1).

As contemplated by the Standard, a compact section is one which can achieve its plastic moment capacity at discrete locations, but may not have sufficient rotation capacity to permit the formation of other plastic hinges and thus attain a mechanism. Sufficient lateral bracing must be provided to ensure this behavior.

In the three classifications noted, non-compact, compact, and suitable for plastic design, the capacity of a member is successively increased. To prevent the possibility of local buckling, the limiting flange and web slenderness ratios must be

correspondingly decreased for a given grade of steel.

Since it has been determined that the critical buckling stress of a plate loaded in uniform edge compression is some function of its width-to-thickness ratio, it follows that the flange plate sections of a beam or beam-column must become progressively stockier in order to preclude buckling as the deformation demands increase on the total cross-section.

Deformation requirements also increase as the yield strength of the material increases. More member deformation is required to develop the higher critical buckling stress. As a result, the critical plate slenderness ratios for higher strength steels must be less than those for the lower strength steels. This requirement is taken into account in the present Standard for the slenderness limits of flanges in compression (see Figure 1.2).

The same general situation exists for the web in a beam-column. As the web deformation requirements become greater, it follows that the critical web slenderness ratio should be decreased to prevent local web buckling.

1.2 Statement of the Problem

Presently, CSA Standard S16 establishes one set of critical web slenderness limitations for all three classifications, non-compact, compact, and suitable for plastic design (Figure 1.3). The only difference in design is that non-compact sections involve a factor of safety against reaching the yield moment (reduced

because of axial load) and the compact and plastically designed sections involve a factor of safety against reaching the plastic moment (reduced for axial load). If the stipulated web slenderness is satisfactory for plastically designed members, then it must be conservative for the design of compact members for which the deformation requirements are not nearly as demanding.

According to the present limits (Figure 1.3), for values of P/P_y (actual load to yield load) less than 0.28, the critical web slenderness ratio for a beam-column is linearly reduced as the applied axial load is increased. For all values of P/P_y greater than or equal to 0.28, the web slenderness ratio must be reduced substantially in order to prevent web buckling.

Both the CSA Standard S16 and the American Institute of Steel Construction Specification[2] have based their web slenderness limitations primarily on a series of tests conducted in 1956 on stub columns and short beam specimens of ASTM-A7 steel[3]. In only three of the tests was failure associated with web buckling.

Recently, a single test has indicated that these present requirements may be overly conservative[4].

1.3 Objectives

The objectives of this investigation are:

1. to examine the present web slenderness limitations for compact members by means of a suitable testing program,
2. to develop and examine existing theories (mathematical models), which describe the behavior of web plate

buckling under combined axial load and moment,

3. and to suggest revisions to the web slenderness limitations for beam-columns, if appropriate.

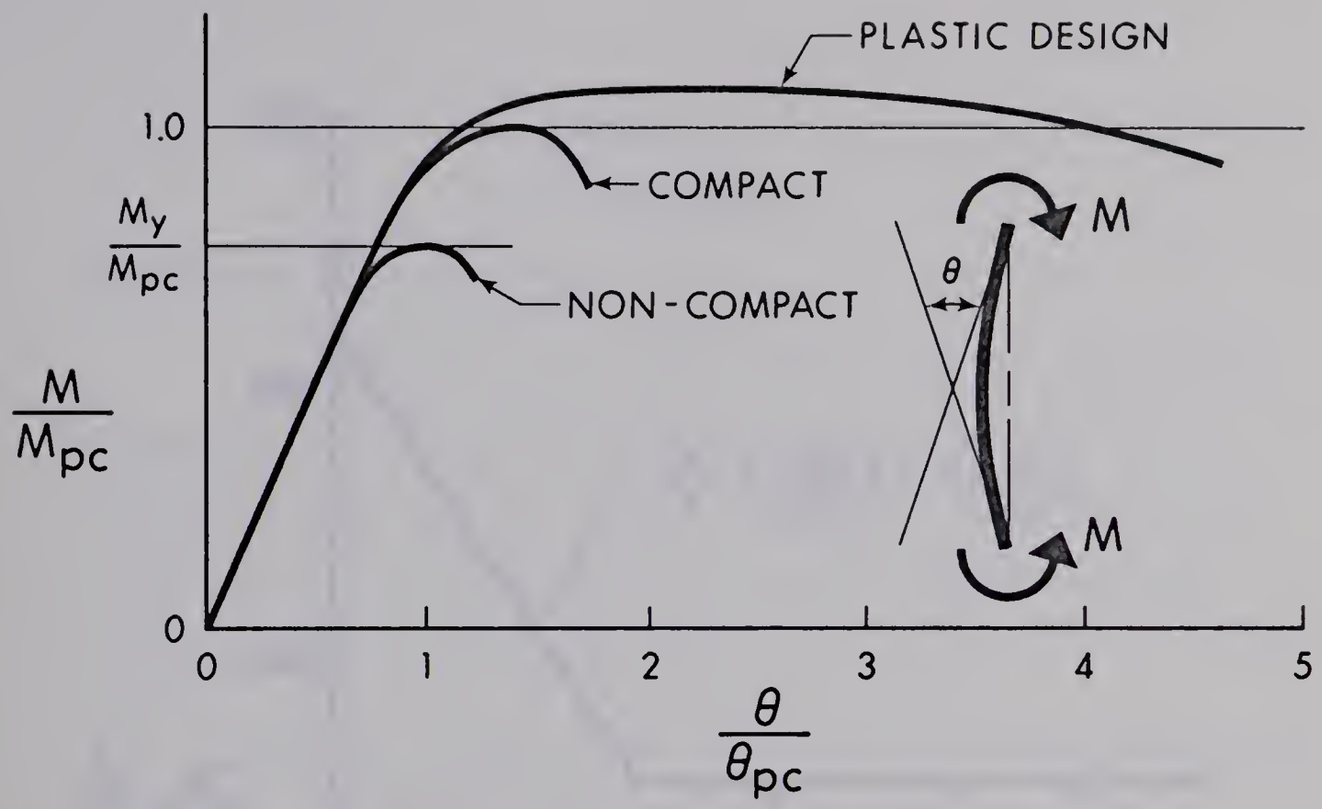

FIGURE 1.1 MOMENT ROTATION BEHAVIOR FOR BEAM-COLUMNS

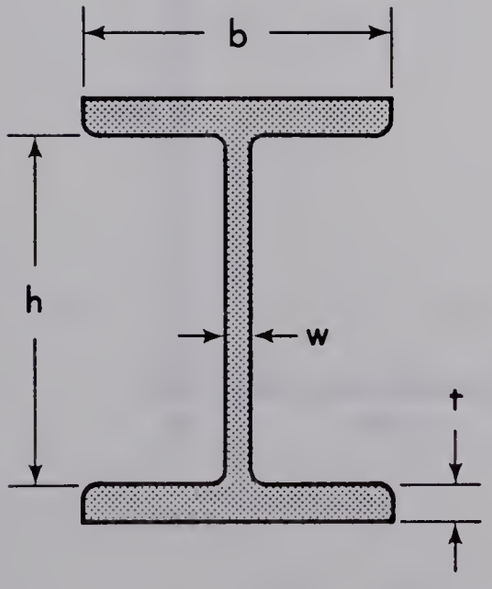

NON-COMPACT $\frac{b}{2t} \leq \frac{100}{\sqrt{F_y}}$

COMPACT $\frac{b}{2t} \leq \frac{64}{\sqrt{F_y}}$

PLASTIC DESIGN $\frac{b}{2t} \leq \frac{54}{\sqrt{F_y}}$

FIGURE 1.2 PRESENT CSA S16 FLANGE SLENDERNESS LIMITATIONS

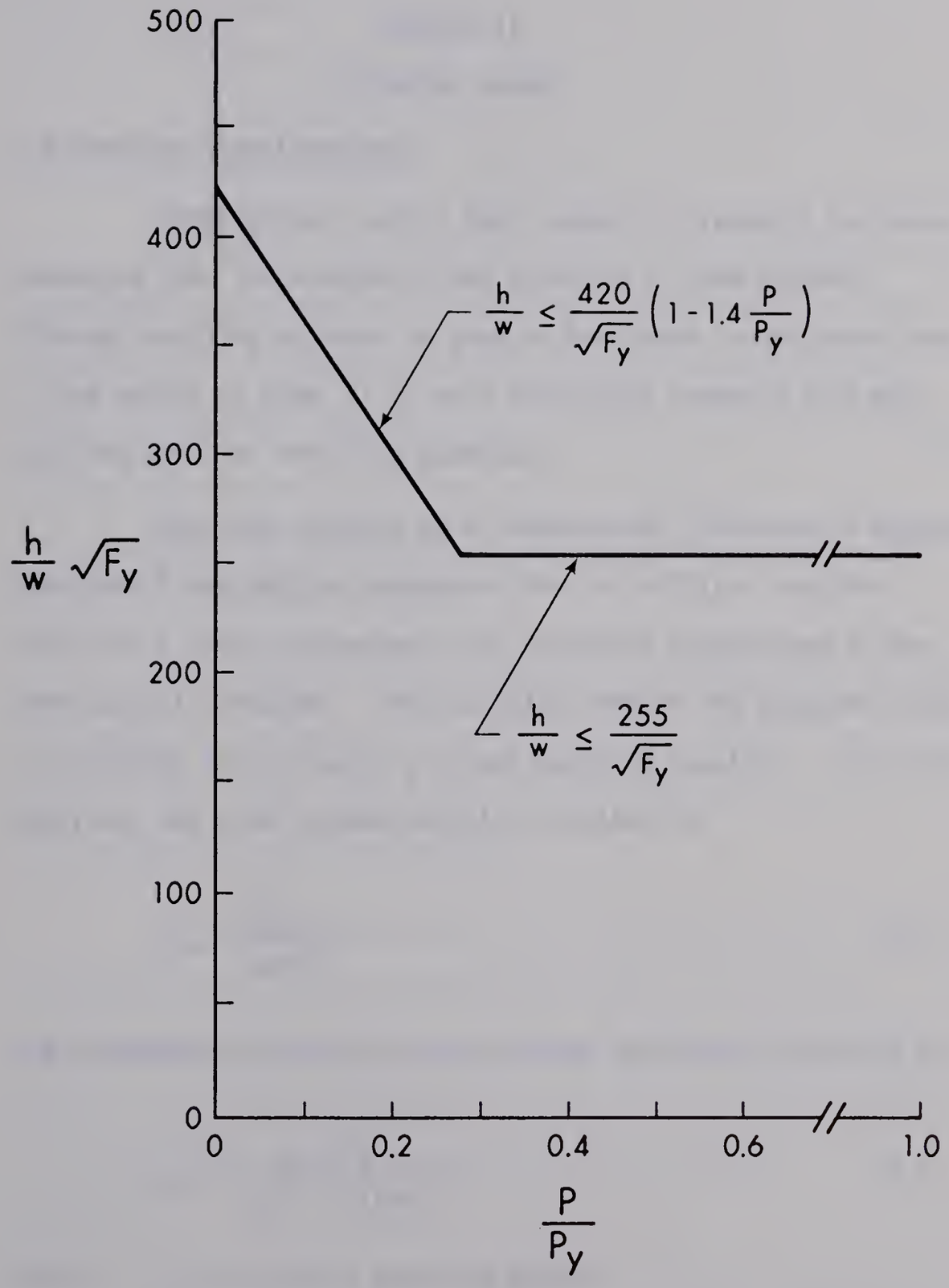

FIGURE 1.3 PRESENT WEB SLENDERNESS LIMITS ACCORDING TO CSA S16

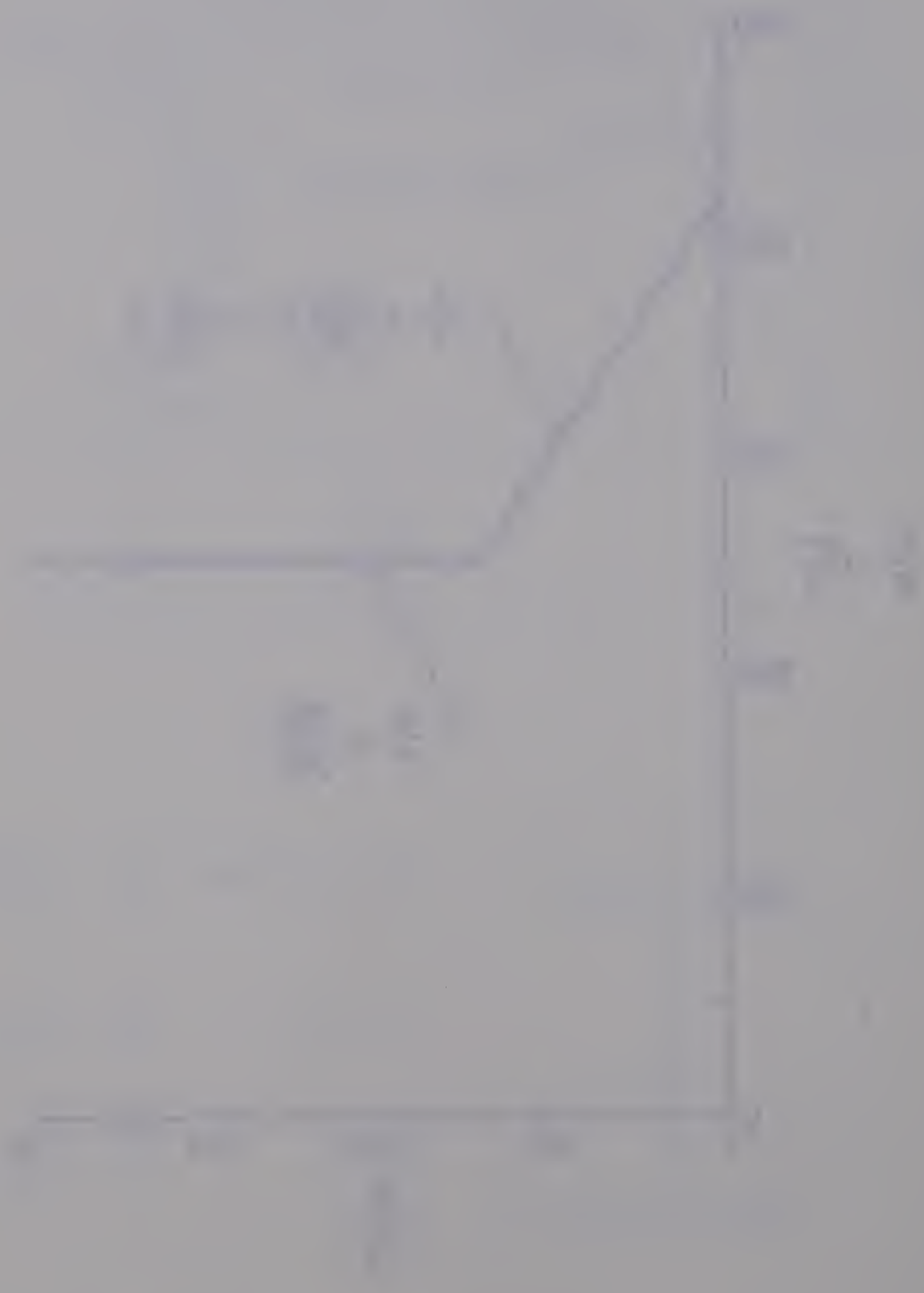

CHAPTER II

LITERATURE SURVEY

2.1 Previous Investigations

Comparatively only a small amount of research has been conducted into the problem of web buckling in beam-columns. Although buckling problems in general have been investigated over a long period of time, it is only relatively recently that web buckling problems have been examined.

From the solution of a fourth-order differential equation, Timoshenko[5] obtained an expression for the critical buckling stress of a simply supported plate uniformly edge-loaded in the longitudinal direction. The resulting form of the equation closely resembled that of Euler's column buckling equation. For elastic buckling, the Euler column buckling solution is:

$$\sigma_{cr} = \frac{\pi^2 E}{(L/r)^2} \qquad 2.1$$

and Timoshenko's plate buckling solution for elastic buckling is:

$$\sigma_{cr} = \frac{K \pi^2 E}{12(1-\nu^2)(h/w)^2} \qquad 2.2$$

where: σ_{cr} = critical buckling stress

E = Young's modulus

ν = Poisson's ratio

r = radius of gyration

L = length of column

h = width of plate

w = thickness of plate

K = plate buckling coefficient

The plate buckling coefficient, "K", was introduced into the equation to account for the various aspect ratios of length to width. For a plate model which was simply supported along the longitudinal and loaded edges, Timoshenko determined that the minimum critical buckling stress could be found when K = 4.0 was substituted into Equation 2.2. This, he showed to be valid for all length to width ratios[5].

The model described by Equation 2.2 closely corresponds to the web of a column in uniform compression, except for the fact that the column flanges do offer some moment restraint to the longitudinal edges of the web.

This major development by Timoshenko opened the field of plate buckling to investigation by others. Of the many plate buckling models developed, some correspond closely to the boundary and loading conditions to which the web component part of a wide-flange beam or beam-column can be subjected. In particular,

1. Bleich[6], in 1952, studied the behavior of plates in non-uniform longitudinal compression, clamped along the longitudinal edges.

2. Noel[7], also in 1952, investigated simply supported plates subjected to longitudinal bending and compression in addition to lateral compression.
3. Johnson and Noel[8] published a study similar to that of Noel's but considered elastically restrained edges.

These investigations were essentially restricted to cases of plate buckling within the elastic range. Even though the plate boundary conditions and loading configurations were varied, the plate buckling equations reduced to the familiar form of Equation 2.2.

None of the investigations referred to analyzed the effects of the inelastic behavior of the material, the amount of actual restraint offered by the plate boundary conditions, or the effects of residual stresses on the resulting critical buckling stresses obtained from the plate buckling equations.

2.2 Development of Present Code Requirements

It was not until 1956 that the first specific investigation into web plate buckling was carried out. Haaijer investigated both flange and web plate buckling, accounting for the inelastic behavior of the material and the restraint existing at the flange to web junction[9]. Good correlation was found to exist between Haaijer's web buckling theory and his pure bending and pure compression tests on ASTM-A7 (σ_y = 33ksi) wide-flange shapes. Some of the compression tests established that both web and flange plates were capable of reaching strain-hardening before the

occurrence of buckling. However, in his study Haaijer did not assess the effect of residual stresses or the case of combined in-plane bending and axial compression on web plates.

In 1958, Haaijer and Thürliman proposed a plate buckling relationship (Figure 5.3), which included an empirical transition curve for the inelastic range between the proportional limit and the point of strain-hardening[3]. For use with the plate buckling curve, they also developed a web plate buckling equation for combined axial compression and bending. The results was an expression:

$$\alpha = \frac{h}{\pi w}\sqrt{\frac{12\sigma_y(1-\nu^2)}{KE}} \qquad 2.3$$

where α = plate buckling modulus,

σ_y = yield stress of material,

and K = plate buckling coefficient for a fully plastified wide-flange section.

For a member that may be required to deform plastically, the following assumptions were made to develop a web buckling curve for design purposes:

1. A/A_w (total area of wide-flange to area of web) = 2.0,
2. h_t/h (total depth of wide-flange to clear depth of web) = 1.05,
3. $\varepsilon_m/\varepsilon_y$ (maximum strain in compression flange to yield strain) = 4.0.

Using these assumptions (for an average wide-flange

section), it followed that the neutral axis in a beam-column subjected to M_{pc} (plastic moment reduced for axial load) and $P/P_y = 0.28$, would have just reached the tension flange. Thus the whole web would theoretically be in compression (not necessarily in uniform compression).

A theoretical design curve was first established, then approximated by two straight lines (Figure 2.1). It was decided to make the approximation applicable to ASTM-A36 steel since its properties were close to those of ASTM-A7 steel, which it had by now replaced. This design curve has since been modified to make the web slenderness limitations applicable to all steel grades (Figure 1.3) and now forms the basis for the present CSA Standard S-16 web slenderness limitations.

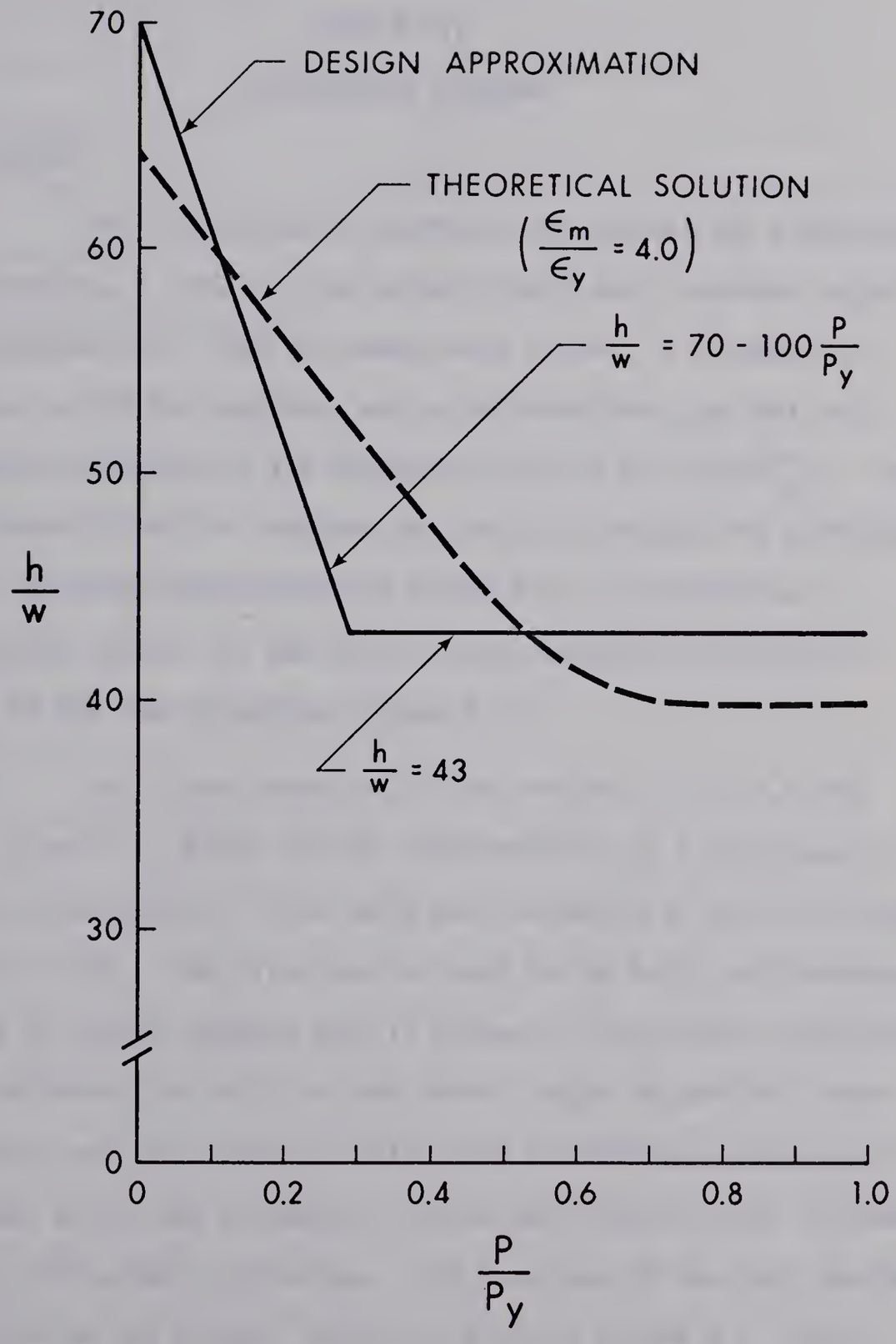

FIGURE 2.1 ALLOWABLE WEB SLENDERNESS RATIOS FOR ASTM-A36 WIDE-FLANGE BEAM-COLUMNS

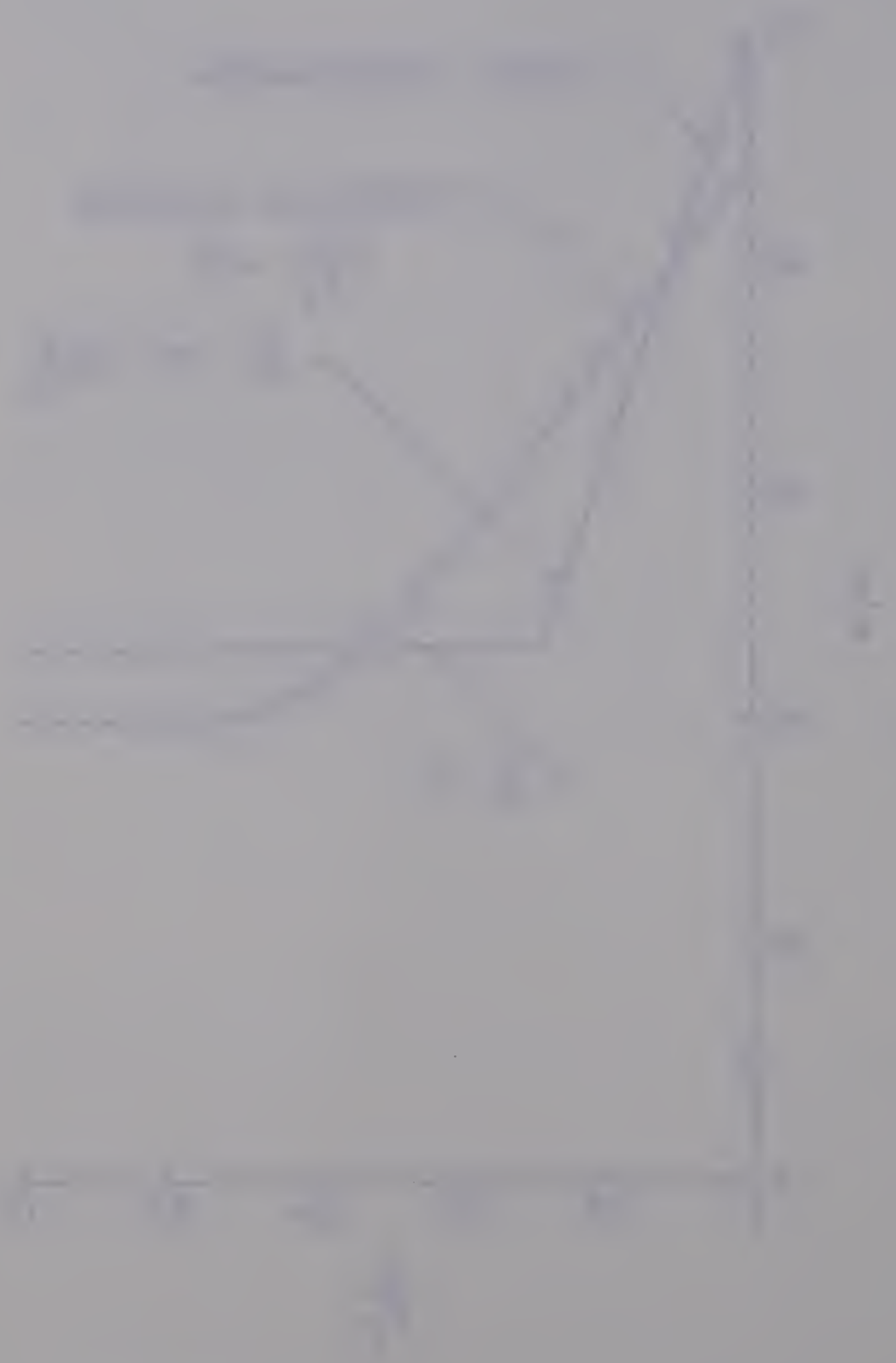

CHAPTER III

EXPERIMENTAL PROGRAM

3.1 Scope

For the purpose of examining the present web slenderness limitations, a total of nine welded wide-flange specimens subjected to combined axial load and moment were tested. A flange size common to all the specimens was established that just met the compact limitation of the Standard (that is, $b/t = 64/\sqrt{F_y}$). The web depth (h) of the specimen was varied to produce the different web slenderness ratios desired (Table 3.1). For the nine specimens tested, all had similar cross-sectional shapes with webs of the same thickness (Figure 3.1).

Tests were conducted at P/P_y ratios of 0.2, 0.4 and 0.8 in order to obtain results representative of a wide range of beam-column design. Three tests were conducted at each individual ratio of P/P_y. The first test in each series had a web slenderness about 12 percent greater than is allowed by the present limitations. The following two tests in each series became successively more critical and the allowable limits were exceeded by as much as 51 percent as the web slenderness ratios were progressively increased above the current limitations. The locations of the test specimens relative to the present limits are shown in Figure 3.2. Here, the web slenderness is expressed as $(h/w)\sqrt{F_y}$ in order that the effect of the yield point of the steel may be included.

By observation of the failures of the wide-flange beam-column specimens, whether by web buckling, flange buckling, or by both, the possibility of a limit at which flange and web buckling occurs simultaneously should exist. This new limit would then establish to what extent the current limitations might be increased.

3.2 Specimen Description

All the specimens were simply supported at their ends, with the moment applied by means of a concentrated load (P_2) placed eccentrically as shown in Figure 3.3. A major concentrated load (P_1) was applied concentrically with the specimen. Thus, the total axial load (P) acting on the specimen was the sum of the two individual concentrated loads and the moment (M) was the product of the eccentric load (P_2) and its eccentricity (e) from the centerline of the specimen. Because of the manner in which the concentrated loads were applied, the beam-column was essentially subjected to uniform compression and constant moment throughout its length. It was therefore theoretically possible that buckling could occur at any point along the length of the member. However, it was expected that buckling would not occur at the ends because of the added stiffness contributed to the web and flanges in these regions by the corner connection stiffeners. If centerline deflections became significant during testing, the axial load acting through the deflection might also increase the moment at the mid-section enough to initiate buckling at this location.

The moment produced by the eccentrically placed axial load was transmitted by arms fabricated from channel sections. These were welded to stiffened corner connections at the top and bottom of the beam-column (Figure 3.3). The arms and stiffened corner connections were designed to be somewhat stronger than the beam-column portion of the specimen. They were checked against premature failure by local or lateral buckling, bending, and shear.

The beam-column portions of the specimens were fabricated from CSA G40.12 steel plate[10]. For plates up to 1 1/2 inches thick, the specified minimum yield point (F_y) for this material is 44 ksi. The flanges of all nine beam-column specimens had dimensions of 7 1/4 inches by 3/8 inches, and all were fabricated from plate of the same mill rolling. This resulted in a width-to-thickness ratio for the flanges of 9.67, which just meets the compact limitation of 9.65, as established by CSA S16. The webs of the beam-columns were fabricated from 1/4 inch thick plate, again all from the same mill rolling, and cut to the required web depth (h).

The clear length of the beam-column was established at 45 inches. This length provided adequate room for the attachment of required gauges and recording equipment. The clear length also provided sufficient span over which buckling could occur without being restricted by the boundary effects at the ends. However, the length was short enough to prevent premature overall buckling about the strong axis during testing.

To prevent lateral buckling about the weak axis, lateral bracing was provided to the tension and compression flanges of each of the beam-columns. A bracing arrangement based on Watt's straight line mechanism[11] was attached by threaded pins welded at mid-height to the centerline of the flanges. This produced a short beam-column in the weak direction which met the bracing spacing requirements for plastic design.

Although the lateral bracing prevented movement perpendicular to the weak axis, no other movement was restricted. The bracing did not interfere with lateral movements perpendicular to the strong axis nor did it interfere with local buckling of the flanges and webs. However, the beam-column was torsionally restrained at its mid-height by the manner in which the lateral braces were attached. Since the beam-column itself was torsionally stable, this was not expected to affect the test results.

The first of the three series of tests to be conducted was at a P/P_y ratio of 0.2 (Figure 3.2). For this particular loading condition, the present web slenderness limit ($(h/w)\sqrt{F_y}$, based on F_y = 44 ksi) is 302. The three beam-column specimens to be tested had web slenderness ratios (based on the actual yield stress of the material used) of 332, 368, and 437. For the two series with P/P_y ratios of 0.4 and 0.8, the present web slenderness limit is set at 255 (F_y = 44 ksi). Three specimens were tested at each of these loading conditions, with web slenderness ratios of 285, 324 and 385 (based on actual yield stress).

3.3 Test Setup

The major concentric load (P_1) was applied using an MTS (Materials Testing System 908.14) testing machine, capable of applying 1,400,000 pounds in compression (Figure 3.4). The base and bottom loading surface of the machine is fixed to the laboratory floor, while the cross-head, which contains the hydraulic ram, is moveable to accept specimens of various heights.

The minor eccentric load (P_2) was applied using a hydraulic centerhole jack rated at 60 kips maximum capacity (see Figure 3.5). A 1 1/8 inch diameter high-strength steel rod, threaded at the ends, was bolted into place, passing upward through the upper arm and the centerhole jack and downward through the lower arm and a load cell. With the centerhole jack applying a tensile load to the rod, the resulting reactions tended to pull the arms towards each other. The effect not only created a stable loading arrangement, but the beam-column was thus further restrained against torsional buckling.

Steel rockers were provided at reaction points of the concentric load, that is, at the top and bottom of the specimen. These 7 inch radius rockers acted as simple supports. The bottom rocker, fabricated to the shape of a half-cylinder, permitted rotations only about the strong axis of the beam-column. However the top rocker, part of the compression head of the testing machine, had a ball and socket joint. This permitted rotations about the weak axis of the specimen as well. It was felt, however,

that the effects of weak axis rotations would be negligible and would not affect the test results.

Steel rockers 1 1/2 inches thick were provided at the reaction points of the eccentric load. These were placed between the centerhole jack and the top surface of the upper arm and between the load cell and the bottom surface of the lower arm. Each of the rockers, fabricated with a radius of curvature of 4 1/2 inches and drilled to provide passage of the tension rod, rotated about a line parallel to the strong axis of the beam-column.

As a result of the precautions taken as to the physical assembly, no overall instability problems of the setup were encountered during the testing.

Almost all measurements recorded during the testing program were collected by means of electronic equipment. Where electronic devices proved inconvenient or uneconomical, manual readings were taken (Figure 3.5).

An electronic load cell calibrated to a maximum load of 100 kips was used to measure the eccentric load. This centerhole load cell through which the tension rod passed, recorded the compressive loads applied by the hydraulic jack during testing.

Because of the magnitude of the concentric load and possible instabilities in compression, use of a load cell was ruled out. Instead, although not quite as precise, the magnitudes of the concentric load were measured from an electronic transducer connected to an oil pressure line located within the compression

head of the testing machine. The accuracy of this system is considered to be ± 0.5%.

In order to monitor deflections during the tests, thirteen rod and plunger type electronic transducers were used. Six transducers were used to measure lateral deflection in the plane of the web. Five of these were connected at equal increments of 11 1/4 inches along the 45 inch length of the specimen. From these readings, deflections relative to the chord joining the ends of the tension flange of the beam-column portion could be determined. Because the bottom rocker, unlike the top one, tended to travel as it rotated, the sixth transducer was mounted so as to monitor its lateral translation.

Rotations of the specimen were recorded using a rotation meter. This consisted of two light channel sections securely clamped to the top and bottom corner compression stiffeners, between which three transducers were placed. Two were mounted at distances of 21 inches and 42 inches respectively from the centerline of the beam-column. From the results of these two transducers, an average rotation could be determined. The third transducer was mounted coincident with the beam-column centerline and recorded the axial shortening. This was applied as a correction to determine the actual rotations.

Four transducers were mounted horizontally between the tips of the tension and compression flanges at equal increments along the length of the beam-column. With the flange in tension

being relatively stable, the movements of the compression flange could thereby be monitored for possible signs of flange buckling.

Out-of-plane deflections of the web were measured using a web deflection meter, consisting of two (or three, depending on the depth of the web) dial gauges supported on an adjustable mounting frame. Measurements could be taken at equal increments along any depth of web. Placing the tips of the frame legs at the web-to-flange junctions of the beam-column, deflections relative to a chord joining the leg tips were measured. To calibrate the device, it was necessary to first place it on a surface known to be flat. All measurements taken throughout the tests were then compared to the initial readings.

By taking both flange and web deflection readings at four cross-sections along the length of the beam-column, it was possible by observation of the results to determine whether the failure was caused by flange buckling or by buckling of the web, or by a combination of both.

The strain distribution at the mid-height of the specimen was measured by means of a set of eight SR-4 electric resistance strain gauges (Figure 3.6). Four of these were placed on the inside faces of the flanges, close to the edge of the flange tips. The remaining four were placed on the web at the two locations that divide the web depth into three equal increments. At each location, one gauge was placed on

either side of the web in order to obtain an average reading. However, if web buckling had occurred at this location, it would be noticed before any visual observation because of a marked difference in the strain readings.

The readings from the web deflection meter and the strain gauges were read and recorded manually. All the remaining data was fed into a multi-channel recorder and punched onto paper tape for later processing.

Prior to testing, each specimen was whitewashed in order to aid in the observation of yield patterns.

3.4 Testing Procedure

Although the top and bottom ends of the specimens were to be prepared square and true, imperfections were considered inevitable. As a result, before a specimen could be tested, it had to be aligned[12]. This was done by loading the specimen concentrically (in increments of about one fifteenth to one twentieth of the total concentric load P) and reading the four strain gauges mounted near the flange tips. Care was taken not to exceed the proportional limit of the material and cause premature yielding. The specimen ends were shimmed until no strain gauge reading deviated more than about five percent from the average reading of the four gauges.

Once the specimen had been aligned, the concentric load was reduced to about 5 kips (to hold the specimen in position) and all initial readings were taken.

To begin testing, the concentric load was applied in increments of approximately one fifth of the total axial load (P), with readings being taken after each increment. Upon reaching the total axial load, it was then necessary to start applying the moment. Since the testing arrangement was such that this also produced additional axial load, the concentric load was reduced in increments of about one fortieth of the total axial load (P). Thus, the total axial load was kept in balance in an incremental fashion. The net effect was to apply moment to the beam-column, with the axial load remaining constant.

After each increment, and while holding the loads constant, all deformations were allowed to stabilize before a set of readings were taken. Web deflection and strain gauge readings were taken after every second increment until the specimen approached the point at which a local buckle might occur. At this time, all gauges were read following every increment. Throughout the test the behavior of the specimen was monitored on a plotter, tracing a moment-rotation relationship.

All test specimens were deformed well into the unloading range as measured on the moment-rotation curve. At this point, all loads were released and a final set of readings were taken.

The data on the paper tape was then reduced and plotted for observation by means of a prepared computer program.

Prior to the beam-column tests, two series of standard coupon tests were conducted to determine the material behavior.

Six coupon tests were performed on each of the web and flange plate materials.

TABLE 3.1 DETAILS OF BEAM-COLUMN TEST SPECIMENS

SPECIMEN	WEB DEPTH h (inches)	P/P_y	$* \frac{h}{w} \sqrt{F_y}$
1	12.09	0.2	332
2	13.43	0.2	368
3	15.82	0.2	437
4	10.27	0.4	285
5	11.64	0.4	324
6	13.97	0.4	387
7	10.28	0.8	286
8	11.65	0.8	324
9	13.88	0.8	385

* based on actual F_y

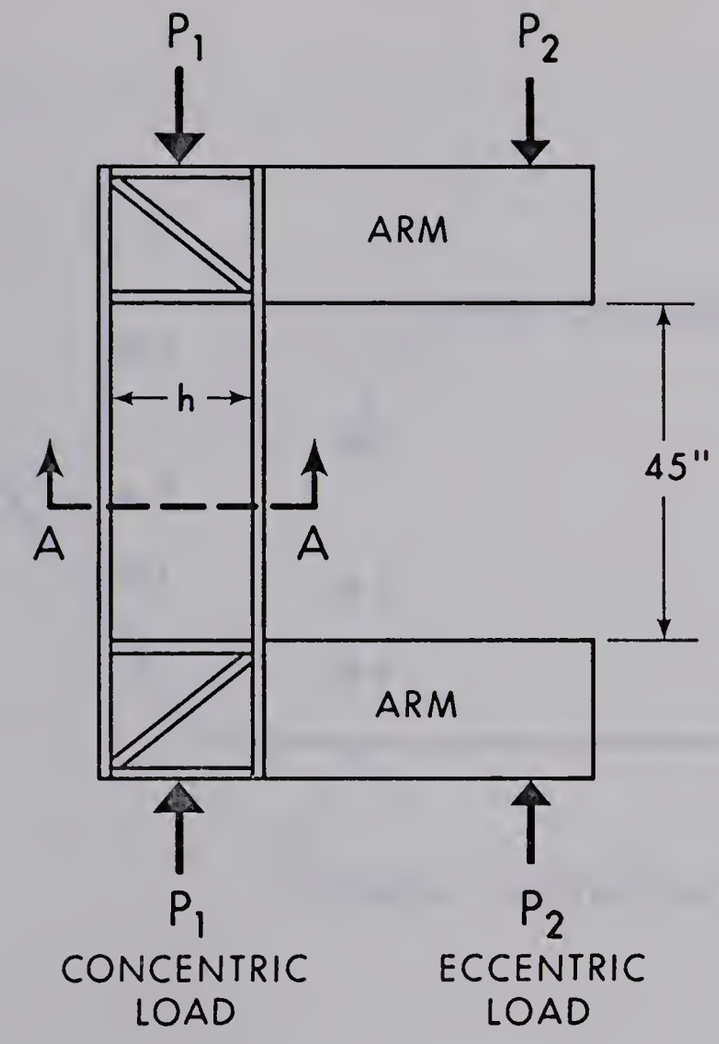

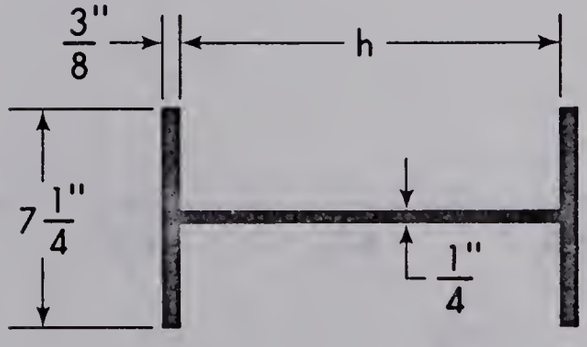

section A - A

FIGURE 3.1 DETAILS OF BEAM-COLUMN TEST SPECIMENS

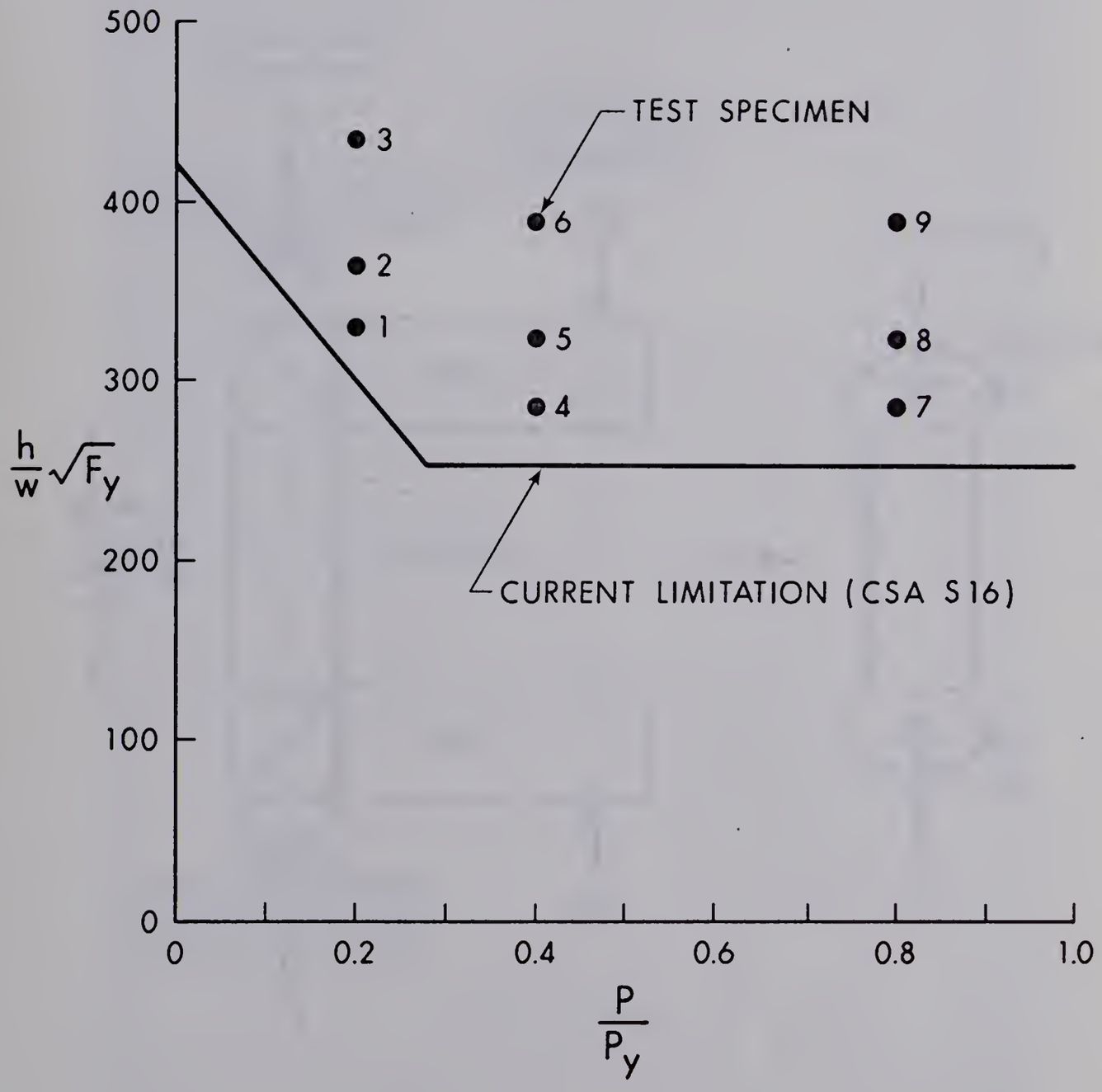

FIGURE 3.2 THE CURRENT WEB SLENDERNESS LIMITS AND THE PROPOSED TESTS

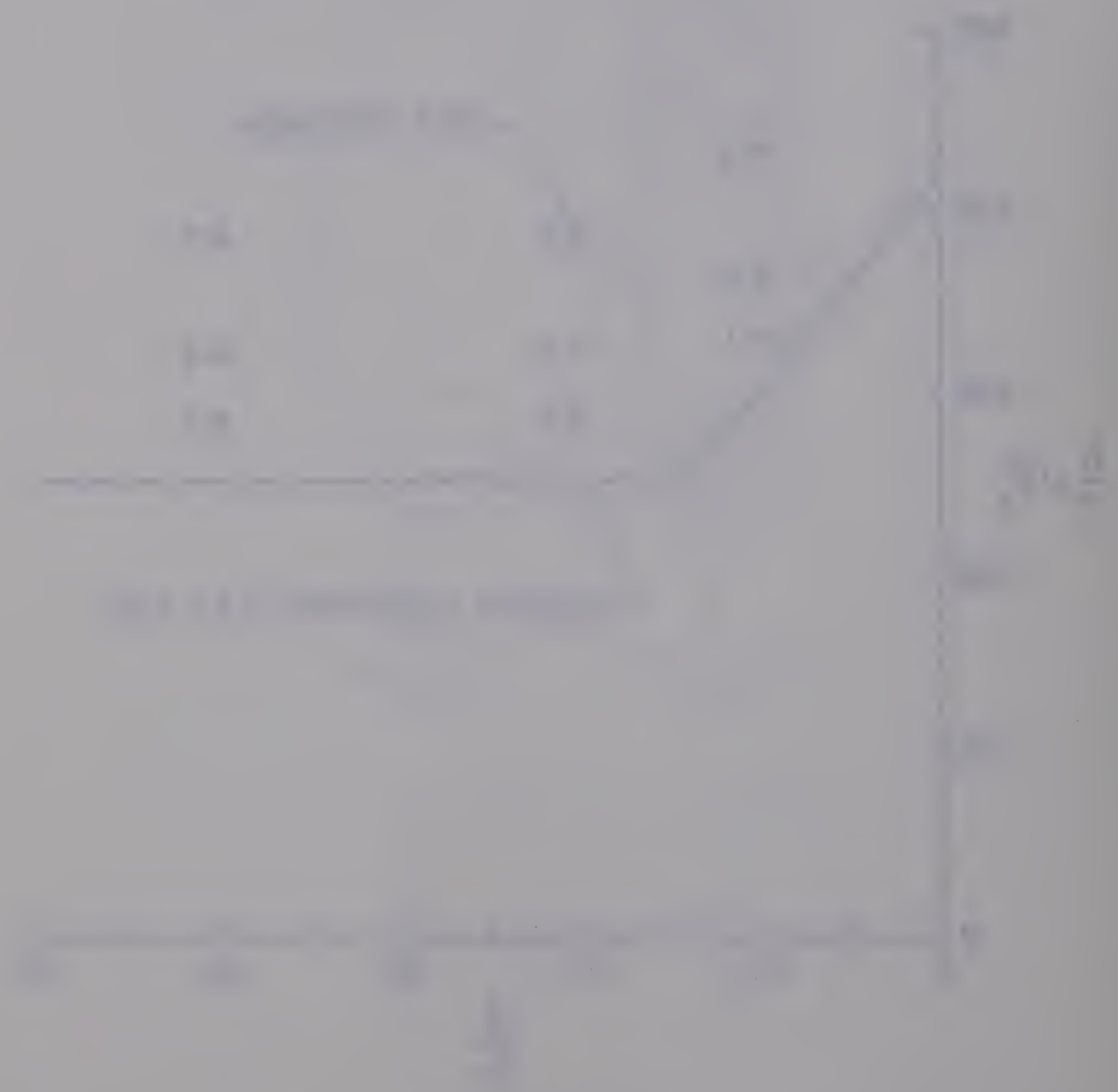

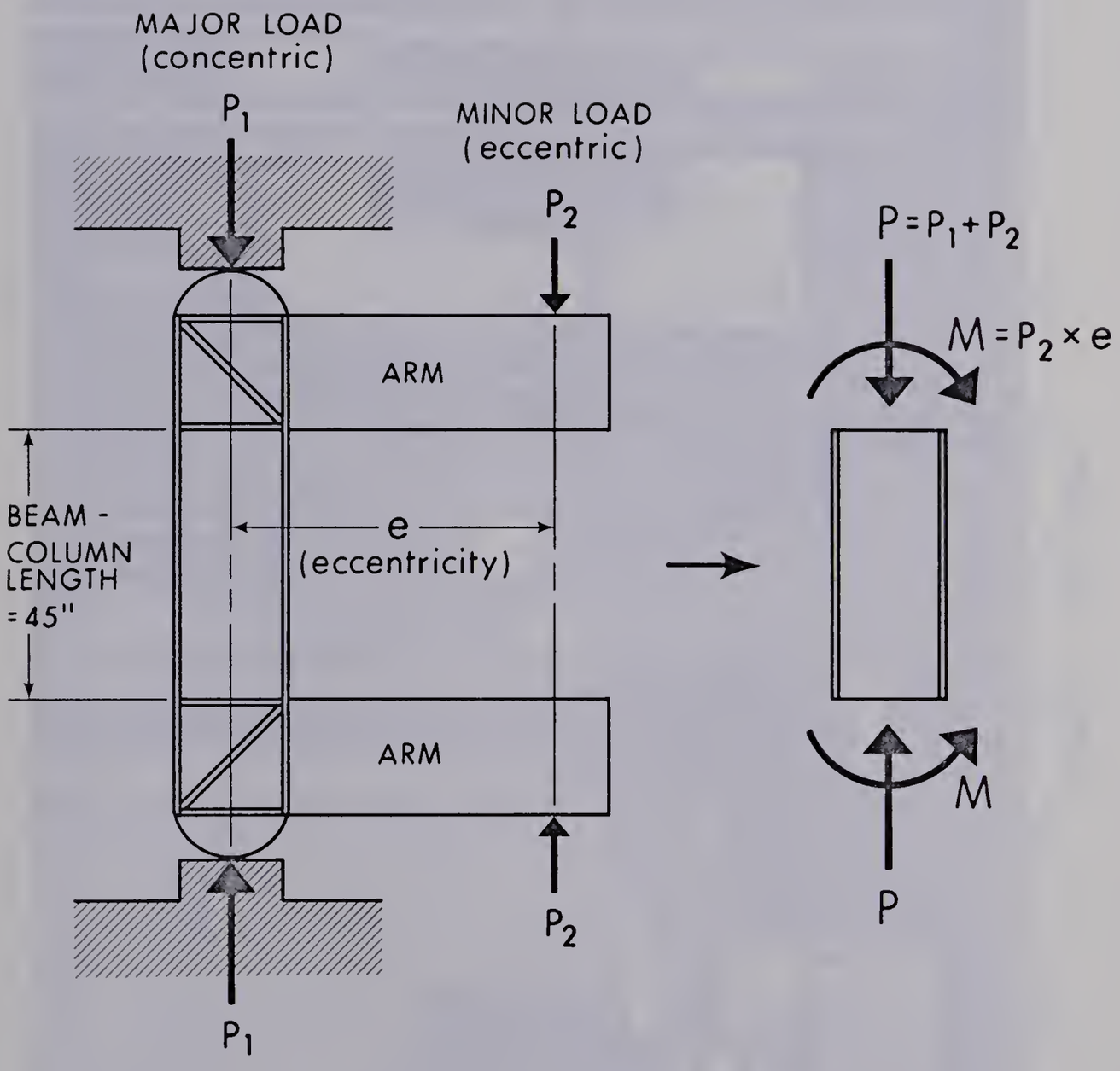

FIGURE 3.3 IDEALIZED TEST SETUP

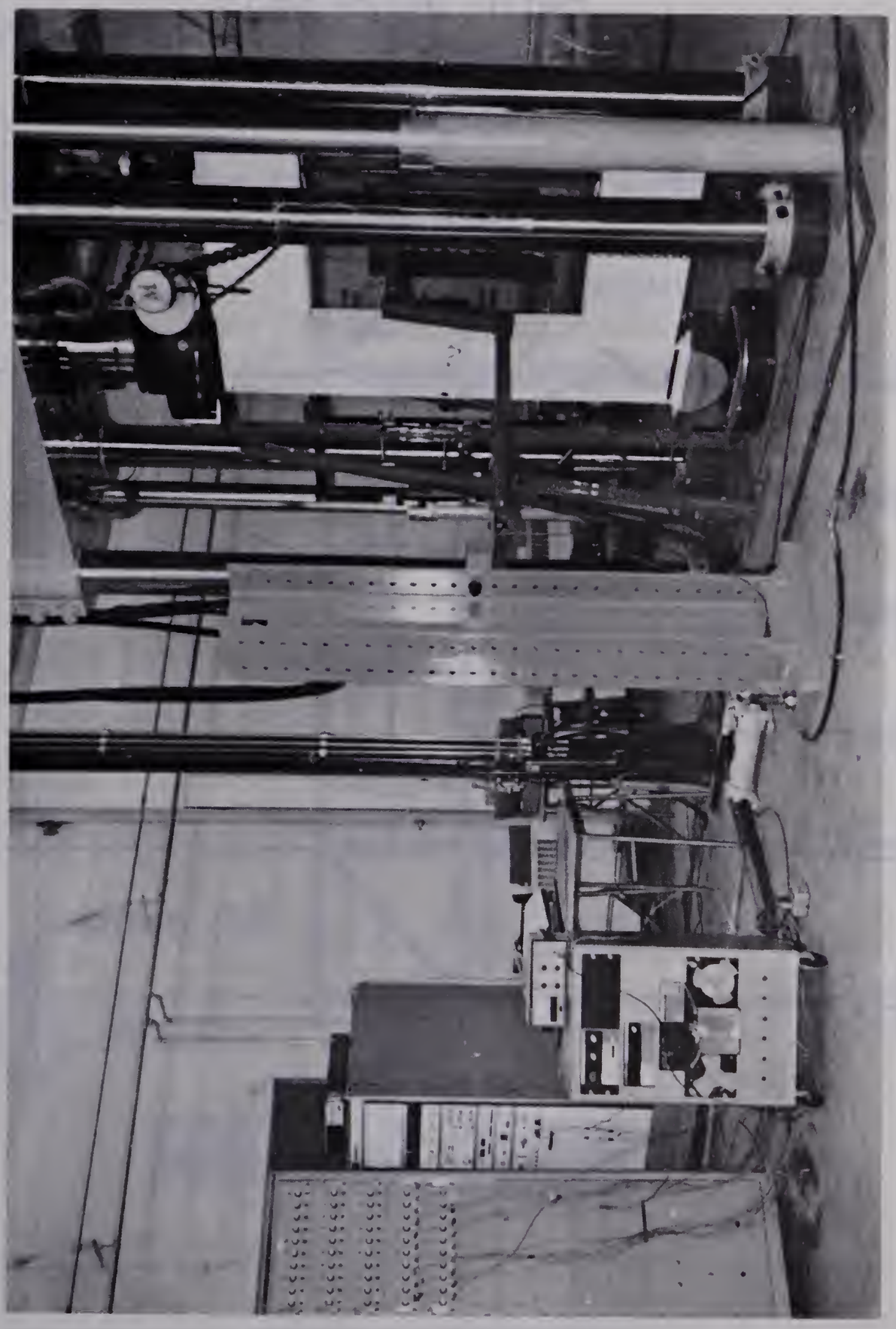

FIGURE 3.4 TEST SETUP

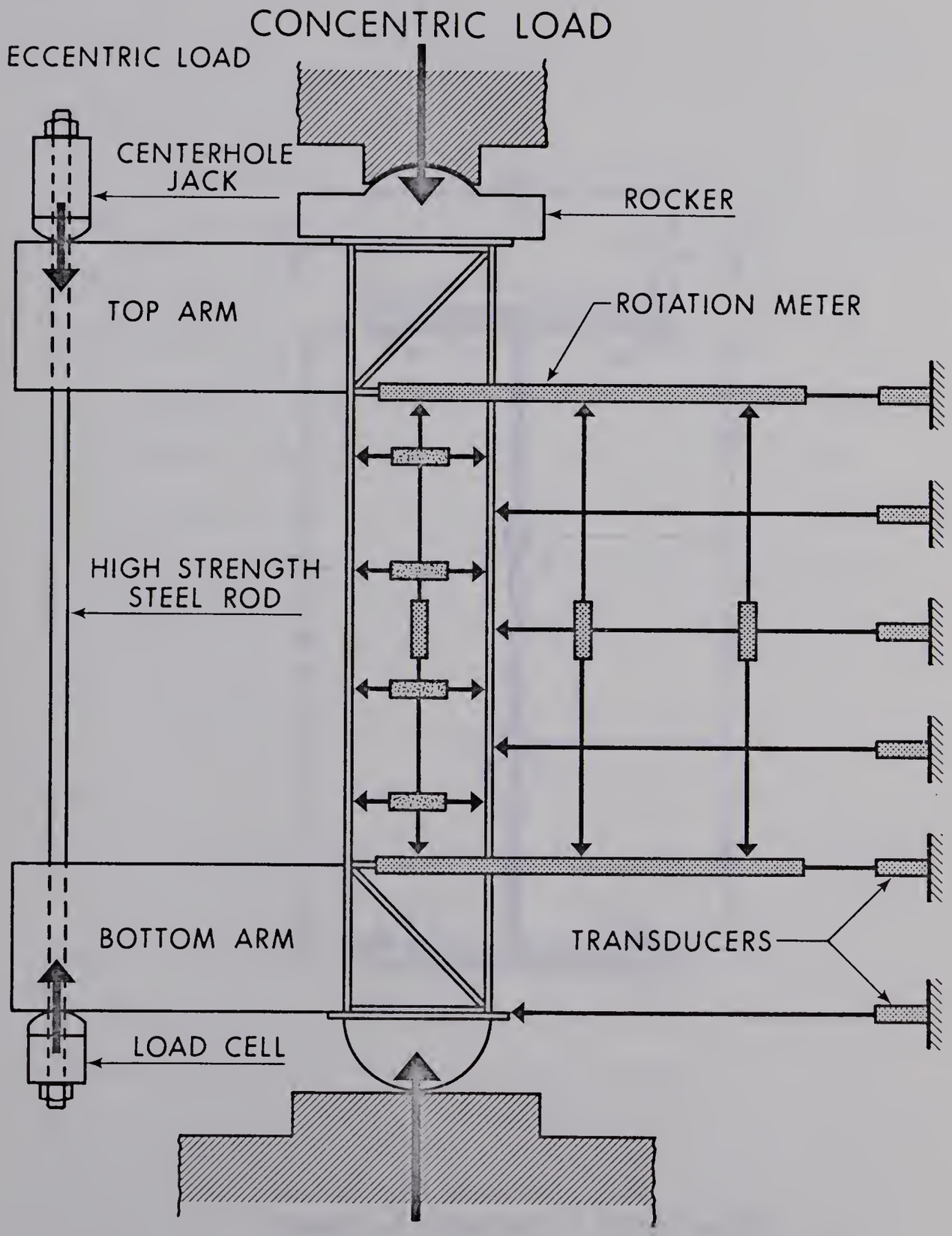

FIGURE 3.5 INSTRUMENTATION

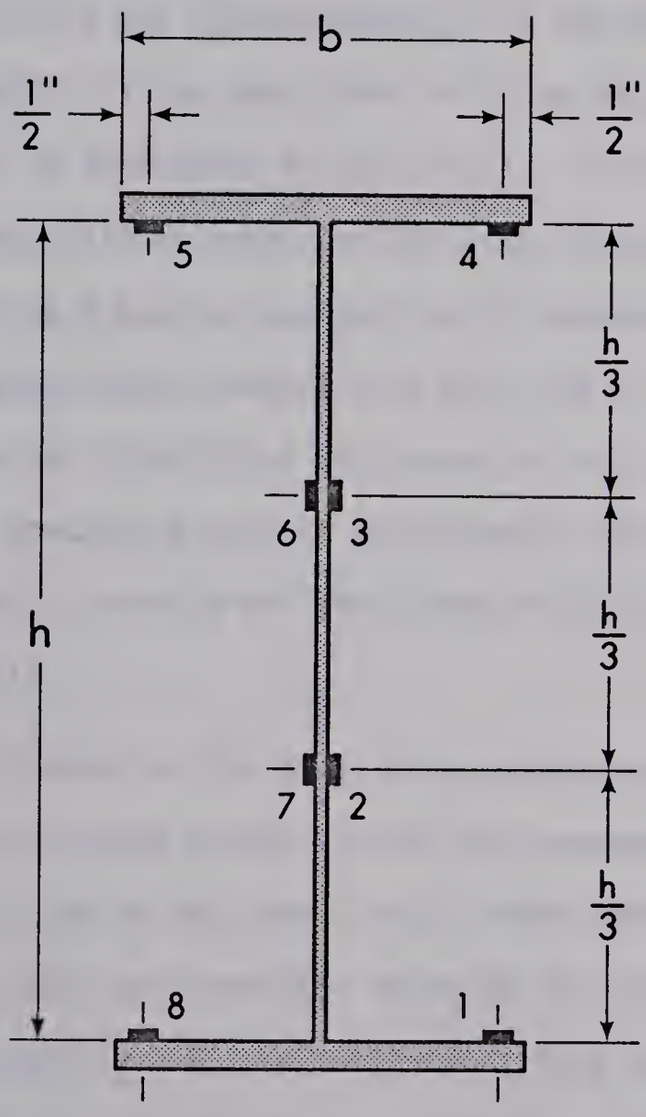

FIGURE 3.6 MOUNTING OF STRAIN GAUGES

CHAPTER IV

TEST RESULTS

4.1 Description of a Specific Test

To illustrate the general behavior of the test specimens, the results of one test, BC-6, will be described in detail. This test is considered to be typical. Significant differences, if any, will be noted for the other tests.

Specimen BC-6 had the greatest web slenderness ratio in the series of three tests conducted at $P/P_y = 0.4$. With a web slenderness ratio $((h/w)\sqrt{F_y})$ of 387, based on the measured value of F_y, this specimen proved to be extremely close to the web slenderness ratio at which web and flange buckling would occur simultaneously.

After alignment in the test setup, specimen BC-6 was then loaded axially to its total axial load (P) in increments of approximately one fifth of the final load. After each increment, all readings were taken and carefully observed for any noticeable changes. At increment 5, when the total axial load had been reached, observations showed that only negligible movements had occurred. Movements of the flange tips and overall deflections of the beam-column did not exceed three one-thousandths of an inch. The web maintained its position during the application of the axial load, in spite of an initial out-of-plane deflection. Significant initial out-of-plane deflections tend to increase when a specimen is subjected to axial load. This is discussed in

detail later.

The application of moment began at increment 6 (Figure 4.1 (f)). For this and each successive increment, the major axial load was first decreased by approximately one fourtieth of the total axial load. The minor (eccentric) load was then increased until the total axial load was restored.

During the application of moment, the moment rotation curve exhibited a non-linear relationship (concave downward), as it was monitored by a plotter. The curve followed above,but closely to,the line of theoretical behavior.

At increment 13 (0.68 M_{pc}), horizontal yield lines in the compression flange were first observed. These occurred along the entire length of the beam-column. The yield lines started at the tips of the compression flange and progressed inward towards the flange-to-web junction as the moment was applied.

At increment 16 (0.944 M_{pc}), horizontal yield lines had appeared in the web, close to the compression flange-to-web junction. Continued application of moment advanced the yield lines towards the tension flange.

Beyond increment 17 (0.988 M_{pc}), it was noticed that the rates of deflections were increasing with each successive load increment. In addition, periods during which deflections were allowed to stabilize before readings could be taken were becoming more prolonged. As a result, deflections were used as

a guide in regulating the loading rate for the remainder of the test. Up to and including increment 21, no visual change was observed in the shape of the specimen's cross-section.

The ultimate moment (M_u) was attained at increment 22 (1.18 M_{pc}). At this point in the test, it was noticed that both the web and the compression flange had begun to move slightly, although no extensive yielding patterns had appeared. The movement was observed in the region just below the point of maximum moment, that is, the mid-height of the specimen.

From this load increment onward, the moment-carrying capacity of the specimen began to decrease. It was necessary to increase the axial load, rather than decrease it, in order to maintain the total axial load required.

At increment 24 (0.886 M_{pc}), a local buckling of the web and adjacent compression flange suddenly appeared. This was preceded by flaking of the mill scale and whitewash. Upon taking measurements and comparing them to measurements from the previous increment, it was found that the maximum out-of-plane deflection of the web had changed more than the movement of the compression flange tips.

Although it is probable that the web initiated buckling of both plate elements, it should be noted that the stiffness of the compression flange-to-web junction at this point in the test had been reduced substantially by yielding. Thus, it is probable that it acted more like a hinge. Since both plate

elements started to move at the same time and both moved throughout the test, it is more likely that both buckled simultaneously.

After increment 26 (0.75 M_{pc}), the local buckling of the web and flange had become more severe. The centerline deflection had become so large that the axial load acting through this deflection accounted for a fifteen percent increase above the nominal value of the moment. This accelerated the decrease in the specimen's capability to sustain the eccentric load for small increases in deflection.

Since the specimen was now deformed well into the unloading range, the test was stopped at increment 31 (0.35 M_{pc}). It was decided that continued deformations could damage the head of the testing machine.

4.2 Coupon Tests

From two series of tension tests done on standard coupons, it was determined that the average static yield strength of the flange material was 46.8 ksi and that of the web material was 51.1 ksi. Each series consisted of six coupon tests. Each coupon was loaded until the material had just entered the range of yielding. At this point in the coupon test, while the strain was held constant, the coupon was allowed to relax with a resulting drop in the load. Once the load had stabilized, the value of the load was recorded and this same procedure repeated two more times to get an average reading for the static yield point (see Figure 4.2).

Since all of the beam-column specimens had been fabricated of material from the same rolling, the yield strength of the material could be expected to be uniform throughout the beam-column test series.

4.3 Discussion of Beam-Column Test Results

Table 4.1 shows the maximum initial out-of-plane deflections that existed in the webs prior to testing. It was found that in no case did initial out-of-plane deflections (δ/h) exceed the CSA W59.1[13] limit of $\delta/h = 0.00667$. Specimen BC-5 had the greatest δ/h ratio which was only 56.8% of this allowable value. The effects of initial out-of-plane deflections are discussed later in section 4.4.

Because of the manner in which the moment was applied, no shear forces perpendicular to the longitudinal axis of the beam-column specimens were introduced. Thus, no interaction between shear and moment existed.

The moment-rotation relationships for the nine beam-columns tested are shown in Figure 4.1 and the test results are summarized in Table 4.2. The rotations plotted in the figure are the relative rotations between the ends of the specimen as shown in the inset of Figure 4.1(a). In order that comparisons may be made between the specimens, the moments and rotations have been non-dimensionalized.

The additional moment caused by the axial load acting through the centerline deflection (Δ) was very small, particularly

prior to reaching M_u. For the nine specimens tested, the average additional moment created by the axial load upon reaching M_u was 1.3 percent. Specimen BC-8 had the maximum increase, 3.15 percent. Thus, the values of M_u/M_{pc} shown in Table 4.2 neglect the very small P - Δ effects.

Upon continued application of moment after reaching the ultimate moment, the P - Δ effects become more significant, however. Mid-height beam-column deflections increased rapidly with each increment of moment application. This resulted in a more substantial contribution to the maximum mid-height moment by the interaction of the load and the deflection. The moment recorded was only that applied to the ends of the specimen by the eccentric load. This accounts for the concave upward curve on the downside portion of the moment-rotation relationships shown in Figure 4.1. However, this had no effect on the results because none of these stubby beam-column specimens had critical buckling occurring at the mid-height cross-section. In most test cases, shortly after reaching M_u, deflections increased so rapidly that the applied end moments decreased quickly. Inclusion of the P - Δ effects would only shift the downside portion of a moment-rotation curve slightly, after the ultimate moment of a specimen had been reached.

In no case did flange buckling occur at the mid-height of a specimen in spite of the additional moment there. The effect of welding the lateral bracing pins at this section was to stiffen the flange plates somewhat. Once the lateral braces were attached,

additional restraint against torsional buckling of the flanges was offered. However, for some tests, web buckling was observed at this section. The lateral bracing pins were noticed to have moved (in some tests) as the flanges were forced to twist as buckling advanced into this region. However, the results were not greatly affected since buckling usually occurred closer to the specimen ends. This means that the moment recorded more closely represented the true moment existing at the point of buckling.

Figure 4.3 is a plot of the out-of-plane deflections of the web and compression flange versus the lateral deflection (Δ) at the mid-height of the specimen. The plots are shown for the locations at which critical buckling first occurred.

Lateral deflection was chosen as the ordinate in the plots, rather than eccentric load, because the load increases at a slower rate as yielding progresses. If load were plotted as the ordinate, this would appear as an increasing rate of web or flange deflection, even if the rates of deflections remained relatively constant.

Using lateral deflection as the ordinate eases the task of determining which plate element had buckled first, and at what point during the test. In order that comparisons could be made between specimens, the ordinate has been non-dimensionalized by dividing by Δ_{pc} (the deflection upon reaching M_{pc}). In the inset in each plot are shown the locations at which the web and flange

deflections were measured. A typical buckling of the web and flange is shown in Figure 4.4.

The web and flange deflections for specimen BC-6 are plotted in Figure 4.3(f). Upon reaching increment 5, it can be seen that for location 3, the flange plate had only shifted slightly. Upon continued moment application (up to but not including increment 22) no significant movement of the web or flange had occurred. Upon reaching the ultimate moment at increment 22, the rate of both the web and flange deflections began to increase. As mentioned previously, the first visual indication of buckling occurred at increment 24. At this point it was observed that both plate elements buckled simultaneously. The measured deflections were taken at a location approximately 2 inches below the point where the maximum buckle eventually occurred.

The flange and web deflection plots presented in Figure 4.3, combined with the visual observations, are indications of whether failure was induced by a local flange buckle, local web buckle, or by a combination of both. For example, if a flange deflection plot shows a major rate of change in deflection while the web deflection plot remains relatively constant, then it can be assumed that the flange plate element initiated buckling of the specimen cross-section. This was the case for a specimen such as BC-1, shown in Figure 4.3(a).

The first plate element to buckle, whether it be the web or compression flange, would cause the other plate element to

carry additional stresses. This combined with the reduced torsional restraint offered by the flange-to-web junction due to yielding, could be expected to cause the second plate element to buckle shortly after the first.

The plots for specimens BC-1 and BC-2 (Figures 4.3(a) and 4.3(b) respectively) show that both failed by flange buckling. For specimen BC-1 ($(h/w)\sqrt{F_y} = 332$), it was observed that the flange tips moved throughout the whole test. Failure eventually occurred due to a local flange buckle. Very little movement of the web had occurred until the ultimate moment was reached at increment 29.

Specimen BC-2 ($(h/w)\sqrt{F_y} = 368$), behaved similarly to BC-1, although at the location of buckling BC-2 had a greater initial out-of-plane deflection of the web. A more substantial initial web deflection increases the probability that web buckling will initiate the failure of a specimen. It should be noted that at increment 26 the buckling of the flange forced the web buckle to move towards the compression flange.

From Figure 4.3(c) it would appear that specimen BC-3 ($(h/w)\sqrt{F_y} = 437$) failed by simultaneous buckling of the web and flange. Visual observations showed, however, that the slight web movement occurring at increment 16 caused a rapid loss in the eccentric load. This slight buckling of the web then caused the flange to carry more stress. In the loading increments following, the flange and web only moved slightly. After reaching

the ultimate moment at increment 21, both the web and compression flange deflection rates began to increase. Therefore, it can safely be said that the web initiated the buckling of the section.

Specimens BC-4 and BC-5 ($(h/w)\sqrt{F_y}$ = 285 and 324, respectively), like specimens BC-1 and BC-2, both exhibited flange buckling failures. Specimen BC-4 (Figure 4.3(d)), showed no major movement of the web plate throughout the test. When flange buckling was noted at increment 24, no web movement had yet been observed.

Although specimen BC-5 (Figure 4.3(e)), had a more substantial initial web deflection than did BC-4, buckling of the flange element caused failure of the cross-section. Flange buckling was observed at increment 19, just after reaching the ultimate moment at load increment 17.

As described previously, specimen BC-6 was an example of simultaneous web and flange plate failure. As shown in Figure 4.3(f), this specimen ($(h/w)\sqrt{F_y}$ = 387) showed only slight movements during the early stages of the test. From increment 5 until reaching the ultimate moment at increment 22, no significant movement of either the web or compression flange was noted. From increment 22 onward, recorded measurements show that both plate elements were buckling simultaneously. This was confirmed visually at increment 24.

Specimens BC-7, BC-8 and BC-9 were subjected to a high axial load (P/P_y = 0.8). Specimen BC-7 ($(h/w)\sqrt{F_y}$ = 286), developed

a multitude of yield lines in the flanges and web during application of the axial load. However, during the application of moment, no web movements were observed. The flange buckled abruptly just after reaching the ultimate moment at increment 24.

Specimens BC-8 and BC-9 ($(h/w)\sqrt{F_y}$ = 325 and 385, respectively) were significantly affected by axial load. The initial web deflections were amplified as the axial loads were applied to the specimens. As a result, because the buckled webs did not carry their full share of the load, the flanges were forced to take on additional load. Even before the application of moment, it was predictable from observation of the specimens that the webs would initiate buckling.

4.4 Effect of Initial Web Deflections

In fabricating reasonable cross-sectional shapes for testing, relatively light steel plate had to be used (3/8 of an inch for flanges and 1/4 of an inch for webs). It is probable that as a result of residual stresses resulting from the welding of these thin plates, that initial web deflections developed.

Initial web deflections (at the location of buckling) can be seen in Figure 4.3 as the web deflection present at Δ/Δ_{pc} equal to zero. The maximum initial out-of-plane deflections (taken from the entire web length) are tabulated in Table 4.2. As mentioned previously, no specimens exceeded the out-of-flatness requirements established by the CSA Standard W59.1[13] (δ/h = 0.00667).

It was thought possible that the specimens failing by web buckling would not reach M_{pc}, that is, that the web would

initiate the failure of the flanges before reaching M_{pc}. However, this was not the case as only specimen BC-9 failed to reach M_{pc}. Of all specimens, BC-9 had the maximum initial out-of-plane web deflection recorded at the location of buckling. For specimens subjected to low axial loads, initial web deflections do not greatly affect the test results. However, initial web deflections play an important part when high axial loads are present, as can be seen in specimens BC-8 and BC-9. The high axial loads amplify the web deflections to the point where web buckling inevitably initiates the failure of the specimen.

TABLE 4.1 INITIAL WEB DEFLECTIONS

Specimen	Web Depth h (inches)	Deflection δ (inches)	δ/h
BC-1	12.0	0.019	0.00158
BC-2	13.5	0.046	0.00341
BC-3	15.7	0.052	0.00331
BC-4	10.3	0.019	0.00184
BC-5	11.6	0.044	0.00379
BC-6	13.9	0.018	0.00129
BC-7	10.3	0.015	0.00145
BC-8	11.7	0.016	0.00137
BC-9	13.9	0.038	0.00273

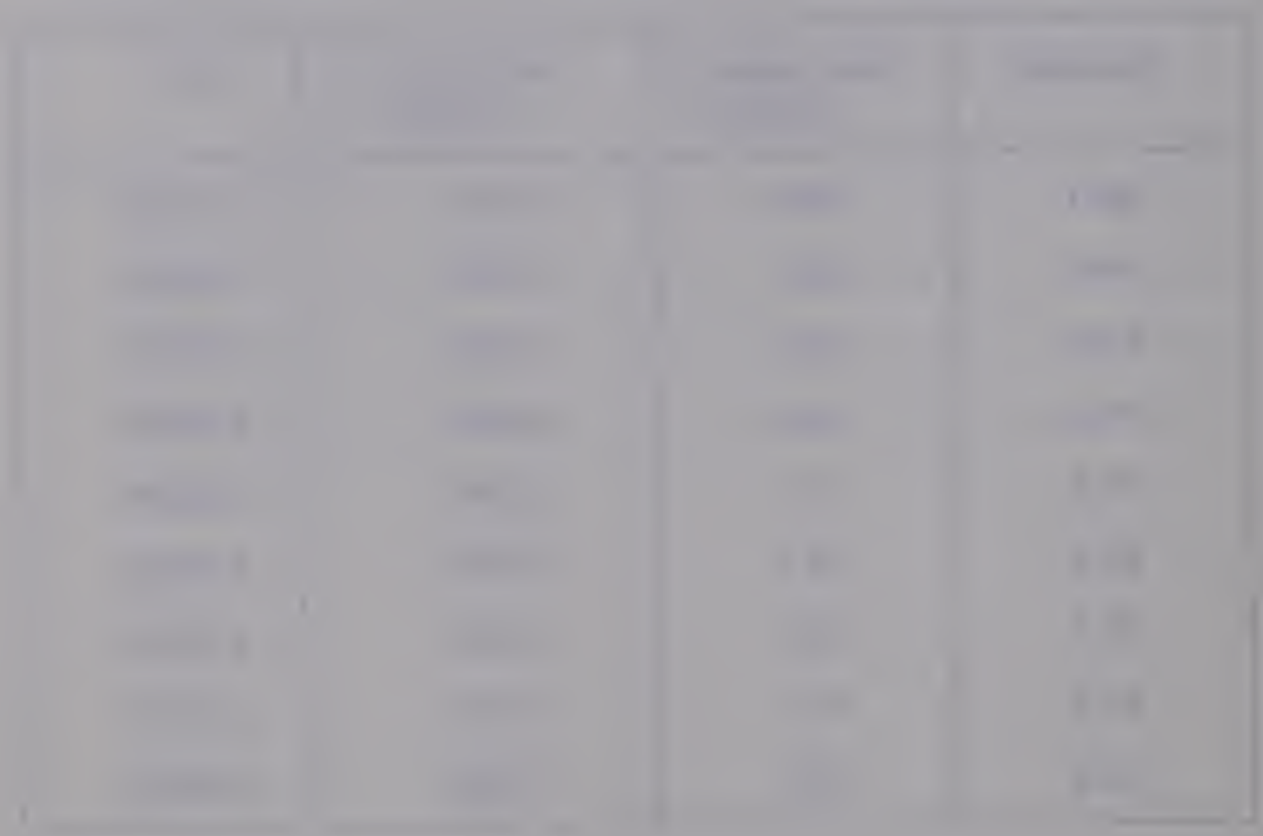

TABLE 4.2 BEAM-COLUMN TEST RESULTS

Specimen	$\frac{h}{w}\sqrt{F_y}$	M_u (inch kips)	M_u/M_{pc}	Buckled Element
BC-1	332	2370	1.18	Flange
BC-2	368	2732	1.18	Flange
BC-3	437	2887	1.04	Web
BC-4	285	1606	1.21	Flange
BC-5	324	1829	1.19	Flange
BC-6	387	2303	1.18	W and F
BC-7	286	738	1.67	Flange
BC-8	324	694	1.34	Web
BC-9	385	582	0.90	Web

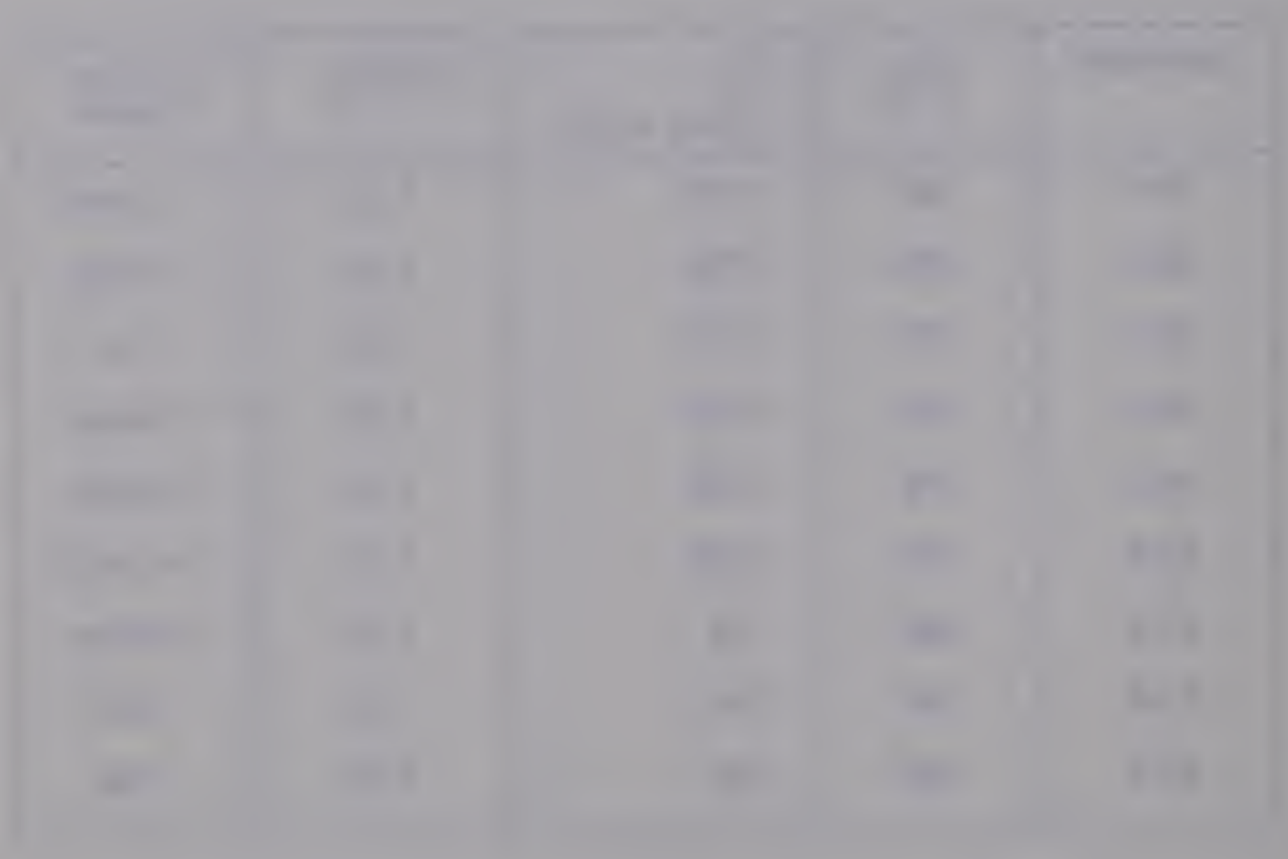

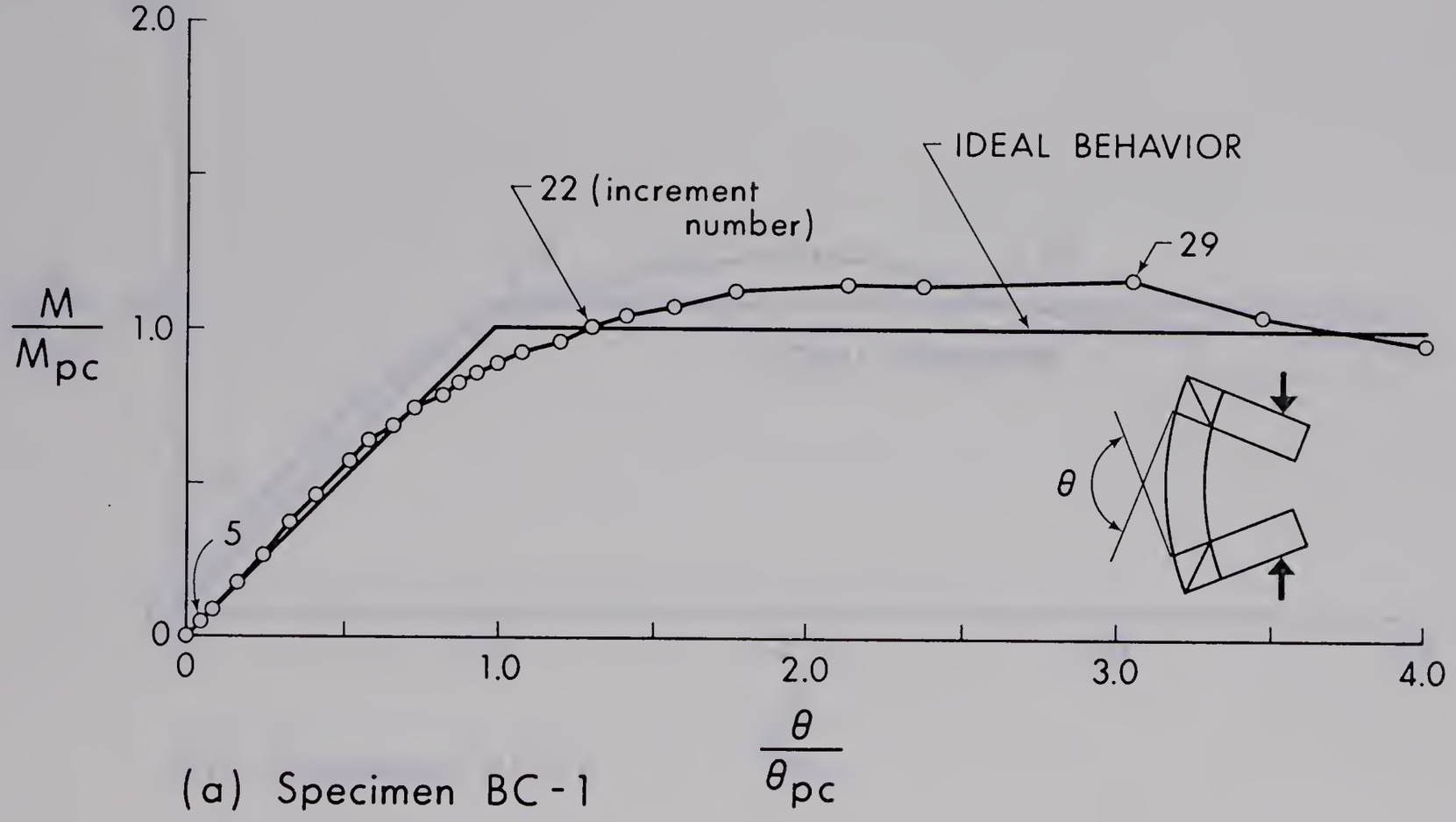

FIGURE 4.1 MOMENT-ROTATION RELATIONSHIPS

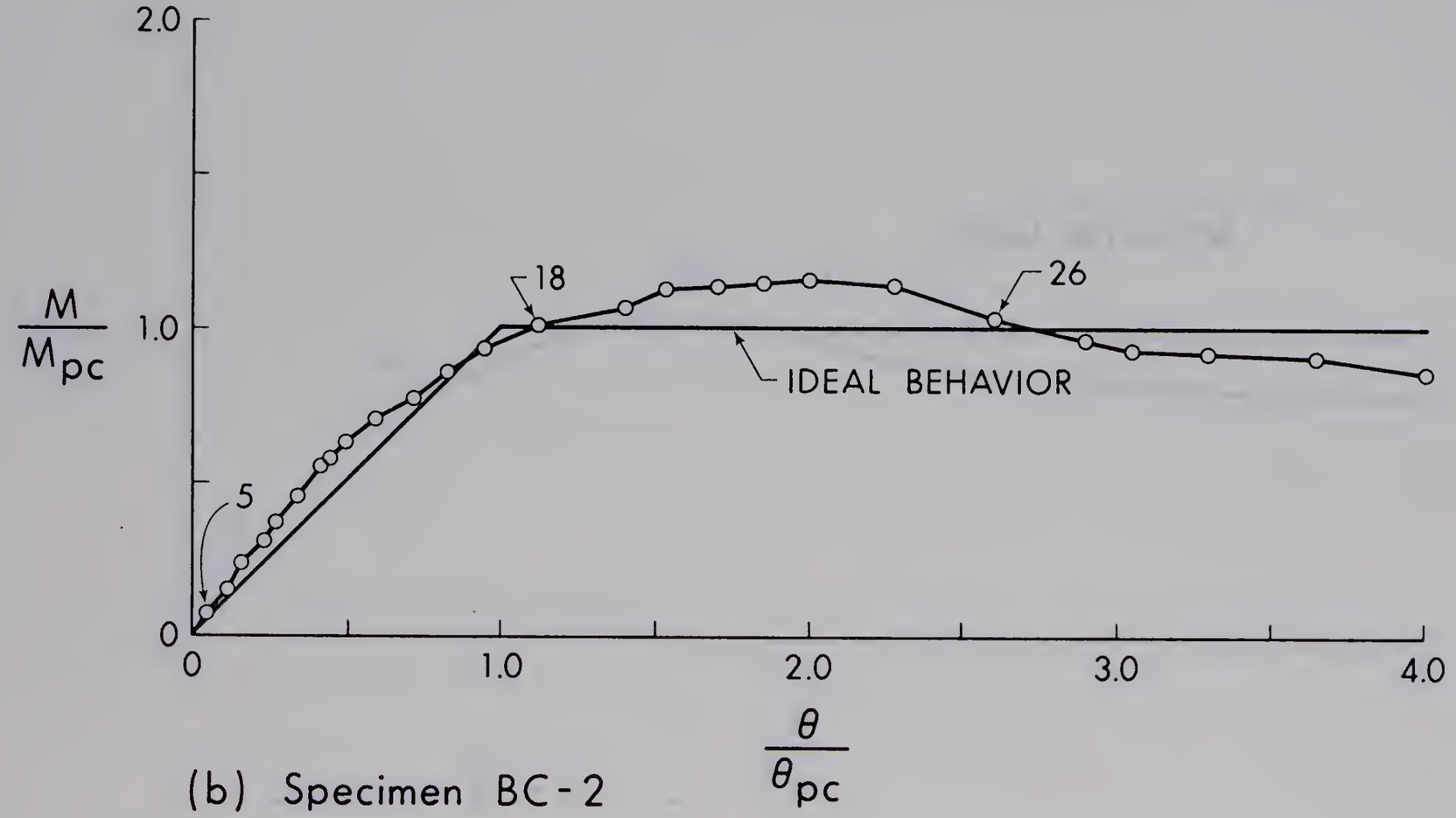

FIGURE 4.1 MOMENT-ROTATION RELATIONSHIPS (Cont'd)

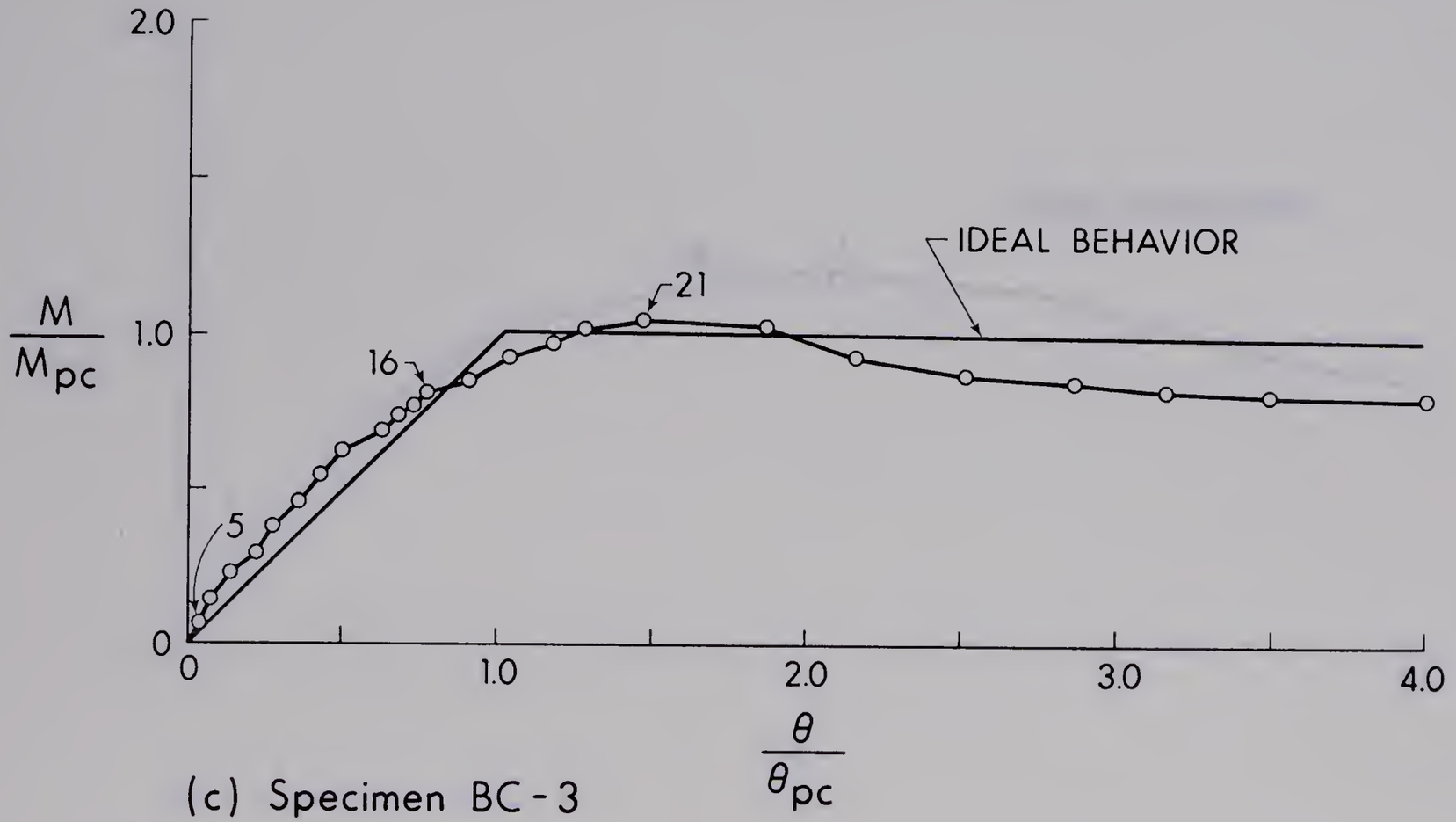

(c) Specimen BC-3

FIGURE 4.1 MOMENT-ROTATION RELATIONSHIPS (Cont'd)

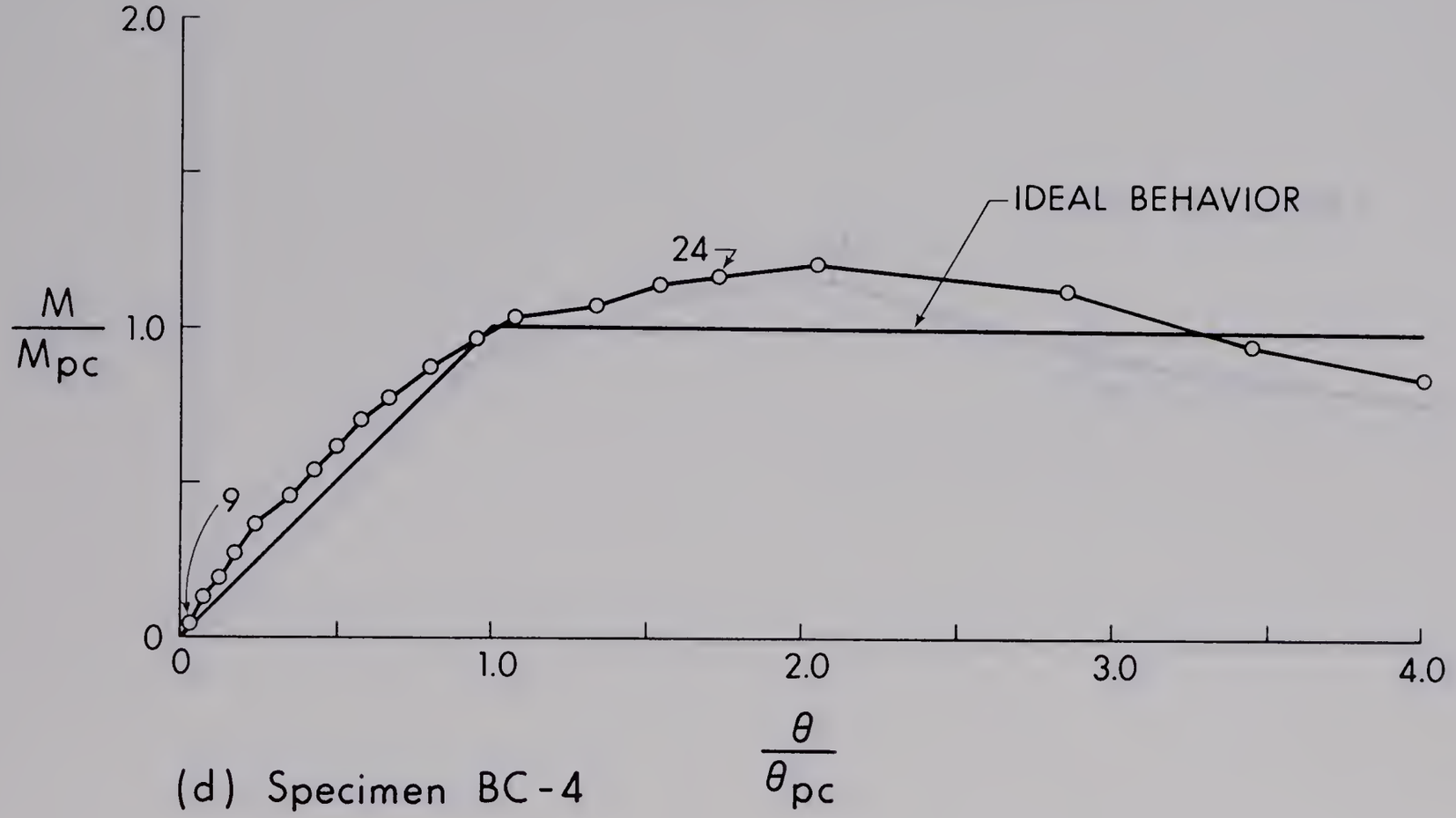

(d) Specimen BC-4

FIGURE 4.1 MOMENT-ROTATION RELATIONSHIPS (Cont'd)

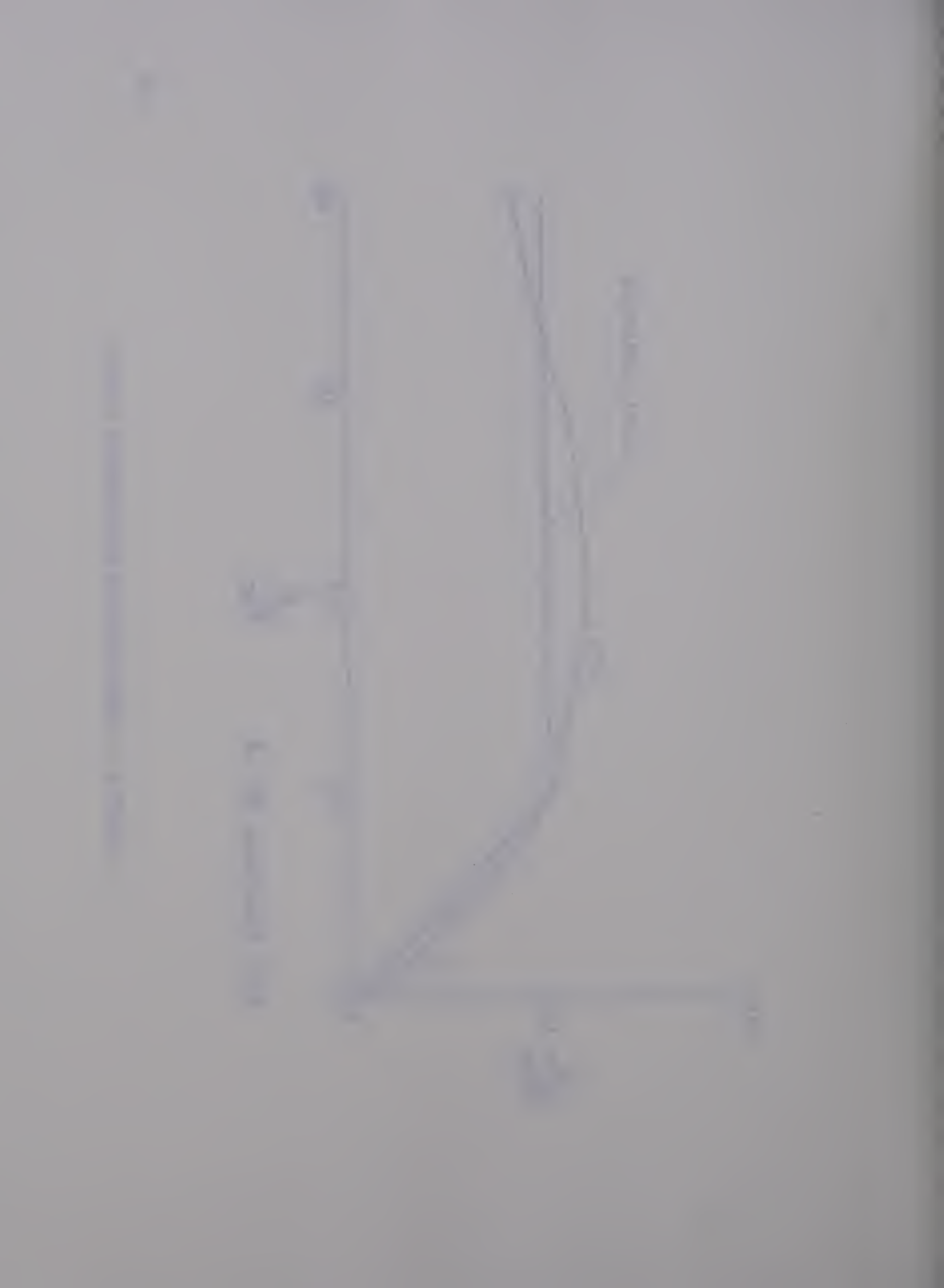

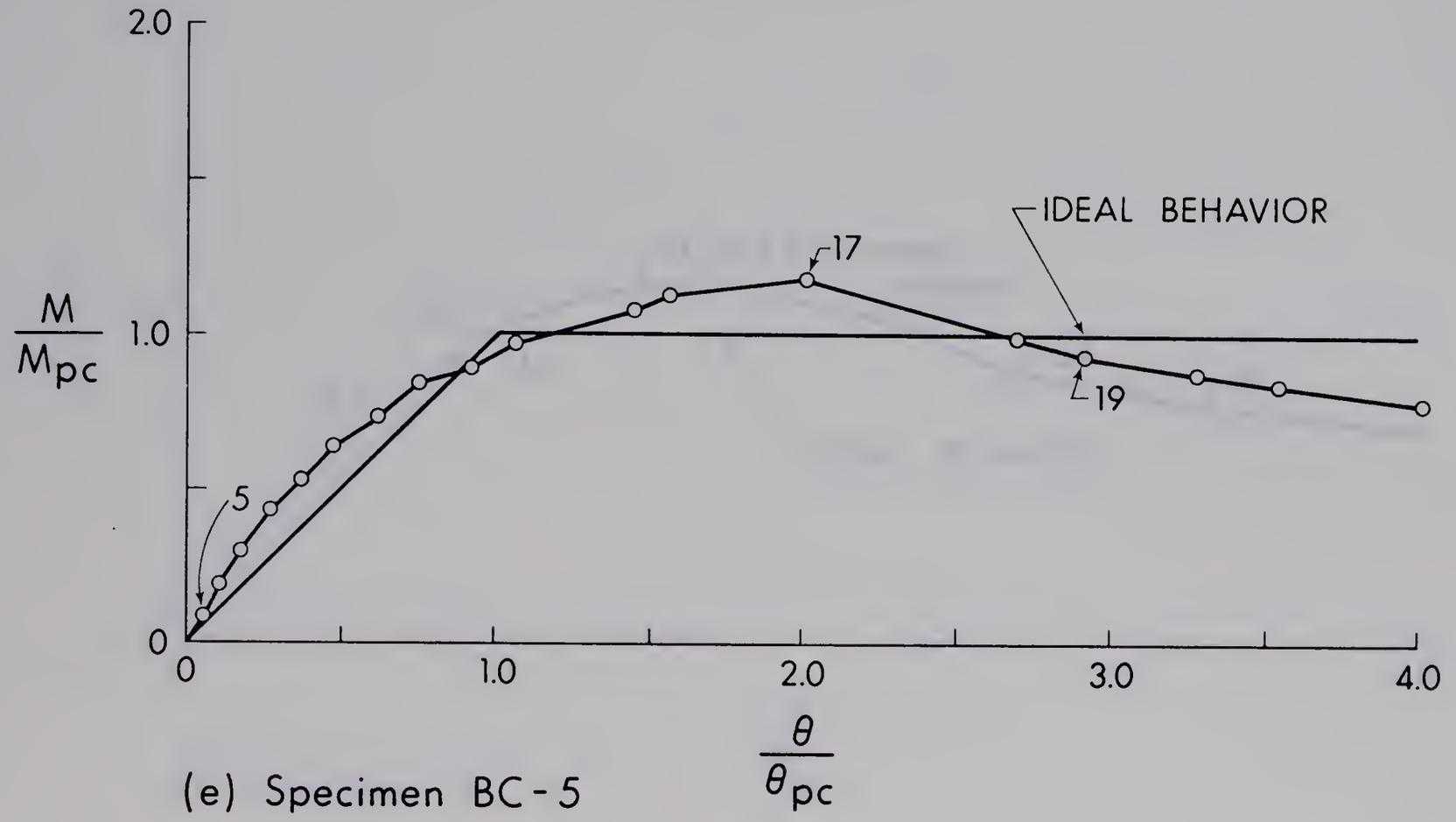

(e) Specimen BC-5

FIGURE 4.1 MOMENT-ROTATION RELATIONSHIPS (Cont'd)

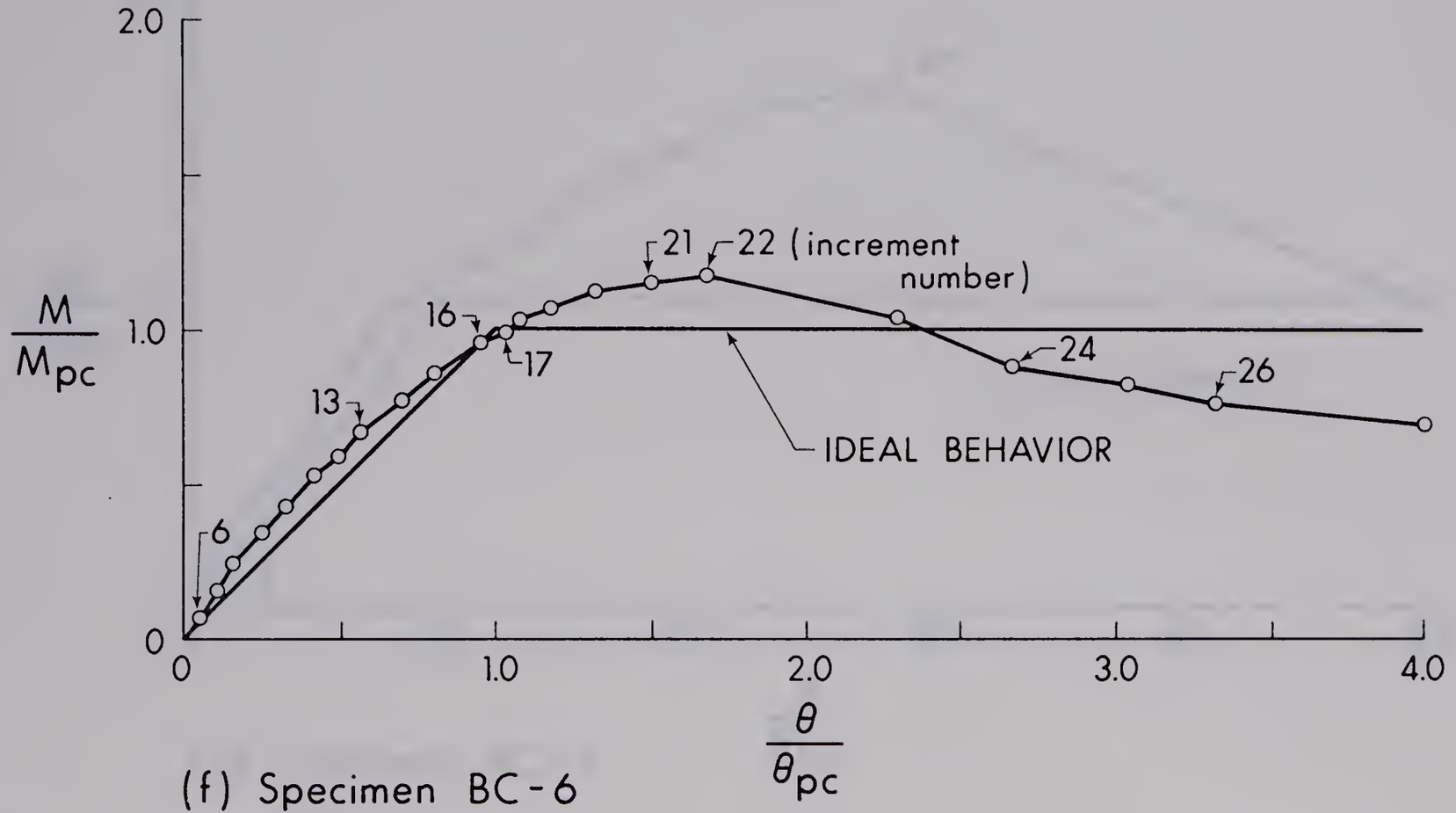

FIGURE 4.1 MOMENT-ROTATION RELATIONSHIPS (Cont'd)

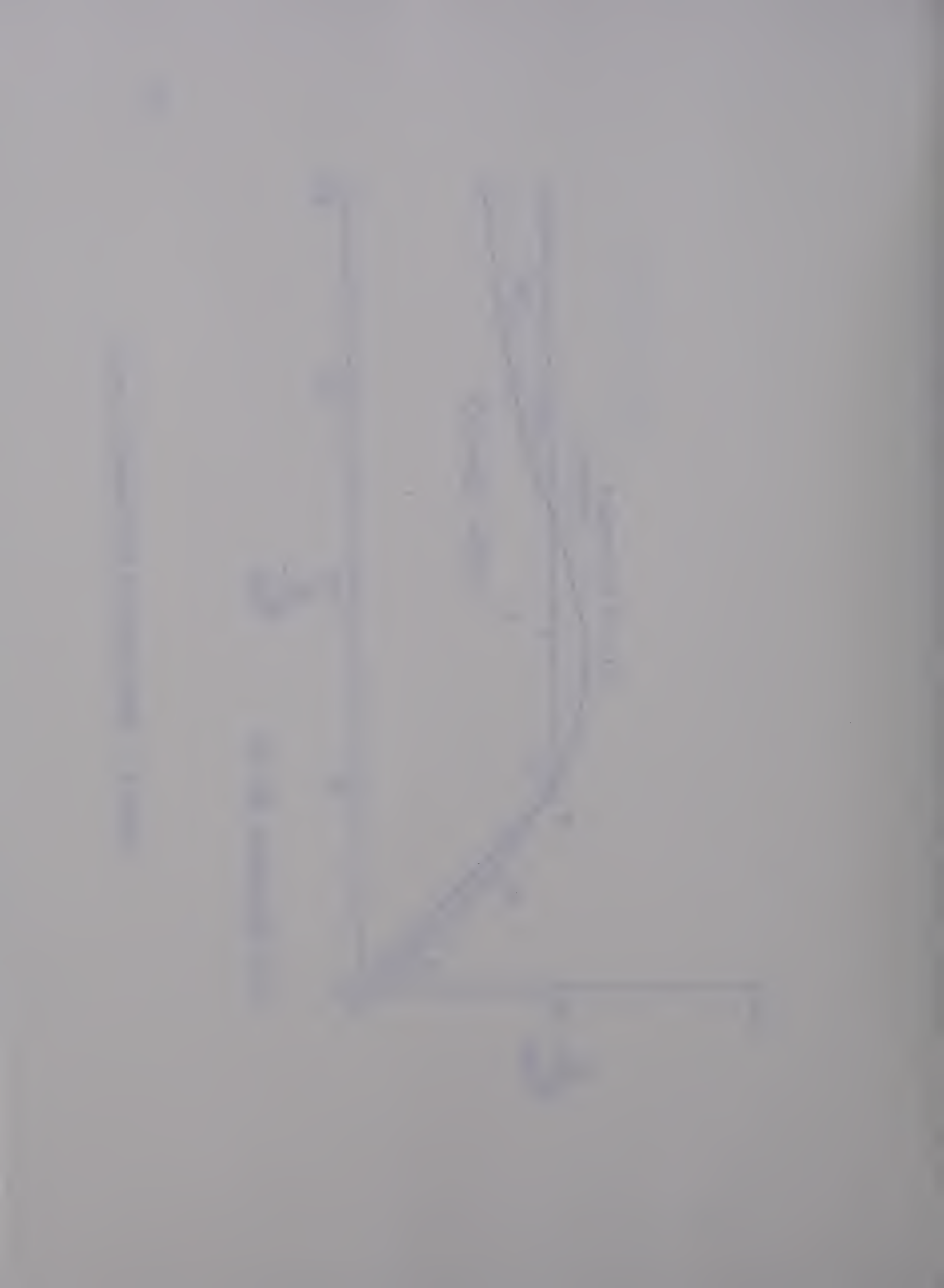

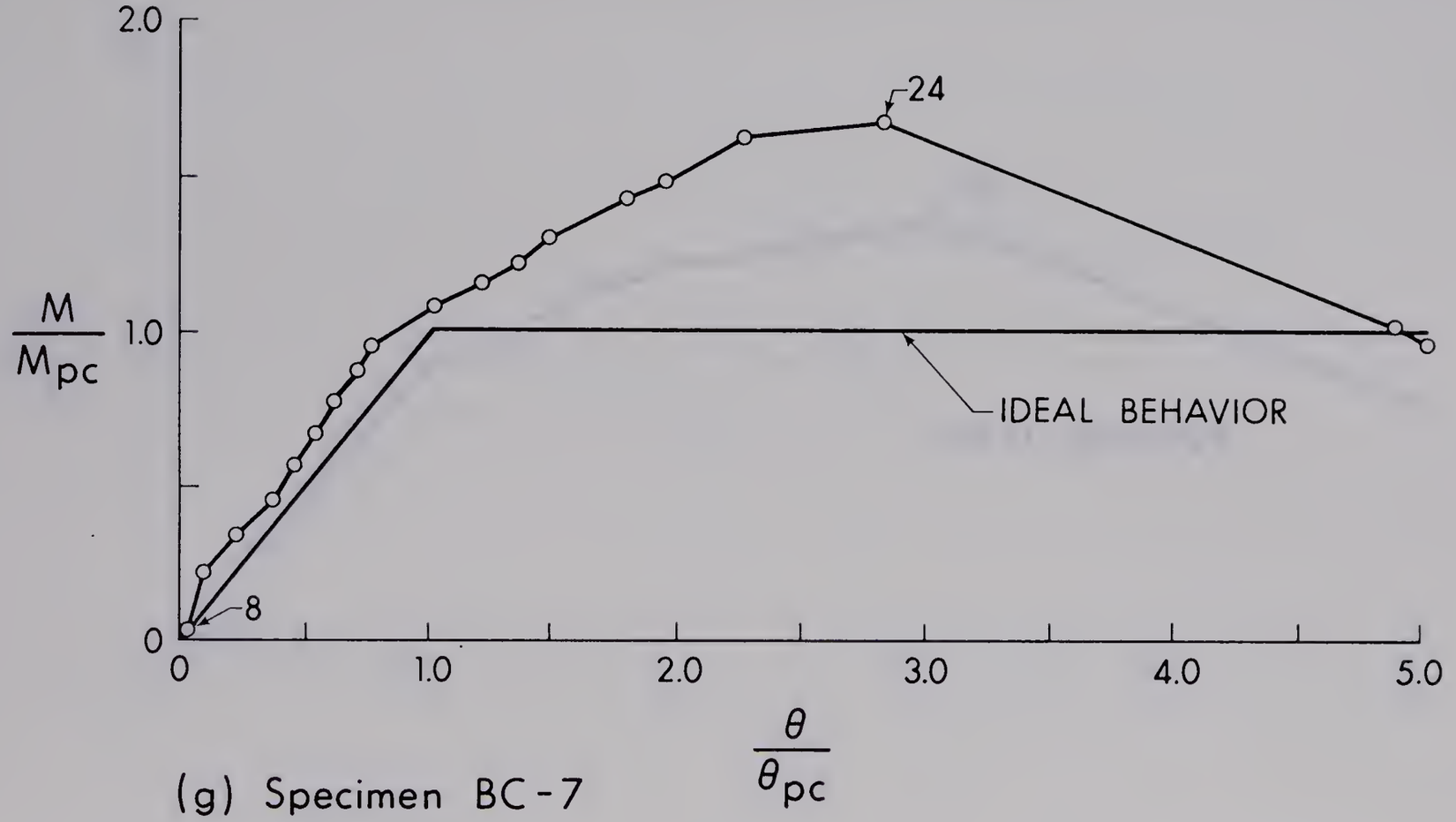

FIGURE 4.1 MOMENT-ROTATION RELATIONSHIPS (Cont'd)

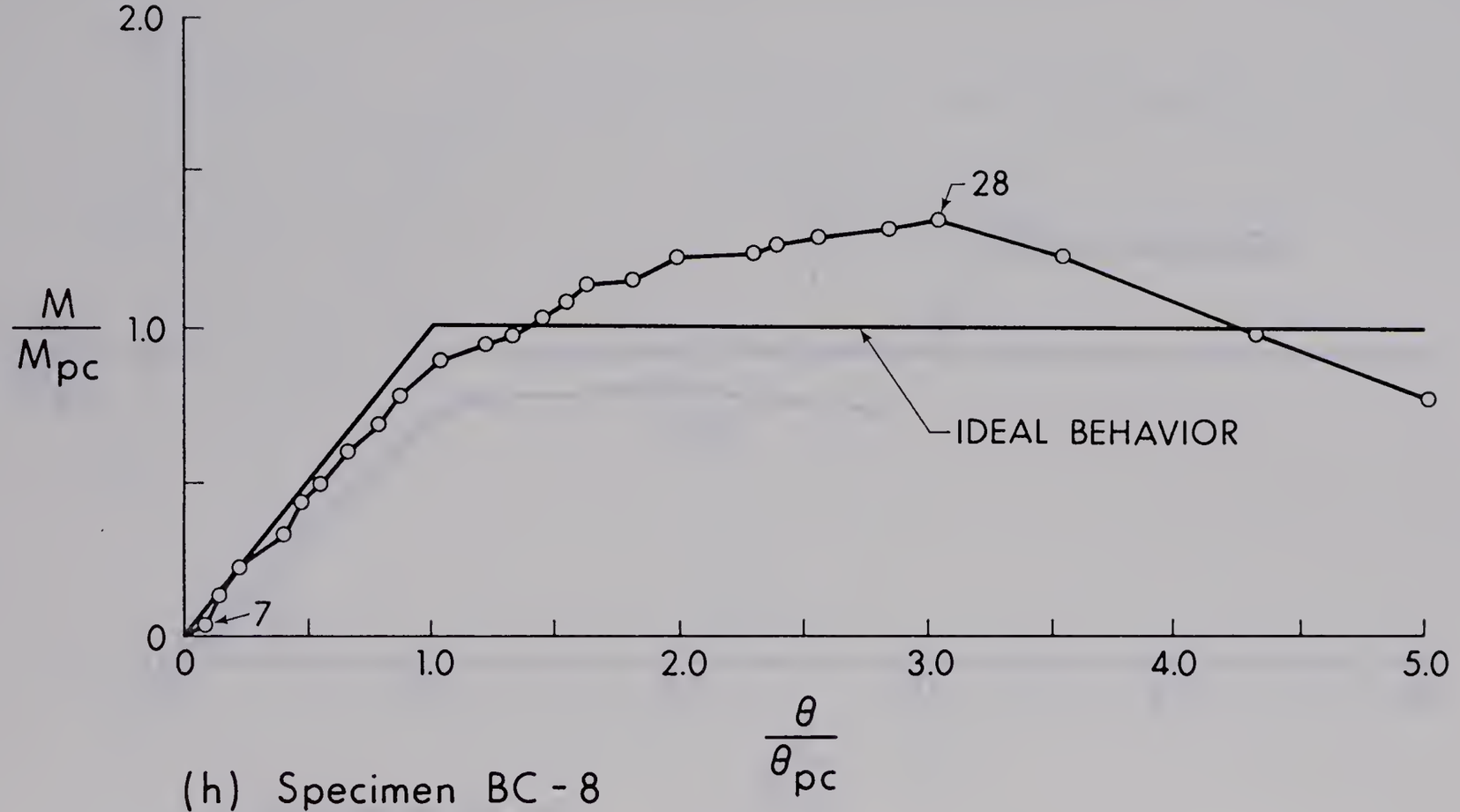

FIGURE 4.1 MOMENT-ROTATION RELATIONSHIPS (Cont'd)

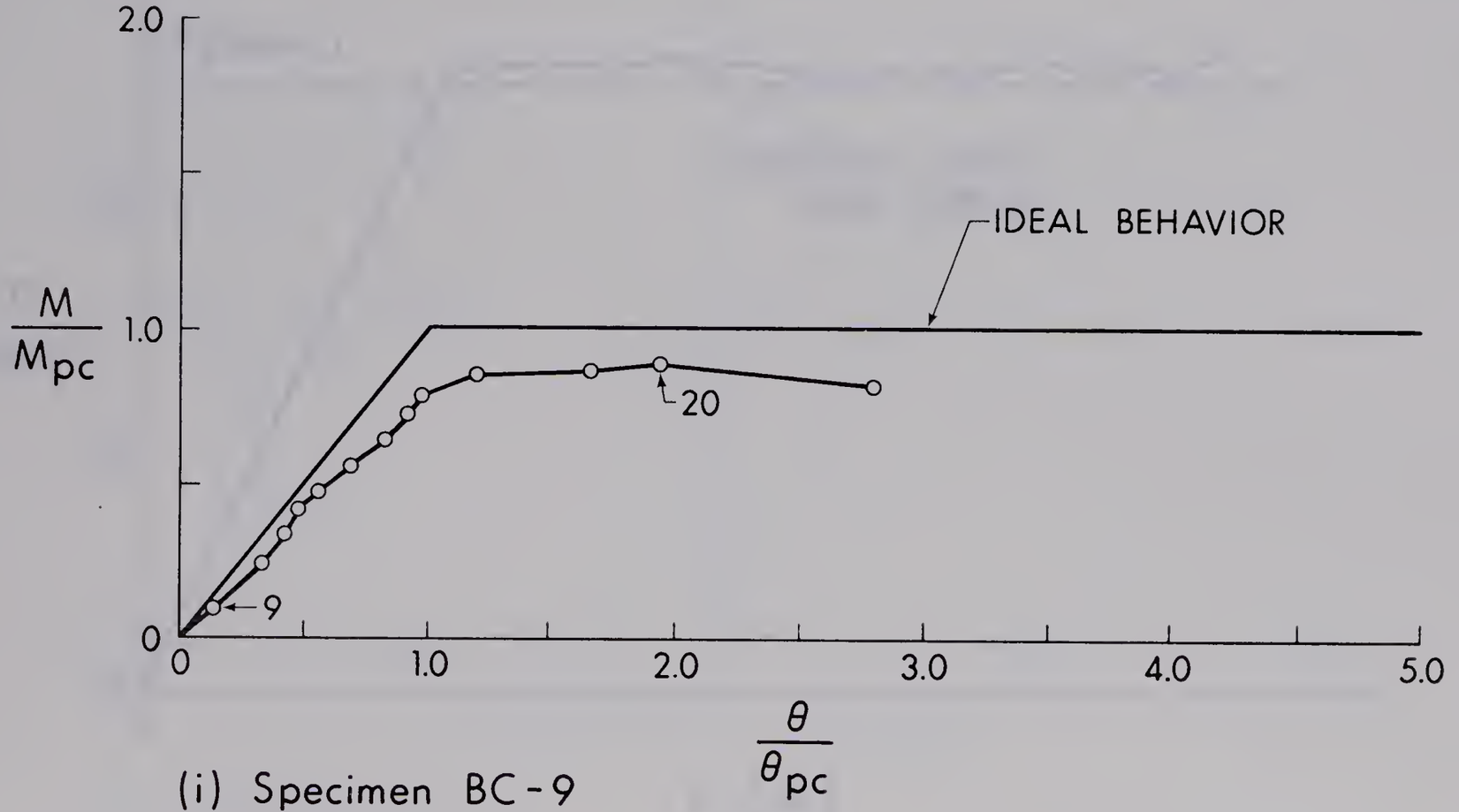

FIGURE 4.1 MOMENT-ROTATION RELATIONSHIPS (Cont'd)

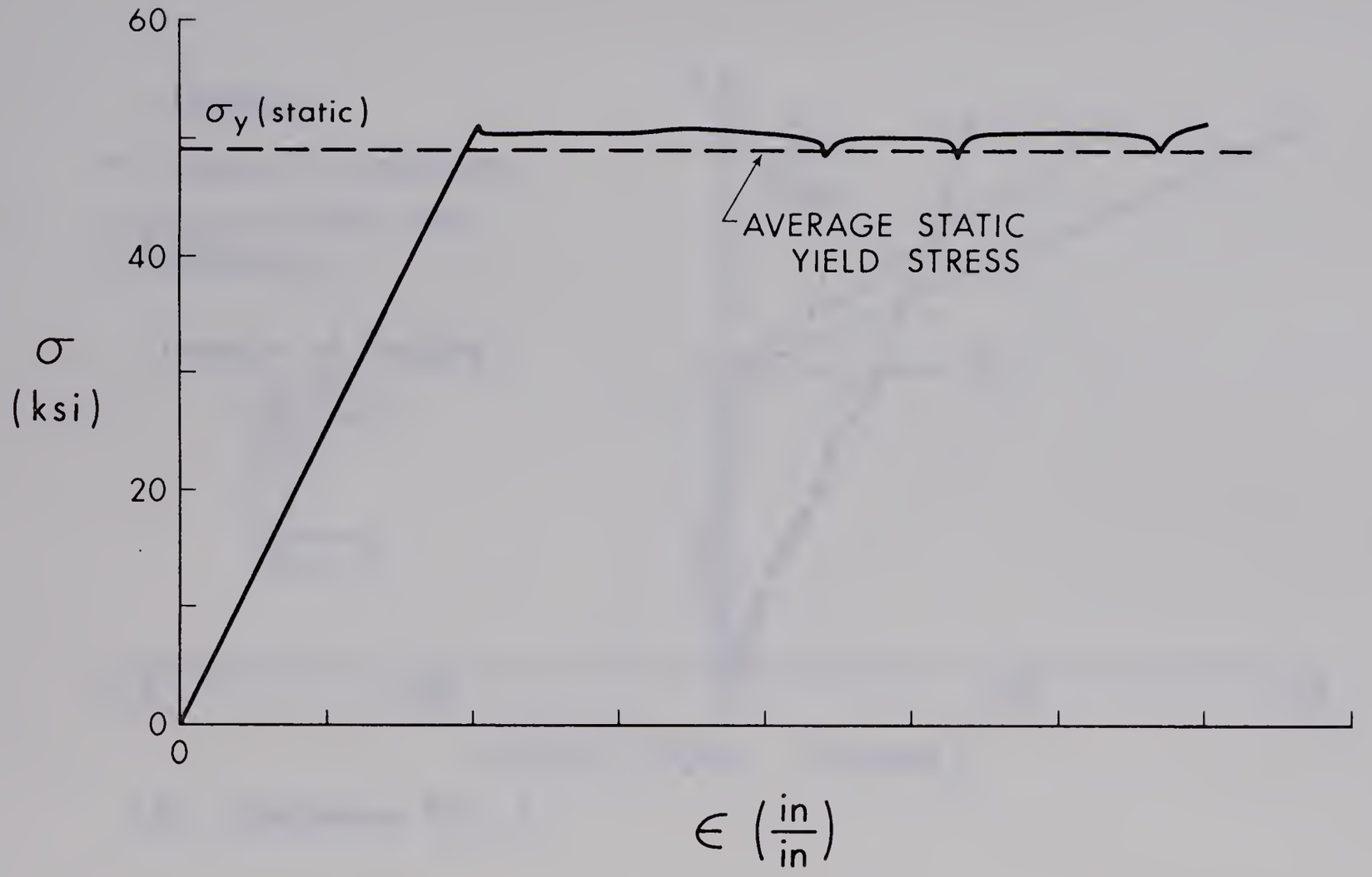

FIGURE 4.2 STRESS-STRAIN RELATIONSHIP FOR A TYPICAL COUPON TEST

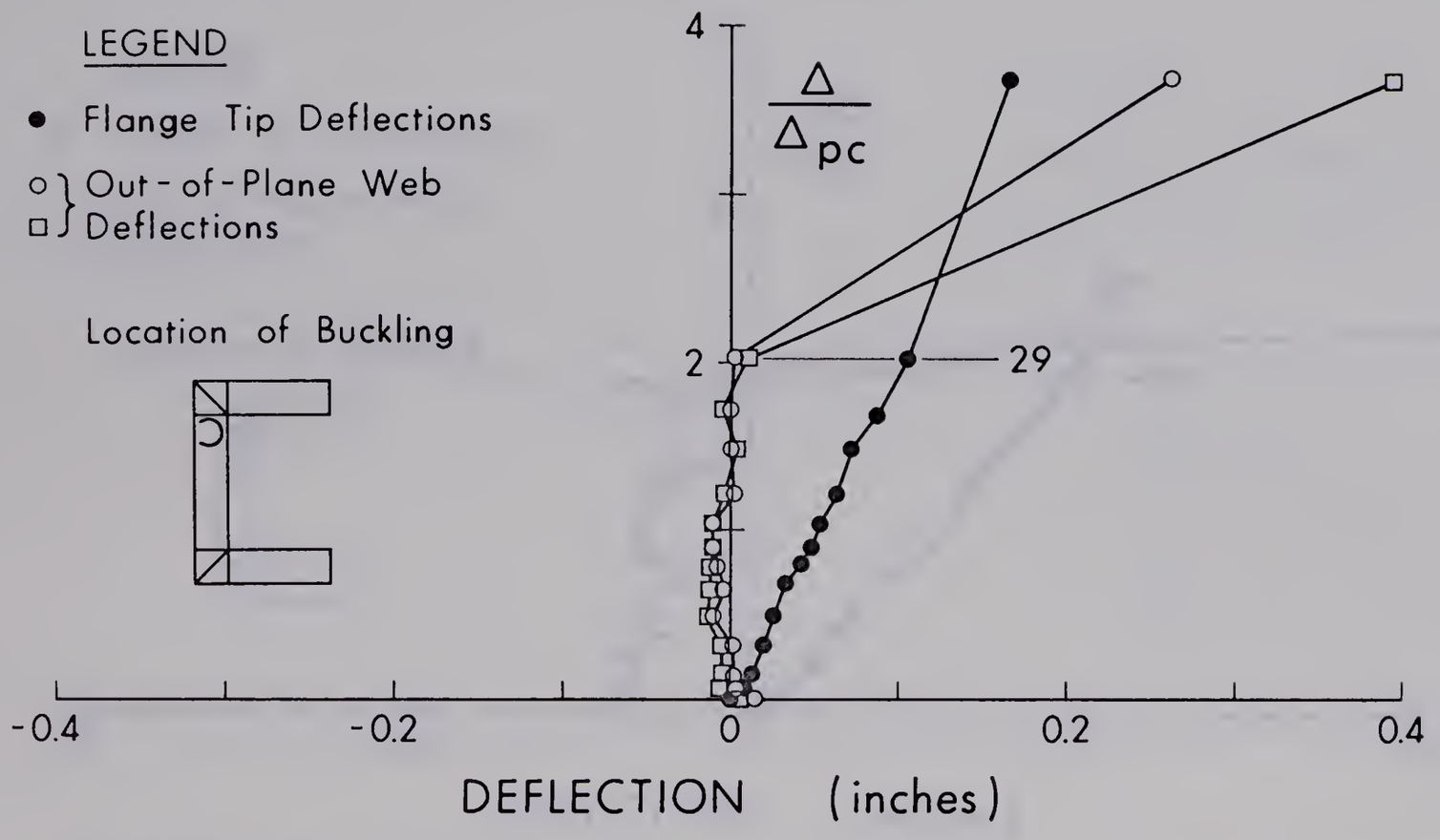

(a) Specimen BC-1

FIGURE 4.3 FLANGE AND WEB DEFLECTION PLOTS

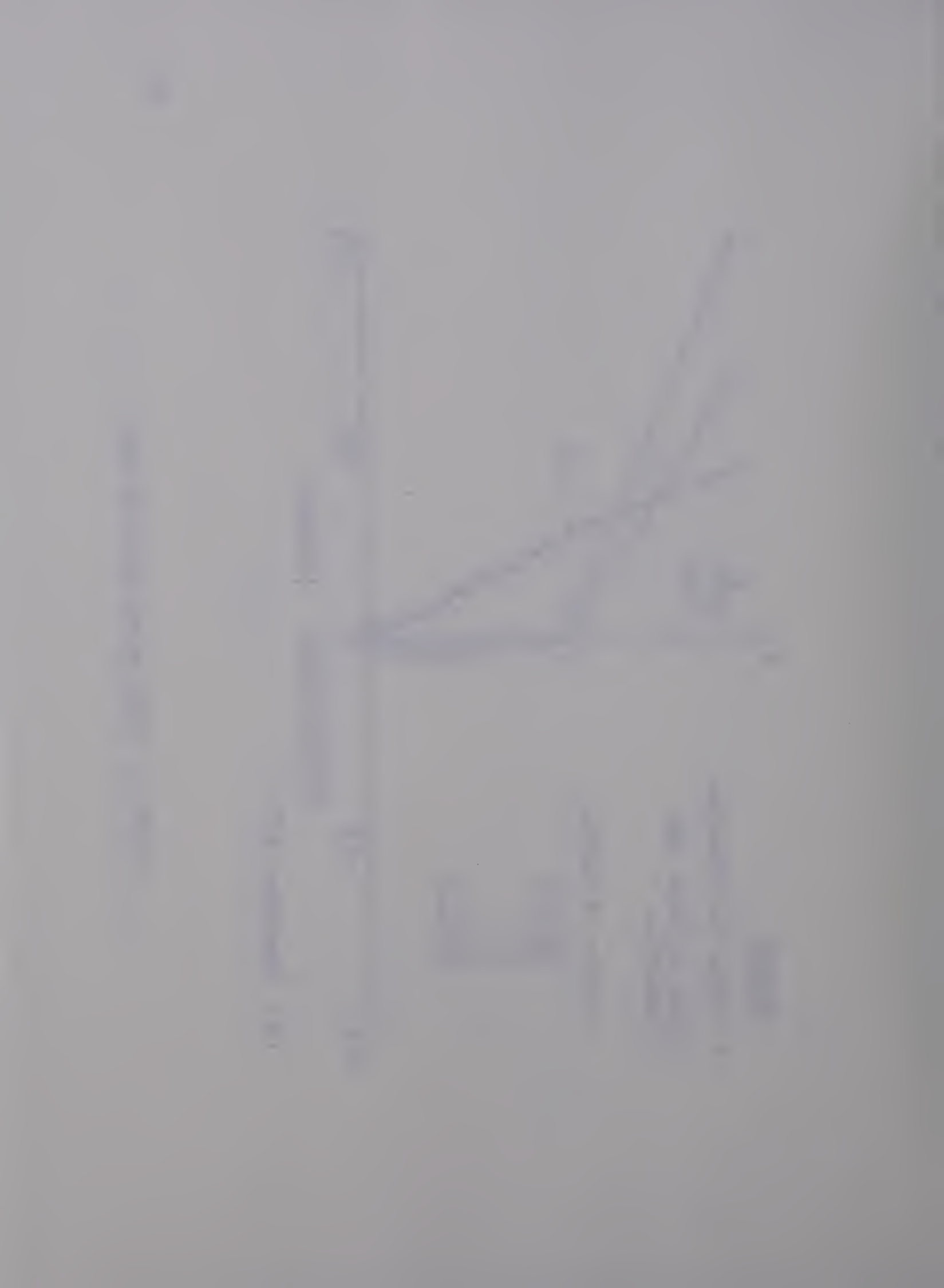

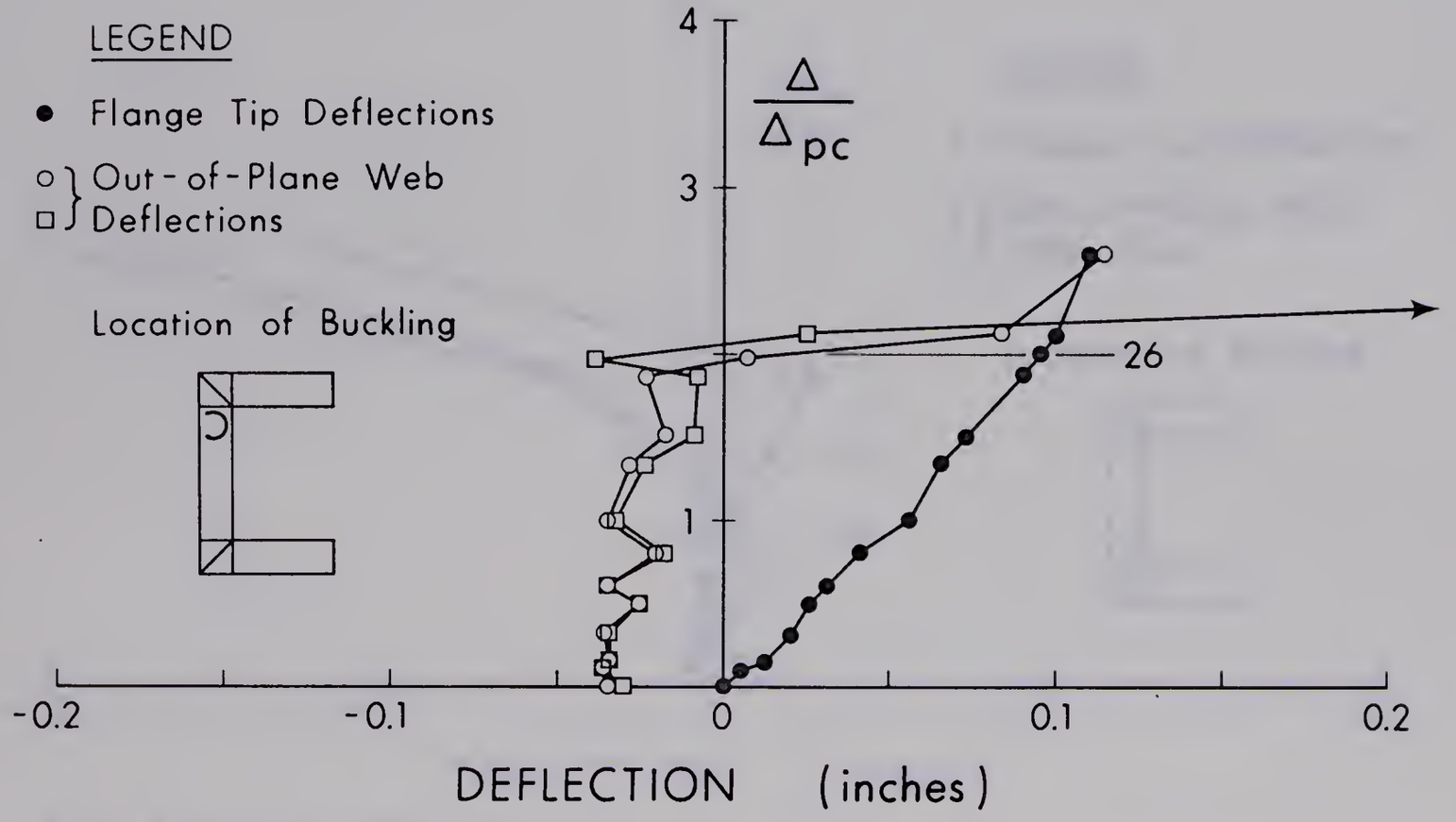

(b) Specimen BC-2

FIGURE 4.3 FLANGE AND WEB DEFLECTION PLOTS (Cont'd)

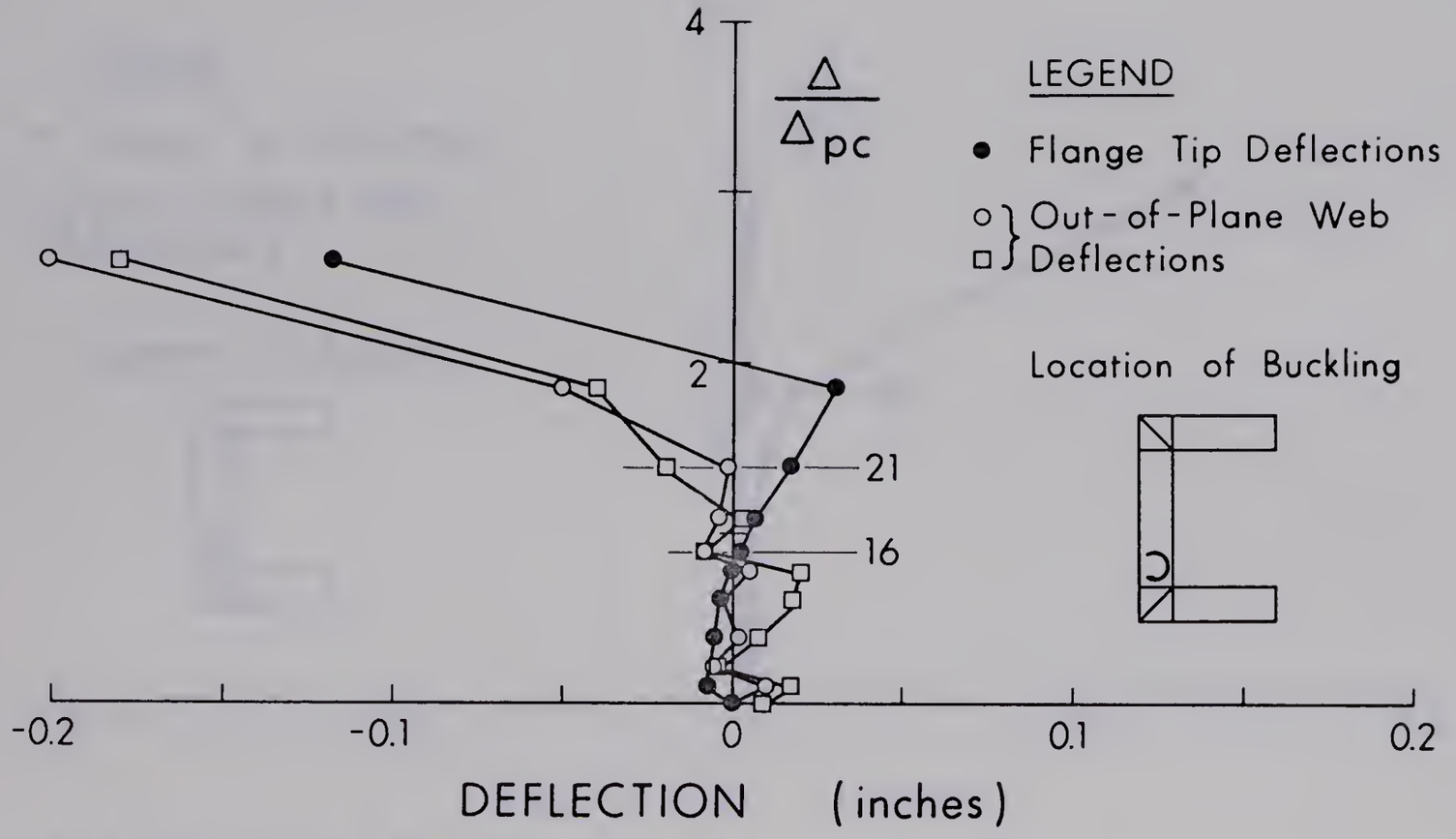

(c) Specimen BC-3

FIGURE 4.3 FLANGE AND WEB DEFLECTION PLOTS (Cont'd)

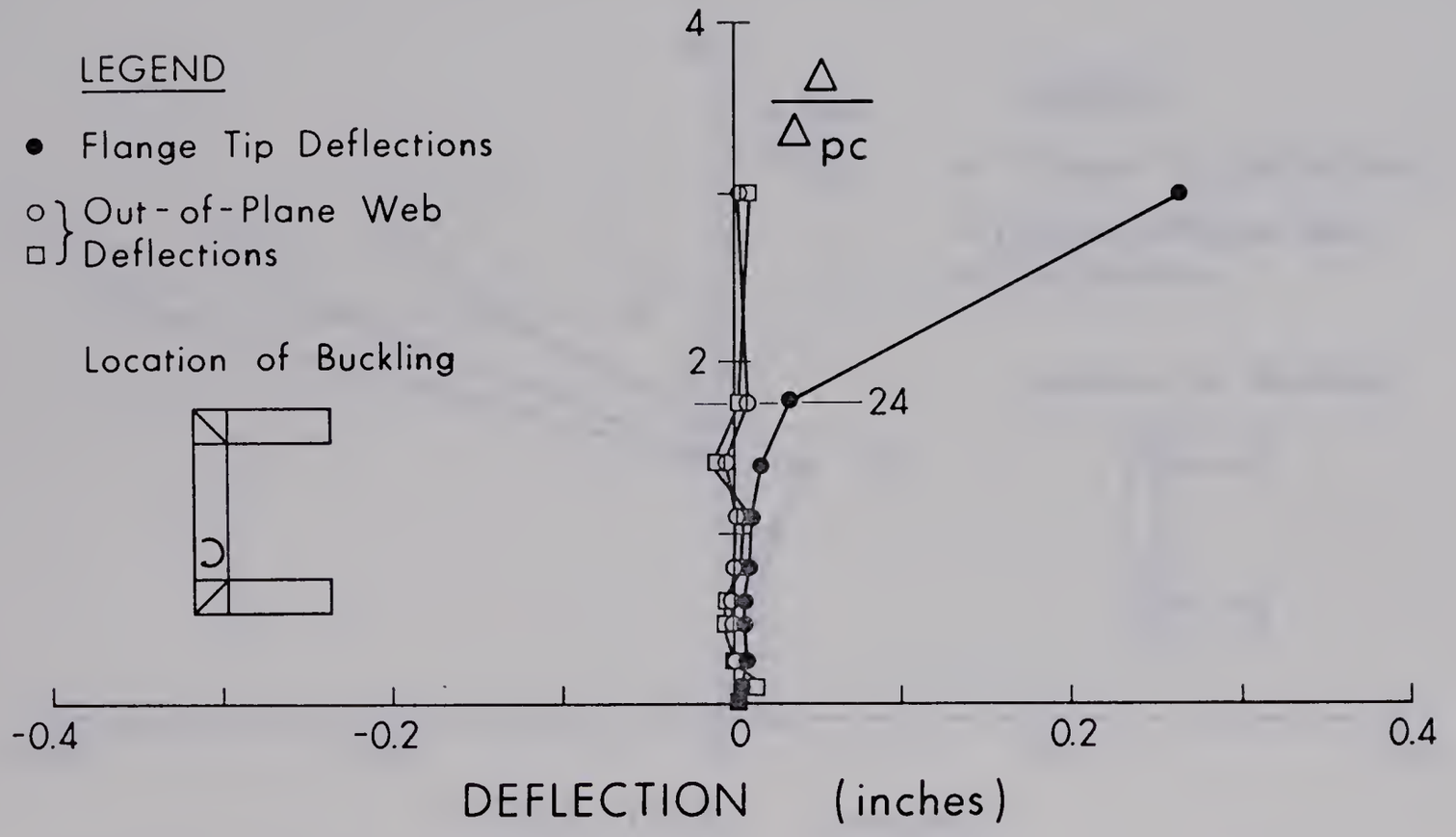

(d) Specimen BC-4

FIGURE 4.3 FLANGE AND WEB DEFLECTION PLOTS (Cont'd)

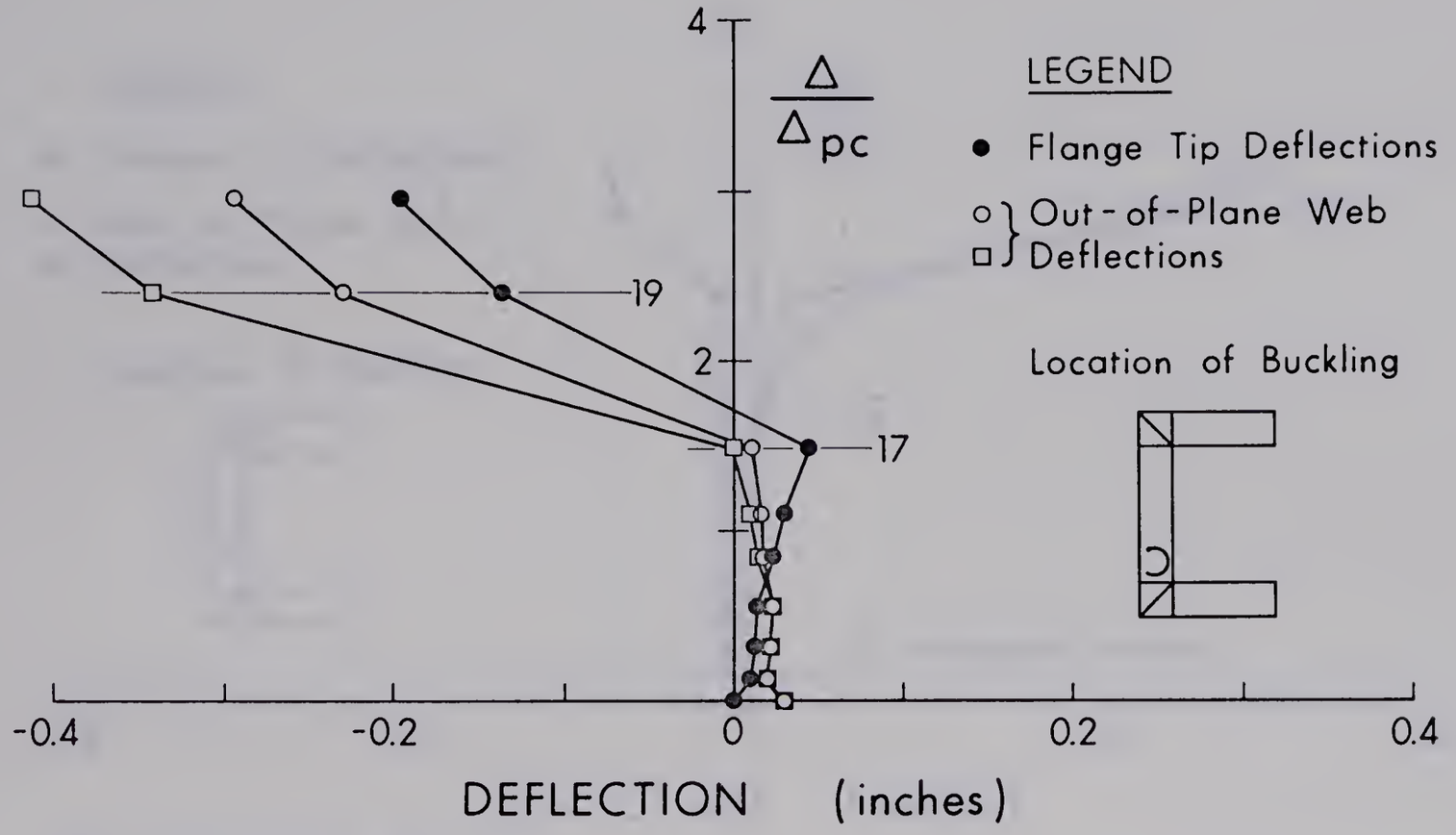

(e) Specimen BC-5

FIGURE 4.3 FLANGE AND WEB DEFLECTION PLOTS (Cont'd)

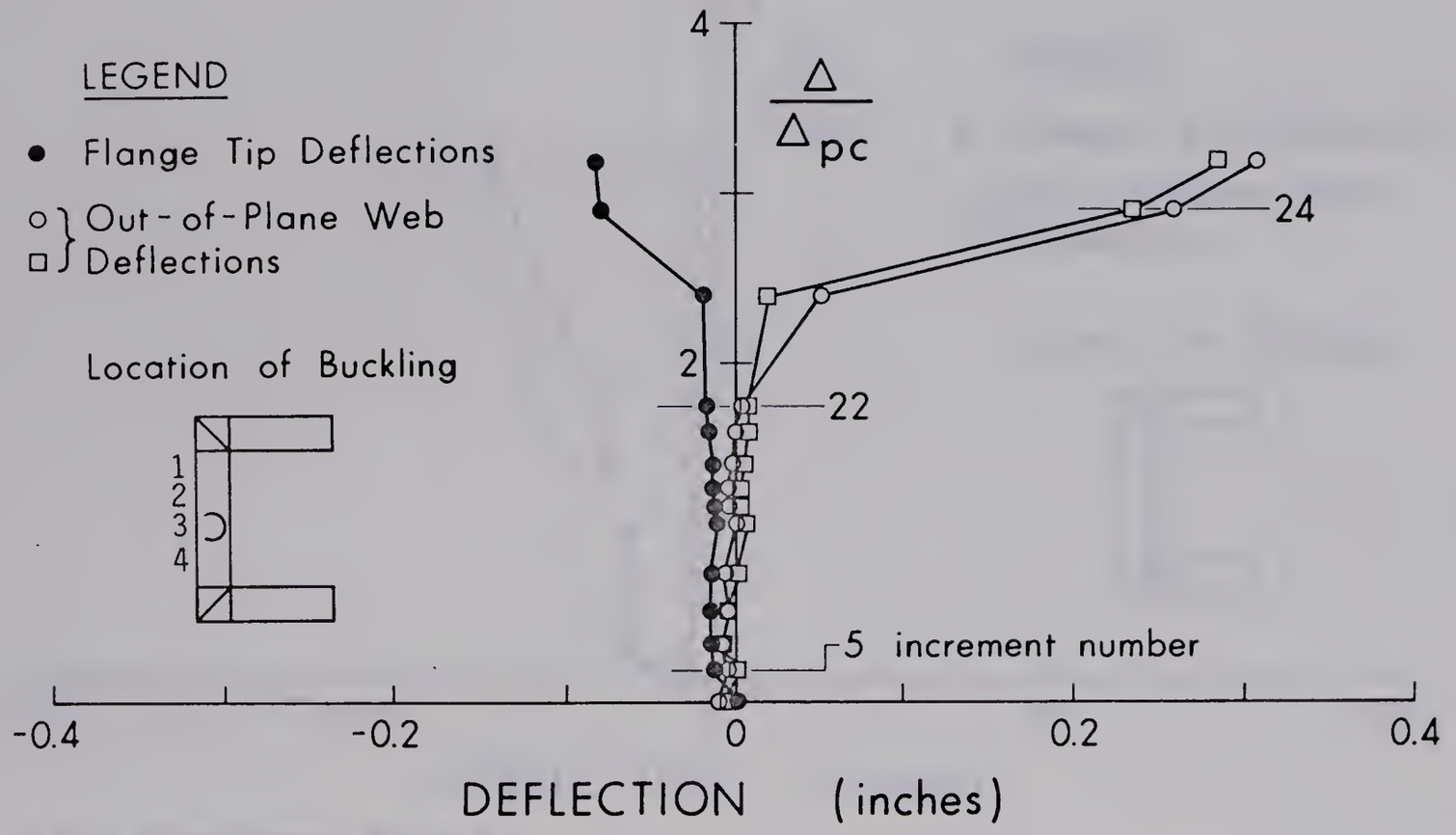

(f) Specimen BC-6

FIGURE 4.3 FLANGE AND WEB DEFLECTION PLOTS (Cont'd)

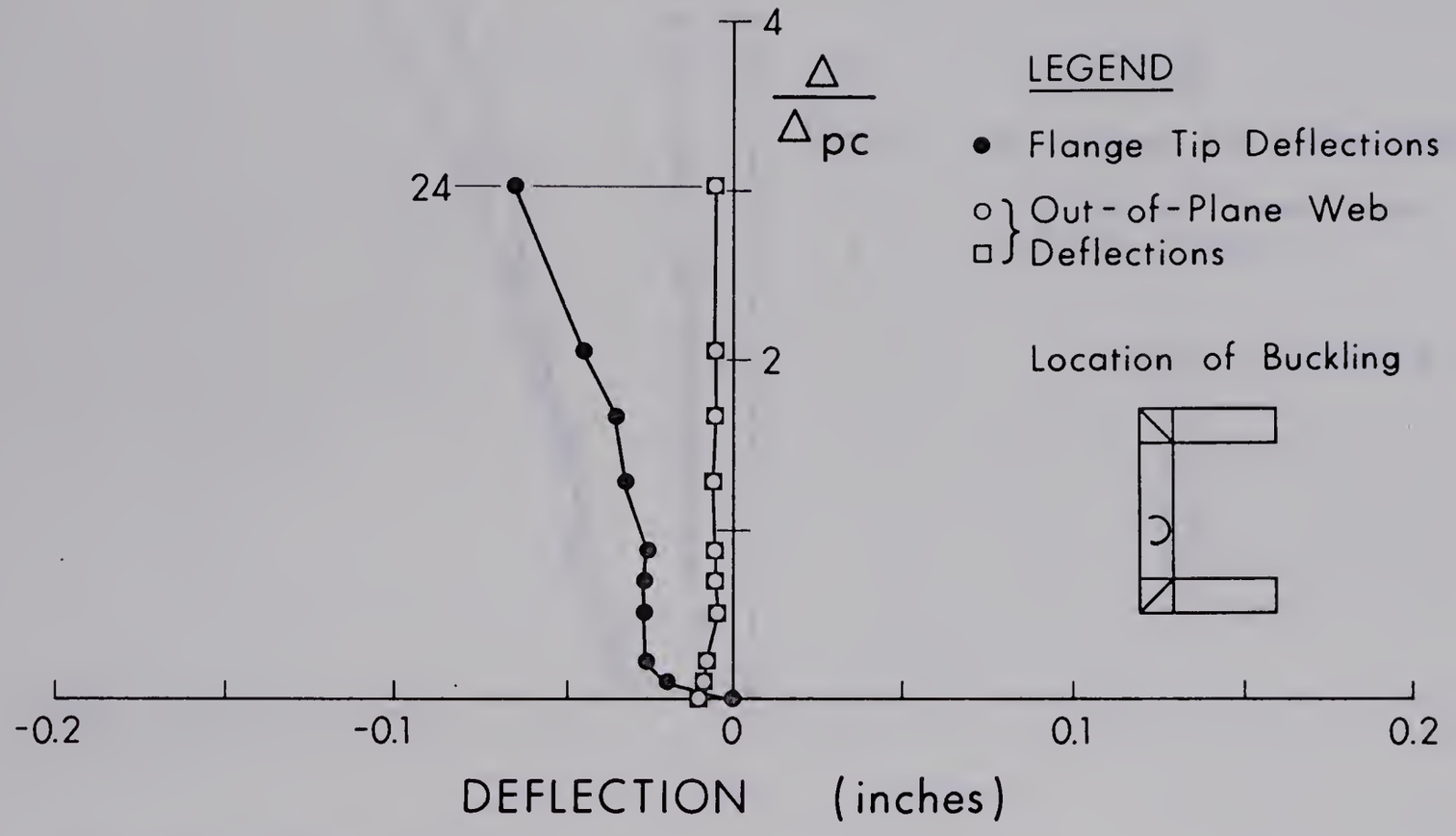

(g) Specimen BC-7

FIGURE 4.3 FLANGE AND WEB DEFLECTION PLOTS (Cont'd)

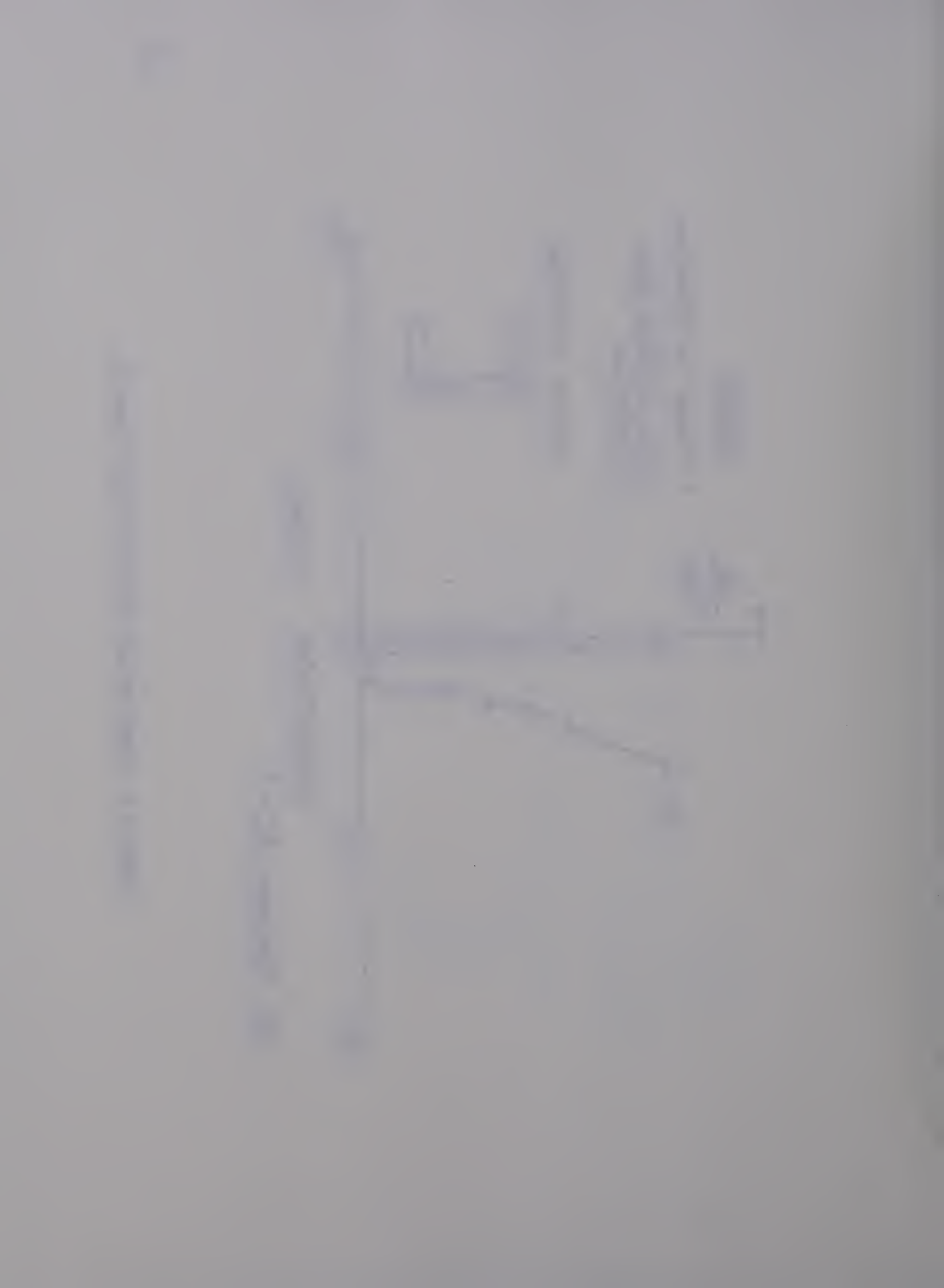

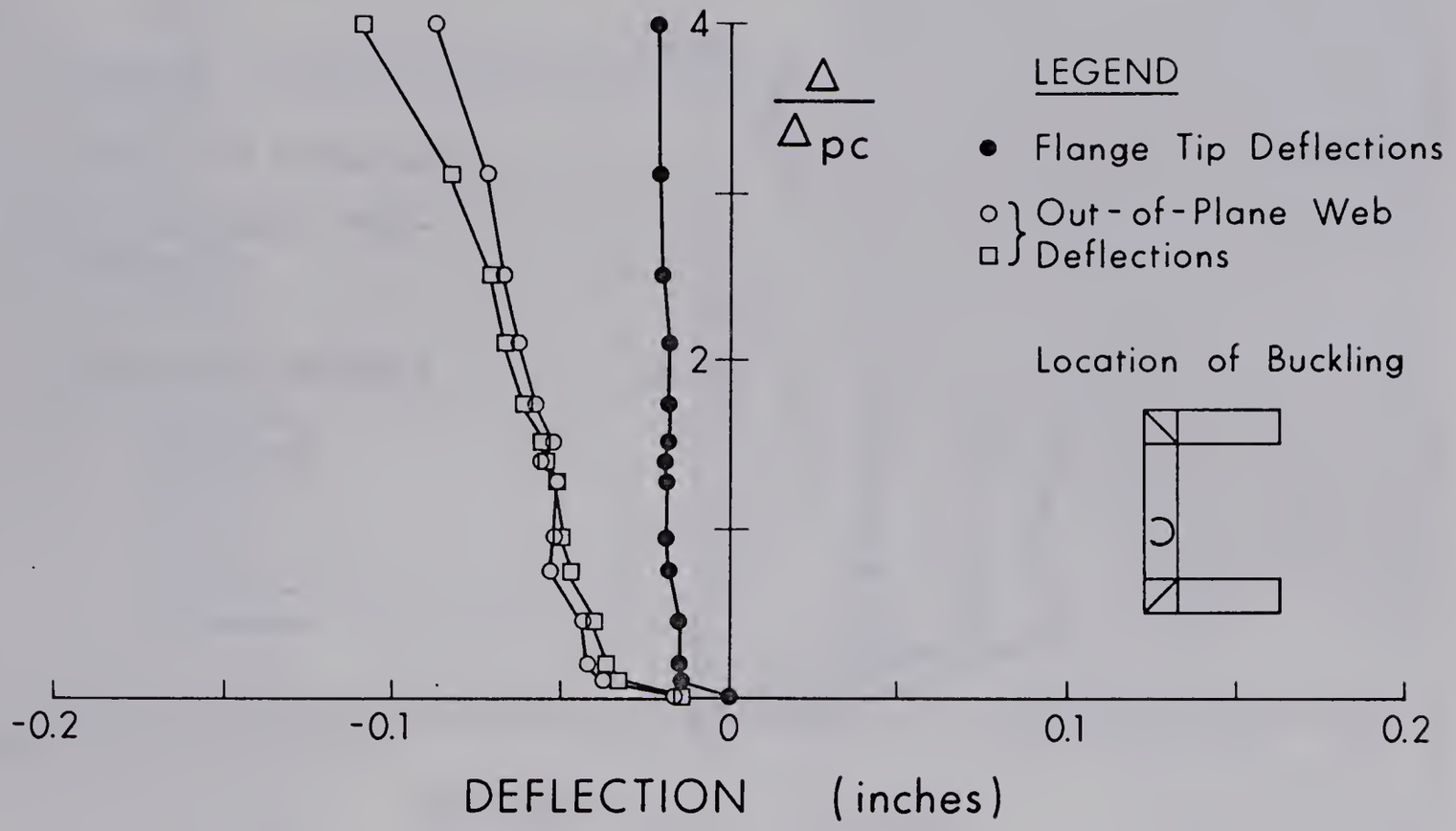

(h) Specimen BC-8

FIGURE 4.3 FLANGE AND WEB DEFLECTION PLOTS (Cont'd)

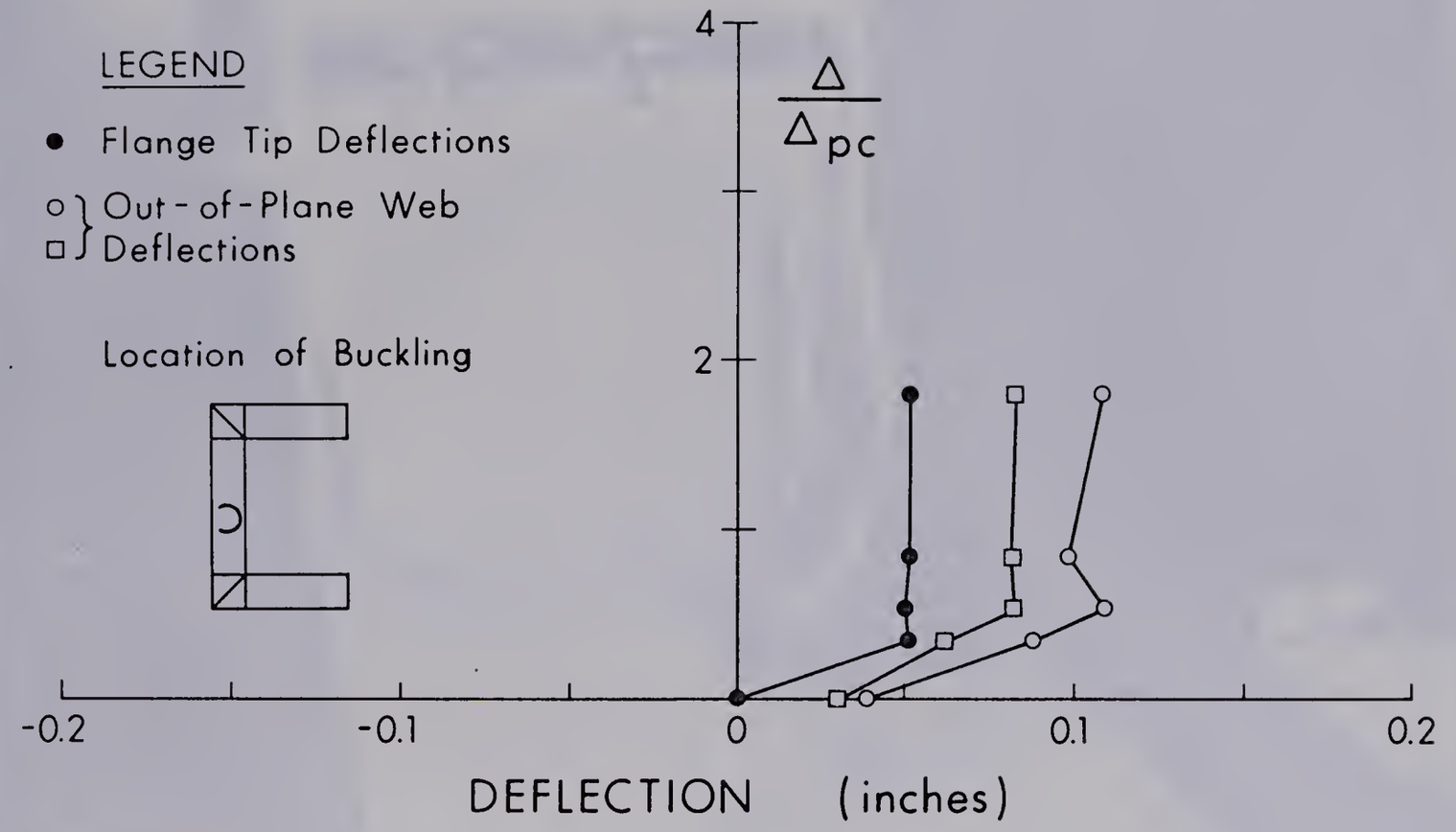

FIGURE 4.3 FLANGE AND WEB DEFLECTION PLOTS (Cont'd)

FIGURE 4.4 TYPICAL BUCKLING OF WEB AND FLANGE

CHAPTER V

ANALYSIS

5.1 Analysis of Present Specification Requirements

Haaijer conducted the first major investigation into the buckling of flange and web plates[9]. Accounting for the possibility that web and flange plates may reach strain-hardening before buckling, the theoretical analysis was based on the assumptions that:

1. An idealized stress-strain diagram can be used (see Figure 5.1),

2. Yielding occurs in slip bands, so that the material is either in the elastic range or the strain-hardening range,

3. The material is homogeneous and isotropic in the elastic range and homogeneous and orthotropic in the strain-hardening range,

4. A linear strain distribution exists before and after the buckling of a plate that is supported on all four edges (that is, no strain reversal occurs),

5. Yielding starts at the loaded edges of a column specimen and progresses inwards, or starts at the center and progresses outwards towards the loaded edges. (Haaijer uses this assumption to show that columns can buckle at stresses above the yield stress, then assumes that the same may hold true for plates[9].),

6. An incremental stress-strain relationship, as applied by Handleman and Prager[14], can be used (initial imperfections of a plate are accounted for by the introduction of effective moduli for the strain-hardening range),

7. The interaction between the web and flange plate can be accounted for by using a coefficient of restraint (β).

Once the possibility of column buckling at stresses above the yield stress was shown to be true[9], Haaijer devoted his attention to developing a plate buckling equation applicable to the strain-hardening range.

On the assumption that buckling occurs without strain reversal, the condition that the bent position is in equilibrium for a web plate element of orthotropic material subjected to uniform edge compression (Figure 5.2) can be expressed by the following differential equation:

$$D_x \frac{\partial^4 u}{\partial x^4} + \frac{2H\ \partial^4 u}{\partial x^2 \partial y^2} + D_y \frac{\partial^4 u}{\partial y^4} = - \frac{w\ \sigma_{cr}}{I} \frac{\partial^2 u}{\partial x^2} \qquad 5.1$$

where: $D_x = \frac{E_x}{1-\nu^2_{xy}}$, $D_y = \frac{E_y}{1-\nu^2_{xy}}$,

$D_{xy} = \frac{\nu_y E_x}{1-\nu^2_{xy}}$, $D_{yx} = \frac{\nu_x E_y}{1-\nu^2_{xy}}$,

$2H = D_{xy} + D_{yx} + 4G_t$,

G_t = tangent shear modulus,

u = deflection of plate at center,

w = plate thickness,

σ_{cr} = critical buckling stress at which bifurcation of equilibrium occurs,

$$I = \frac{w^3}{12}$$

The condition that the in-plane and bent positions are equilibrium positions can be expressed in terms of work. Any additional work done by the external forces (due to bending of the plate) must equal the change in the internal energy of the plate. This yields the following integral equation:

$$\frac{\sigma_{cr} w}{I} \iint \left(\frac{\partial u}{\partial x}\right)^2 dx\,dy = \iint \left[D_x \left(\frac{\partial^2 u}{\partial x^2}\right)^2 + D_y \left(\frac{\partial^2 u}{\partial y^2}\right)^2 + (D_{xy}+D_{yx})\left(\frac{\partial^2 u}{\partial x^2}\right)\left(\frac{\partial^2 u}{\partial y^2}\right) + 4\, G_t \left(\frac{\partial^2 u}{\partial x \partial y}\right)^2\right] dx\,dy \qquad 5.2$$

Equation 5.2 will give an approximate solution if some appropriate deflection surface is assumed. Although the degree of approximation depends upon the correctness of the assumed deflection surface, the result will be conservative in any case. For a rectangular plate (supported along all four edges, Figure 5.2), with the loaded edges x=0 and x=L being hinged and the edges y= ±h/2 having equal restraint against rotation, Haaijer assumed the following deflected surface:

$$u = \left[B\,\pi\left(\frac{y}{h} - \frac{1}{4}\right) + (A+B)\cos\frac{\pi y}{h}\right] \sin\frac{\pi x}{L} \qquad 5.3$$

where:

the coefficient of restraint $\beta = \frac{B}{A} = \frac{\chi h}{2 D_y I}$,

and χ = moment per unit length required for a unit of rotation.

Substitution of "u" from Equation 5.3 into Equation 5.2 and integrating will give the solution for the critical stress, σ_{cr}. In the limiting cases for a web plate subjected to uniform axial compression, when the unloaded edges $y = \pm h/2$ are hinged or fixed, the minimum values of σ_{cr} are:

for $y = \pm h/2$ hinged ($\beta=0$),

$$\sigma_{cr} = \frac{\pi^2}{12} \left(\frac{W}{h}\right)^2 \left[2\sqrt{D_x D_y} + D_{xy} + D_{yx} + 4\, G_t\right] \qquad 5.4$$

and for $y = \pm h/2$ completely fixed ($\beta=\infty$),

$$\sigma_{cr} = \frac{\pi^2}{12} \left(\frac{W}{h}\right)^2 \left[4.554\sqrt{D_x D_y} + 1.237\,(D_x+D_y) + 4.943\, G_t\right] \qquad 5.5$$

Substituting the appropriate values of the moduli (ie. D_x, D_y, D_{xy} and G_t) for the strain-hardening range, Equations 5.4 and 5.5 can be used to give the critical buckling stresses of plates subjected to strains greater than or equal to ε_{st} (Figure 5.1).

For the simplified stress-strain curve of Figure 5.1, substitution of the elastic values of the moduli in Equations 5.4 and 5.5 will give valid elastic buckling solutions for σ_{cr} less than σ_y. However, whether buckling is to occur in the elastic range or strain-hardening range, the most conservative estimate for σ_{cr} would be

found using Equation 5.4 (all edges simply supported).

Haaijer conducted tests on wide-flange shapes of ASTM-A7 steel subjected to either pure bending or to pure compression. It was concluded that the theory, summarized by Equations 5.4 and 5.5, adequately described the behavior obtained in the test results. At this time, however, the behavior of a web plate subjected to combined in-plane bending and uniform axial compression was not investigated.

Equations 5.4 and 5.5 only pertain to plate elements that are free of residual stresses, that is, they apply to annealed specimens. However, as-delivered specimens generally contain residual stresses of such magnitude that partial yielding will occur at an applied stress considerably less than the yield stress. The elastic solutions obtained from Equations 5.4 and 5.5, are only valid up to a limiting stress σ_p. The magnitude of σ_p is determined such that the applied stress (σ_p) plus the maximum residual compressive stress (σ_r) equals the yield stress (σ_y).

A more realistic approach to the range $\sigma_p<\sigma_{cr}<\sigma_y$ (Figure 5.1) was put forward in 1958 by Haaijer and Thürliman[3]. They proposed a more rational plate buckling equation which took into account the effects of residual stresses. A plate buckling curve (similar to a column buckling curve) was developed which had an empirical transition curve to describe the buckling behavior of a plate subjected to stresses between its proportional limit and yield stress (Figure 5.3).

Starting with Equation 2.2, a non-dimensionalized form for the elastic buckling stress of a perfectly plane plate of isotropic material subjected to uniform in-plane compression can be written as:

$$\frac{\sigma_{cr}}{\sigma_y} = \frac{K \pi^2 E}{12 \sigma_y (1 - \nu^2)} \left(\frac{w}{h} \right)^2 \qquad 5.6$$

Defining

$$\frac{\sigma_{cr}}{\sigma_y} = \frac{1}{\alpha^2} \qquad 5.7$$

the result is Equation 2.3. For convenience, Equation 2.3 is given again, with all terms defined:

$$\alpha = \frac{h}{\pi w} \sqrt{\frac{12 \sigma_y (1-\nu^2)}{K E}} \qquad 2.3$$

where: h = clear depth of web plate,

w = thickness of web plate,

σ_y = yield stress of material,

ν = Poisson's ratio (0.3, as suggested by Bleich[6], is used in the analysis of the beam-column tests),

E = Young's modulus,

K = plate buckling coefficient (discussed below),

α = plate buckling modulus.

Equation 5.7 is valid for values of α greater than some limiting value, α_p (see Figure 5.3). Corresponding to α_p is the non-

dimensionalized limiting stress σ_p/σ_y. From the point given by $(\sigma_p/\sigma_y, \alpha_p)$, some transition curve must be followed to the point at which the buckling stress is equal to the yield stress $(\sigma_{cr}/\sigma_y = 1.0, \alpha_o)$. A specimen reaching this latter point has, by definition, had all of its material yielded and has reached the strain-hardening range. The equation for the transition curve, put forward by Haaijer and Thürliman, is:

$$\frac{\sigma_{cr}}{\sigma_y} = 1 - \left(1 - \frac{\sigma_p}{\sigma_y}\right)\left(\frac{\alpha - \alpha_o}{\alpha_p - \alpha_o}\right)^n \qquad 5.8$$

where: σ_{cr} = critical buckling stress for uniform compression,

$\sigma_p = \sigma_y - \sigma_r$ (the proportional limit),

σ_r = maximum value of the compression residual stresses,

$$n = \frac{2(\alpha_p - \alpha_o)}{\alpha_p(\alpha_p^2 - 1)},$$

$$\alpha_p = \sqrt{\sigma_y/\sigma_p}\ .$$

Reference 3 suggests values of α_o for three types of compression elements and shows that they are nearly independent of the amount of edge restraint offered at the boundary. For example, Haaijer and Thürliman found that for hinged webs, $\alpha_o = 0.588$ and for the condition of fixed webs, $\alpha_o = 0.579$. They suggested that, for simplicity, α_o could be taken as 0.58 for web plates supported along all four edges.

Knowing the properties of the material in a specimen, it is possible using Equation 5.8 to plot σ_{cr}/σ_y versus α. Using Equation 2.3, it is possible to determine the limiting value of h/w for any value of σ_{cr}/σ_y. This was done for the tests conducted by Haaijer in Reference 9. Good correlation was found to exist for webs and flanges subjected to pure compression. As was mentioned previously, no tests were conducted to determine the behavior of web plates subjected to combined in-plane bending and uniform axial compression.

Haaijer and Thürliman realized, however, the practical importance of extending previous considerations to cases of plates subjected to combined bending and axial load. The web of a wide-flange beam-column, subjected to an axial load P and a bending moment M, presents such a case. Depending on the P/P_y ratio (P_y being the yield load of the axially loaded member), the neutral axis may lie inside or outside of the web.

For the case of combined in-plane bending and compression, Haaijer and Thürliman suggested that Equation 2.3 could be used to describe the behavior of a web plate since α (a function of the maximum critical strain in the web) was still a function of the h/w ratio and that an appropriate plate buckling coefficient (K) could be determined.

The minimum values of K for a stress distribution of a "fully plastified" wide-flange section are shown in Figure 5.4. In this figure, h is the depth of the web and y_0 corresponds to the position

of the neutral axis. For the two limiting cases, pure bending is represented by $y_o/h = 0.5$ and $y_o/h = 1.0$ is analogous to pure compression. In any case (except pure compression), to achieve such a stress distribution the ratio of the maximum compression strain (in the compression flange) to the yield strain ($\varepsilon_m/\varepsilon_y$) must be equal to infinity.

The values of K were determined by equating the work of the external forces to the dissipation of the internal energy at the moment of buckling. A work equation similar to the form of Equation 5.2 was used[3].

For an expedient solution of the rather involved problem, Haaijer and Thürliman plotted experimentally determined values of α as a function of the critical strain (ε_{cr}) for Haaijer's three pure compression tests failing by web buckling.

For a beam-column web, defining the maximum strain of the compression flange to be ε_m and assuming that the average strain over the compression zone in the web would be $\varepsilon_m/2$, it was determined graphically for web plates that:

$$\text{for } \frac{\varepsilon_m}{\varepsilon_y} = 12, \quad \alpha = 0.58$$

$$\frac{\varepsilon_m}{\varepsilon_y} = 8, \quad \alpha = 0.60$$

$$\text{and } \frac{\varepsilon_m}{\varepsilon_y} = 4, \quad \alpha = 0.69$$

Using the assumptions stated in Chapter 2 (A/A_w = 2.0, h_t/h = 1.05 and $\varepsilon_m/\varepsilon_y$ = 4.0) and Equation 2.3, web slenderness limits were proposed (Figure 2.1). These form the basis for the present CSA-S16 web slenderness limitations (Figure 1.3). However, it should be noted that no tests on web plates subjected to combined axial load and moment were conducted for verification.

5.2 Validity of the Present Web Slenderness Limits

The results of the nine beam-column tests conducted in the present study are plotted in Figure 5.5. By observation it can be seen that the present web slenderness limitations are too conservative. Eight of the nine specimens tested equalled or exceeded their predicted moment capacities before failure occurred and all of these specimens had web slenderness ratios above the current limitations.

Although good correlation was found to exist between Haaijer and Thürliman's theory for plates in pure compression and their test results, in extending this same theory to apply to web plates subjected to combined axial load and moment, many assumptions of doubtful validity were used. For example:

1. In determining the values of K for Equation 2.3 (Figure 5.4), a stress distribution corresponding to that of a fully plastified wide-flange section was assumed. For all cases of y_o/h (except pure compression), this would mean that a member would be required to deform until the condition that $\varepsilon_m/\varepsilon_y = \infty$ had been reached.

In reality, a member (assuming it to be fabricated of very stocky web and flange plates) would fracture before this condition could be reached. Figure 5.6 shows the actual stress distribution for a typical beam-column test specimen. The significance of this distribution will be discussed later.

2. Referring to Figure 5.4, it was considered in Section 5.1 that the maximum compressive strain in the compression flange would be ε_m and the average strain over the compression zone in the web (depth y_o) would be taken as $\varepsilon_m/2$. This assumption implies that the web plate model being investigated is one which is subjected to uniform compression rather than the true loading of combined in-plane bending and compression.

3. Another assumption made was that the maximum compression flange strain to yield strain ratio ($\varepsilon_m/\varepsilon_y$), would reach a value of four for members required to deform plastically.

Firstly, the value of α obtained in Section 5.1 (for $\varepsilon_m/\varepsilon_y = 4.0$) to establish the proposed web slenderness limits using Equation 2.3 (see Figure 2.1) was based on three of Haaijer's tests. Although the three tests did fail by web buckling, they were only subjected to pure compression. The deformation demands on beam-column cross-sections will not be as severe as this and in the nine test specimens referred to in the present study, none exceeded $\varepsilon_m/\varepsilon_y = 2.0$ at the time that the combination of ultimate axial load and ultimate moment was reached.

Since no satisfactory correlation was found to exist between Haaijer and Thürliman's theory (for web plates) and the beam-column test results, it was decided to find some other way of predicting web buckling. In the following section, two new methods for predicting web buckling are developed.

The first method develops a relationship between h/w and P/P_y. From test results, it can be found that a relationship exists between the relative depth of the compression zone, y/h (Figure 5.6) and P/P_y. A relationship between y/h and h/w can also be obtained. From these two relationships, h/w can be found as a function of P/P_y.

The second method uses a modified form of Equation 2.3. The value of K in Equation 2.3 (shown in Figure 5.4) is replaced by a new value K'. From the test data, K' can be found as a function of P/P_y. When K' is substituted back into Equation 2.3, $(h/w)\sqrt{F_y}$ can be found as a function of P/P_y.

The two methods are then compared and the examination shows that they give comparable, valid results.

Since it is desired to find valid web slenderness limits for beam-columns that may be subjected to loading conditions of pure bending, pure compression, or to some combination of combined axial load and moment, and since the resulting relationships for the two methods must be applicable over a wide range of loading conditions, it was decided to incorporate data from other testing programs. Results from two other investigations, along with Haaijer's tests[9] and the present beam-column tests, are summarized in Table 5.1. The two

additional sets of results are taken from tests done by Holtz[15] and by Lukey[16]. The results are explained as the development of the two methods progresses. From the four sets of test results, the relationships between P/P_y and h/w for wide-flange members subjected to pure bending, pure compression, or a combination of both can be developed with some confidence.

5.3 Method I for Predicting Web Buckling

It is necessary to establish two relationships, one between h/w and y/h, and one between P/P_y and y/h. From the two relationships, h/w can be found as a function of P/P_y.

It was first necessary to find the ratio of y/h for the specimens in all four testing programs. Because residual stresses have an effect on test results, they were taken into account.

By addition of the strain diagrams for axial load, moment, and residual stresses for a particular member, it is possible to find its y/h ratio. A typical example is shown in Figure 5.6 (where stresses are used since the elastic limit is not exceeded). This ratio is not to be confused with the y_o/h ratio for a fully plastified wide-flange section, as was defined by Haaijer and Thürliman (Figure 5.4).

In only one of the four testing programs did the author quantitatively investigate the residual stress patterns of the specimens[16]. Therefore, typical patterns had to be assumed for use as the residual stress patterns for the other test specimens. Since both rolled and welded shapes were used, typical patterns for each of these types were

assumed[17,18]. These are shown in Figure 5.7.

For the nine beam-column tests reported herein, the y/h ratios were obtained after graphically determining the combined strain diagrams for each member at the applied load and ultimate moment. The resulting stress distributions were obtained from the superposition of the strain diagrams for axial load, ultimate moment (M_u) and the assumed residual stresses. A residual stress pattern such as that shown for a welded wide-flange section in Figure 5.7 was used.

Figure 5.8 shows that at ultimate conditions, a slightly different assumed residual stress pattern does not greatly affect the resulting y/h ratio for a member. This is because residual stress patterns possess symmetry and a certain degree of consistency for residual stress magnitudes. The value of 15 ksi for the maximum value of the compression residual stresses, is typical for most of the deep rolled and welded wide-flange sections.

Lukey presented measured residual stress patterns in his report[16]. The y/h ratios for Lukey's test specimens were determined by simply summing the strain patterns due to moment at (M_u) and residual stresses. When the beam specimens had first reached M_y (the yield moment) during these tests, the y/h ratios were as high as 0.66. As the ultimate moments were attained, the y/h ratios reached values of about 0.61 and as rotations increased, the y/h ratios approached 0.5.

Holtz[15], who was investigating web buckling in unstiffened beams, used much deeper sections than did Lukey. In calculating the

y/h ratios for Holtz's tests, results closely agreed with the y/h ratios obtained for Lukey's tests. For a specimen failing by flange buckling, the y/h ratio was about 0.61 and that for failure by web buckling, 0.63.

For Haaijer's six compression tests, only axial load was involved. By definition, the value of "y" locates the position of the neutral axis. If this is the case, the ratios of y/h for Haaijer's compression test specimens must be, theoretically, infinity. It should be noted that in these compression tests, some of the measured P/P_y ratios had reached values greater than 1.0.

The resulting y/h ratios for all four testing programs are tabulated in Table 5.1 and are shown graphically in Figure 5.9.

If y/h versus P/P_y is plotted for all tests (Figure 5.10), a nearly linear relationship is indicated for all values of P/P_y less than about 0.8. The equation of the line shown in Figure 5.10 is:

$$\frac{y}{h} = 0.4463 \frac{P}{P_y} + 0.607 \qquad 5.9$$

At $P/P_y = 1.0$, y/h is theoretically equal to infinity. It is not known how the function actually behaves between $0.8 \leq P/P_y \leq 1.0$. If a member that is loaded into the strain-hardening range ($P/P_y > 1.0$), had the smallest moment applied to its ends, the y/h ratio would quickly diminish from infinity. It can only be assumed that the line shown in Figure 5.10 starts to curve upward at some location greater

than $P/P_y = 0.8$, and becomes asymptotic to $P/P_y = 1.0$ as $y/h \rightarrow \infty$.

In Figure 5.11, y/h is plotted against h/w for the specimens of all four testing programs. (Pertinent data for each specimen can be found by referring to Table 5.1). Two possible boundaries of member behavior can be chosen. One describes the web slenderness limits at which flange buckling ceases to be critical and web buckling becomes the mode of member failure. For web slenderness ratios that plot on this boundary line, $M/M_{pc} \geq 1.0$. The other boundary describes the web slenderness limits at which a member would cease to reach $M/M_{pc} = 1.0$, irrespective of the mode of failure. It should be noted that the flanges of all specimens shown in Figure 5.11 conform to the present CSA-S16 slenderness limits for plates that are subjected to compression and supported along one edge. Although some judgement is involved in locating the curves, they should adequately predict member behavior. It is felt that these two boundaries may lie slightly on the conservative side of the actual behavior.

The curve that estimates the limits at which simultaneous web and flange plate buckling would become the mode of member failure is given by the equation:

$$\frac{y}{h} = \frac{(8.20-0.100(h/w))^{2.6} + 61}{100} \qquad 5.10$$

and the equation for the curve that estimates the condition that a member would just reach $M/M_{pc} = 1.0$ is given by:

$$\frac{y}{h} = \frac{(10.25 - 0.125(h/w))^{2.6} + 61}{100} \qquad 5.11$$

Since this investigation is mainly concerned with web buckling, Equation 5.10 will be discussed in detail.

It should be noted that for all points on the curve described by Equation 5.10, $M/M_{pc} \geq 1.0$. The curve passes on the side of specimens BC-8, BC-6 and BC-3 that would be conservative. Specimen BC-3, during testing, came extremely close to having a simultaneous web and flange failure. The curve could brush this point and still remain safe with $M/M_{pc} = 1.04$. Specimen BC-6 ($M/M_{pc} = 1.18$), was an example of failure by simultaneous web and flange plate buckling. The curve could conservatively pass through this point. However, it was decided to have the curve pass between BC-7 (flange failure, $M/M_{pc} = 1.67$) and BC-8 (web failure, $M/M_{pc} = 1.34$). The curve was shifted closer to specimen BC-7 to guarantee that a web plate failure would not occur. Towards the y/h ratio of 0.6, the curve continues to meet the results of Holtz's test specimen, WS-7-P, with $M/M_{pc} = 0.993$ (essentially equal to 1.0).

Relationships now exist for P/P_y as a function of y/h and for y/h as a function of h/w. By combining these, it is possible to obtain a relationship for P/P_y as a function of h/w.

Equations 5.9 and 5.10 can be combined to give the desired relationship for P/P_y as a function of h/w. This then describes the limits at which simultaneous web and flange buckling would become

the mode of member failure and for which $M/M_{pc} \geq 1.0$. The resulting expression is:

$$\frac{P}{P_y} = \frac{(8.20 - 0.100(h/w))^{2.6} + 0.3}{44.63} \qquad 5.12$$

The curve described by Equation 5.12, shown in Figure 5.12 along with a summary of the beam-column test results reported herein, shows reasonably good correlation with the test points.

Alternatively, if it is desired that a member just reach $M/M_{pc} = 1.0$, whether web buckling occurs or not, higher allowable limits can be found by combining Equations 5.9 and 5.11. The resulting expression is:

$$\frac{P}{P_y} = \frac{(10.25 - 0.125\ (h/w))^{2.6} + 0.3}{44.63} \qquad 5.13$$

The curve described by Equation 5.13 is also shown in Figure 5.12.

5.4 Method II for Predicting Web Buckling

The second method for predicting web buckling finds $(h/w)\sqrt{F_y}$ as a function of P/P_y by using a revised form of Equation 2.3. Knowing the test results for the specimens of all four testing programs (tabulated in Table 5.1), values for α can be found using Equations 5.7 and 5.8 (see Figure 5.3).

Using Equation 2.3, new values of "K" (called K') can be calculated. These K' values are then plotted against $(h/w)\sqrt{F_y}$ to obtain an equation giving K' as a function of $(h/w)\sqrt{F_y}$. Substituting h/w (as a function of K') into Equation 5.12 (or 5.13, depending on which criterion of member behavior is desired), K' can be expressed as a function of P/P_y. Finally, substituting the expression for K' back into Equation 2.3 gives the desired relationship between $(h/w)\sqrt{F_y}$ and P/P_y.

This second method, although it adopts results obtained in Section 5.3, essentially has as its source the Haaijer and Thürliman buckling theory developed in Section 5.1. This is discussed in more detail in Section 5.5.

In determining α from Equations 5.7 and 5.8, it is first necessary to calculate σ_{cr}/σ_y for the specimens of all four testing programs. The maximum strain in the compression flange-to-web junction (at ultimate moment) is determined from the experimental results. This is then converted to stress and divided by the yield stress of the material of the particular specimen to give the ratio σ_{cr}/σ_y (tabulated in Table 5.1).

In none of the four testing programs except Haaijer's[9] did the ratio of σ_{cr}/σ_y reach values greater than unity. Although many tests showed that the yield strains in the compression flange-to-web junction were surpassed, none had attained strain-hardening. Some

of Haaijer's compression tests, however, did reach strain-hardening. This resulted in ratios of σ_{cr}/σ_y ranging between 0.979 and 1.107. Equation 5.8 does not give values of α for σ_{cr}/σ_y values greater than 1.0 (see Figure 5.3). By definition, Equation 5.8 states that once a member has reached $\sigma_{cr}/\sigma_y = 1.0$, it is in the strain-hardening range. Therefore, values of $\sigma_{cr}/\sigma_y \geq 1.0$ will be taken as being equal to 1.0.

Extensive literature exists on the buckling of plates compressed beyond the elastic limit of the material and it is generally accepted that such elements, made out of structural steel, will invariably buckle once the yielding range is reached[5,6]. Taking values of $\sigma_{cr}/\sigma_y \geq 1.0$ as being equal to 1.0, values of α for the specimens in all four testing programs can be obtained.

Since the four testing programs involved the use of six different steel grades (Lukey used 3 types of steel), six curves (similar to Figure 5.3) representing the buckling strength of plates were plotted in Figure 5.13. In establishing these curves, the residual stress patterns shown in Figure 5.7 were again assumed.

It should be noted that as the yield point of the steels decreases, the non-dimensionalized proportional limits (σ_p/σ_y) begin at points lower along the elastic curve described by Equation 5.7. The residual stresses cause the steels with lower yield points to reach their proportional limits before the steels having higher yield points. Once the proportional limit has been reached, the steel behaves in a

non-linear manner.

It should also be noted that $\alpha_o = 0.58$ was used in establishing the plate buckling curves in Figure 5.13. (α_o is the plate buckling modulus for a plate reaching $\sigma_{cr}/\sigma_y = 1.0$; see Figure 5.3). As was suggested in Reference 3, it would be reasonable to use a value of $\alpha_o = 0.58$.

Knowing the ratio of σ_{cr}/σ_y for each of the test specimens, the value of α can be obtained from the curve of the appropriate steel grade. The values of α are tabulated in Table 5.1.

Once the values of α have been determined, enough information exists so that Equation 2.3 can be solved for values of K'. These values, replacing values of Haaijer's K, are also tabulated in Table 5.1.

Figure 5.14 shows K' plotted against the appropriate values of $(h/w)\sqrt{F_y}$ for each specimen. The figure shows that a boundary can be established that defines the limits at which web and flange buckling should occur simultaneously. Since web buckling failures plot above the boundary, the curve must show the limits at which web plate buckling ceases to become the mode of specimen failure. The equation describing this curve is:

$$K' = \frac{0.48(h/w)\sqrt{F_y}}{\sqrt{F_y}} - 9.6 \qquad 5.14$$

Now, K' must be found as a function of P/P_y. This is done by referring

to the expressions obtained in Section 5.3 (Method I). Substitution of h/w from Equation 5.12 (defining the limits not to be exceeded if web buckling is not desired) into Equation 5.14, results in the following expression:

$$K' = 29.76 - 20.68\ (P/P_y)^{(0.3846)} \qquad 5.15$$

Substitution of K' from Equation 5.15 back into Equation 2.3 (replacing Haaijer's K) gives an expression relating $(h/w)\sqrt{F_y}$ as a function of P/P_y. The web slenderness limits not to be exceeded if web buckling is not desired can be found (assuming $E = 3.0 \times 10^6$ psi and $\nu = 0.3$) from:

$$\alpha = \frac{h}{100w}\sqrt{F_y}\sqrt{\frac{0.01241}{1-0.695(P/P_y)^{(0.3846)}}} \qquad 5.16$$

A similar equation can be obtained using Equations 5.13 and 5.14 to guarantee that a member will reach M/M_{pc} equal to 1.0. This results in the expression:

$$\alpha = \frac{h}{100w}\sqrt{F_y}\sqrt{\frac{0.01225}{1-0.619(P/P_y)^{(0.3846)}}} \qquad 5.17$$

Equations 5.16 and 5.17 could be rearranged and used for design purposes (solving for P/P_y) if the value of α were known. Since extensive test data is available from the four testing programs, an appropriate value of α can be chosen for use in Equations 5.16 and 5.17.

Plotting α versus $(h/w)\sqrt{F_y}$ (Figure 5.15), it can be observed that the value of $\alpha = 0.58$ corresponds to the limit at which web buckling ceases to be critical and flange buckling or combined flange and web buckling becomes the mode of failure. The reason that all flange buckling failures plot along the line described by $\alpha = 0.58$, results from the fact that flanges were proportioned so that the yield stress of the material would be reached before the occurrence of buckling. It can be noted that specimens failing by combined flange and web buckling also plot along this line. This means that both the web and flange plates were proportioned to reach the yield stress before buckling occurred. Therefore, the use of $\alpha = 0.58$ in Equation 5.16 will result in web slenderness limits that will guarantee that the web component part of a member will reach the yield stress of the material, to a distance of about h/4 below the compression flange-to-web junction, before web buckling will occur.

For web slenderness limits generated by values of α greater than 0.58, web buckling will invariably occur before flange buckling as shown in Figure 5.15.

5.5 Discussion

Although Method II (outlined in Section 5.4), uses in part results obtained for Method I (outlined in Section 5.3), it must be

noted that the development of the two methods started at different sources.

Method I finds a relationship between h/w and P/P_y by using graphical methods, whereas Method II finds a relationship between $(h/w)\sqrt{F_y}$ and P/P_y by using results from Method I and revising Equation 2.3. It can be shown that both methods yield identical web slenderness limits for various P/P_y ratios. This implies that Equation 2.3, as presented by Haaijer and Thürliman, is basically applicable to the present case. It was necessary, however, to provide a more realistic plate buckling coefficient (K') and an appropriate value for α (the plate buckling modulus), to assure that the web plate of a beam-column would reach the yield stress of the material before buckling occurred.

Table 5.1 Summary of Test Results

Present Beam-Column Tests

Specimen Number	$\frac{P}{P_y}$	$\frac{M_u}{M_{pc}}$	$\frac{y}{h}$	$\frac{\sigma_{cr}}{\sigma_y}$	α	K'	$\frac{h}{w}$	$\frac{h}{w}\sqrt{F_y}$	Failure
BC-1	0.2	1.18	0.70	1.0	0.58	12.20	46.5	332	Flange
BC-2	0.2	1.18	0.69	1.0	0.58	14.98	51.5	368	Flange
BC-3	0.2	1.04	0.71	0.576	1.32	4.07	61.1	437	Web
BC-4	0.4	1.21	0.77	1.0	0.58	8.90	39.8	285	Flange
BC-5	0.4	1.19	0.77	1.0	0.58	11.60	45.3	324	Flange
BC-6	0.4	1.18	0.77	1.0	0.58	16.53	54.1	387	W and F
BC-7	0.8	1.67	0.96	1.0	0.58	9.04	40.0	286	Flange
BC-8	0.8	1.34	0.97	0.961	0.87	5.15	45.3	324	Web
BC-9	0.8	0.90	0.98	0.845	1.04	5.08	53.8	385	Web

Table 5.1 Continued Summary of Test Results

Results of Tests Conducted by Lukey

Specimen Number	$\frac{P}{P_y}$	$\frac{M_u}{M_p}$	$\frac{y}{h}$	$\frac{\sigma_{cr}}{\sigma_y}$	α	K'	$\frac{h}{w}$	$\frac{h}{w}\sqrt{F_y}$	Failure
A-1	0	1.37	0.610	1.0	0.58	4.59	29.3	203	Flange
A-2	0	1.41	0.610	1.0	0.58	4.59	29.3	203	Flange
B-1	0	1.12	0.609	1.0	0.58	11.90	42.7	332	Flange
B-2	0	1.16	0.609	1.0	0.58	11.90	42.7	332	Flange
B-3	0	1.13	0.609	1.0	0.58	11.90	42.7	332	Flange
B-4	0	1.06	0.609	1.0	0.58	11.90	42.7	332	Flange
B-5	0	1.04	0.609	1.0	0.58	11.90	42.7	332	Flange
C-1	0	1.12	0.608	1.0	0.58	17.80	52.2	400	Flange
C-2	0	1.20	0.608	1.0	0.58	17.80	52.2	400	Flange
C-3	0	1.16	0.608	1.0	0.58	17.80	52.2	400	Flange
C-4	0	1.11	0.608	1.0	0.58	17.80	52.2	400	Flange
C-5	0	1.13	0.608	1.0	0.58	17.80	52.2	400	Flange

Table 5.1 Continued Summary of Test Results

Results of Tests Conducted By Holtz

Specimen Number	$\frac{P}{P_y}$	$\frac{M_u}{M_p}$	$\frac{y}{h}$	$\frac{\sigma_{cr}}{\sigma_y}$	α	K'	$\frac{h}{w}$	$\frac{h}{w}\sqrt{F_y}$	Failure
WS-1	0	1.023	0.61	1.0	0.58	26.09	76.5	494	Flange
WS-2	0	0.977	0.61	1.0	0.58	40.83	95.7	618	Flange
WS-3	0	0.893	0.63	0.91	0.91	24.29	115.3	745	Web
WS-4	0	0.863	0.63	0.89	0.94	32.23	137.8	890	Web
WS-6	0	0.879	0.63	1.0	0.58	37.16	91.3	590	Web
WS-7-P	0	0.993	0.61	1.0	0.58	29.76	81.7	528	Flange
WS-8-P	0	0.954	0.63	1.0	0.58	36.43	90.4	584	Web
WS-9	0	1.077	0.61	1.0	0.58	24.88	74.7	482	Flange
WS-10	0	1.147	0.61	1.0	0.58	29.60	81.5	526	Flange
WS-11	0	1.066	0.61	1.0	0.58	35.30	89.0	575	Flange

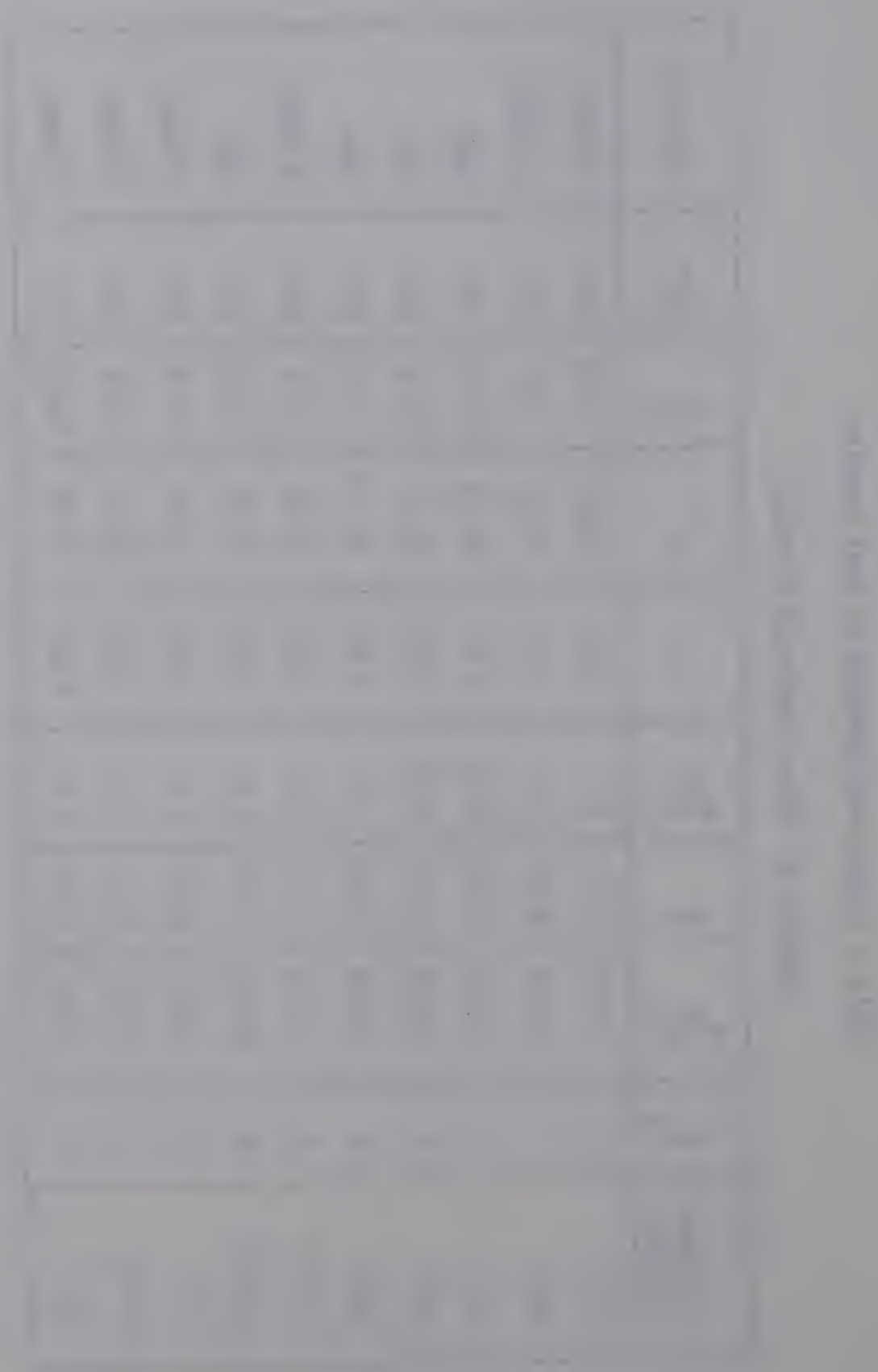

Table 5.1 Continued Summary of Test Results

Results of Tests Conducted by Haaijer

Specimen Number	$\frac{P}{P_y}$	$\frac{M_u}{M_p}$	$\frac{y}{h}$	$\frac{\sigma_{cr}}{\sigma_y}$	α	K'	$\frac{h}{w}$	$\frac{h}{w}\sqrt{F_y}$	Failure
D-1	0.994	-	∞	0.994	0.59	3.45	30.4	178	Flange
D-2	1.00	-	∞	1.00	0.58	3.64	30.7	179	W and F
D-3	1.107	-	∞	1.107	0.58	2.82	27.0	160	Flange
D-4	1.011	-	∞	1.011	0.58	3.76	31.2	185	Web
D-5	1.038	-	∞	1.038	0.58	2.09	23.3	141	Flange
D-6	0.979	-	∞	0.979	0.68	4.46	39.8	246	Web

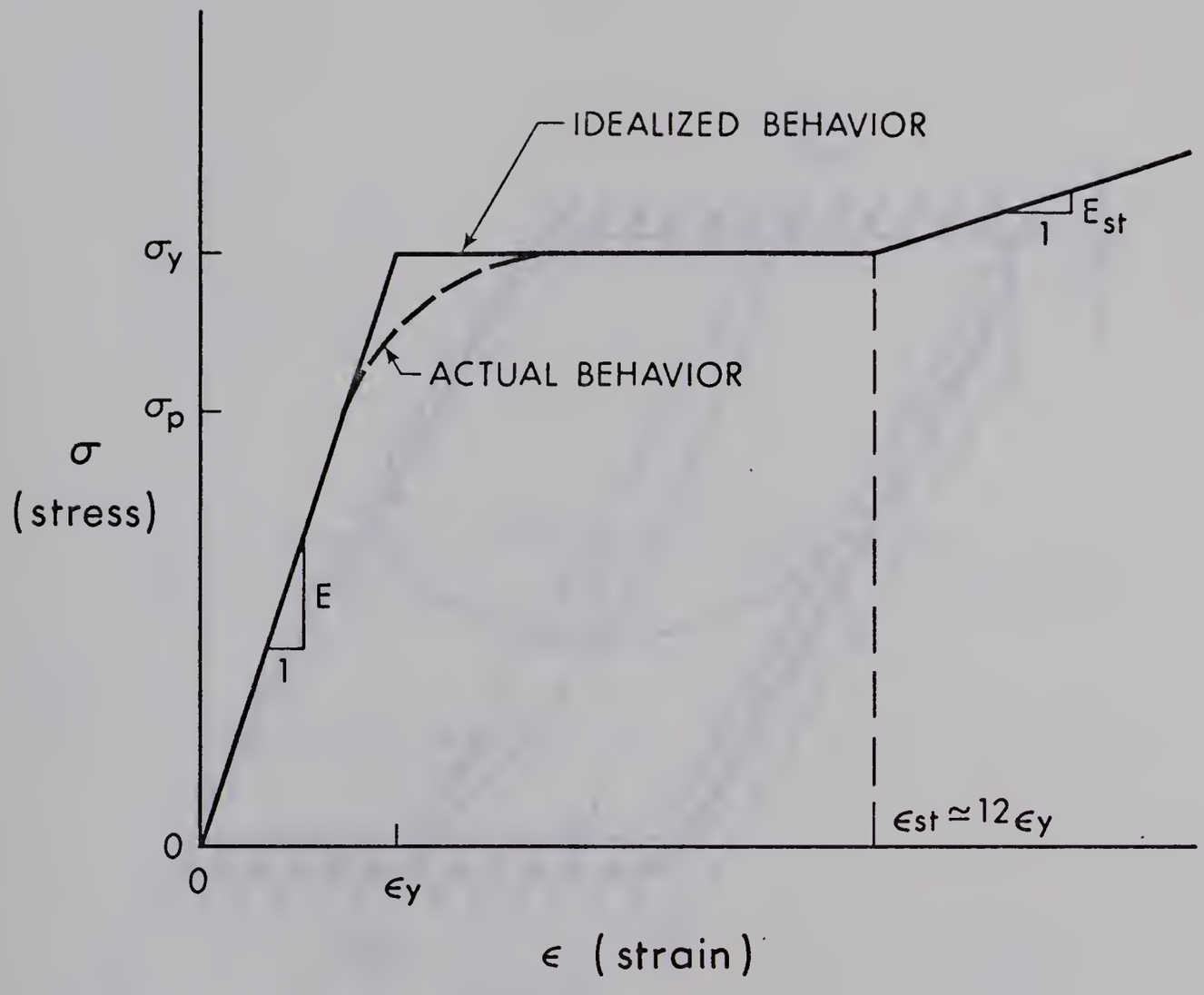

FIGURE 5.1 IDEALIZED STRESS-STRAIN DIAGRAM

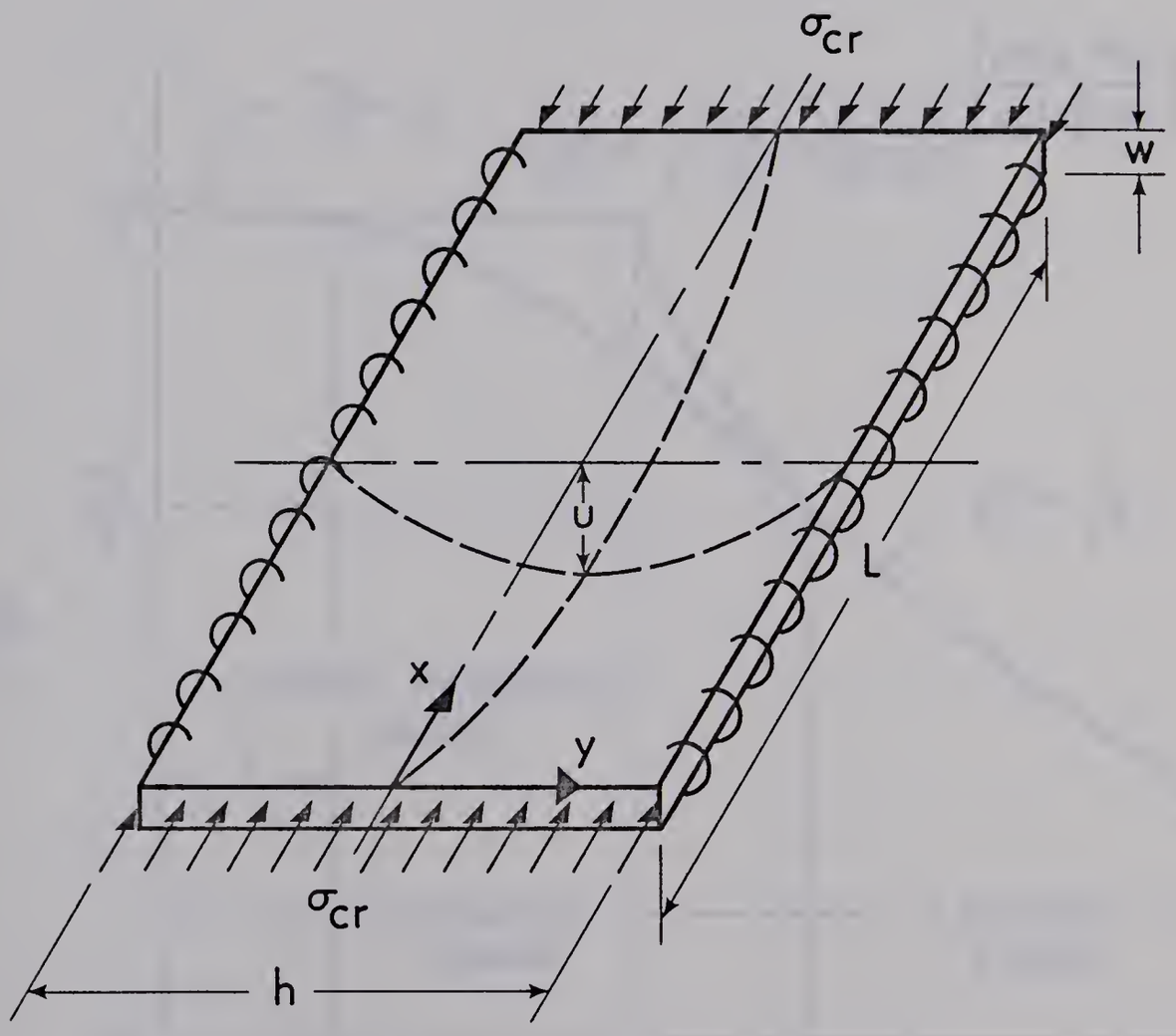

FIGURE 5.2 PLATE BUCKLING MODEL

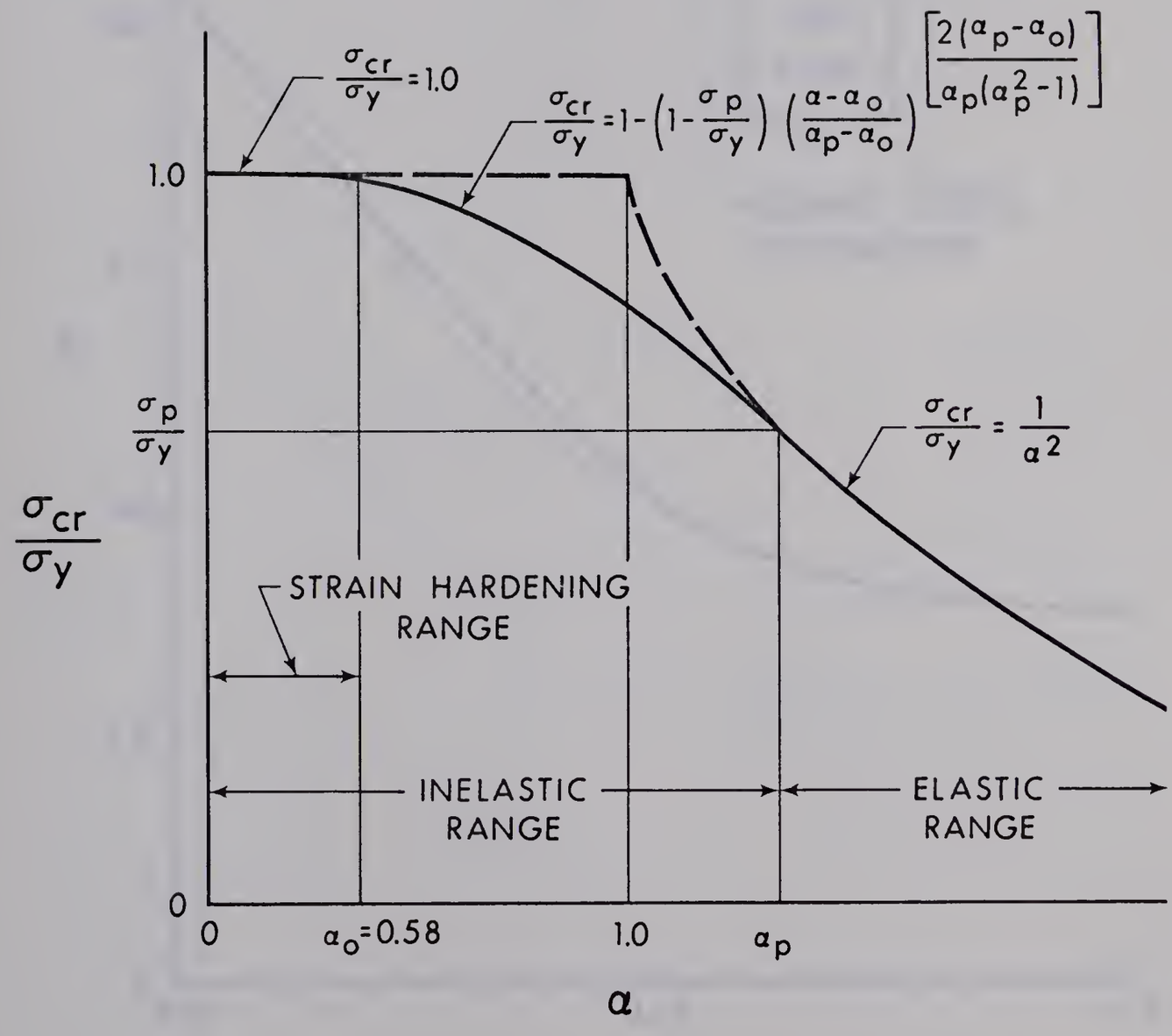

FIGURE 5.3 DIMENSIONLESS REPRESENTATION OF THE BUCKLING STRENGTH OF PLATES (INCLUDING THE EFFECT OF RESIDUAL STRESSES)

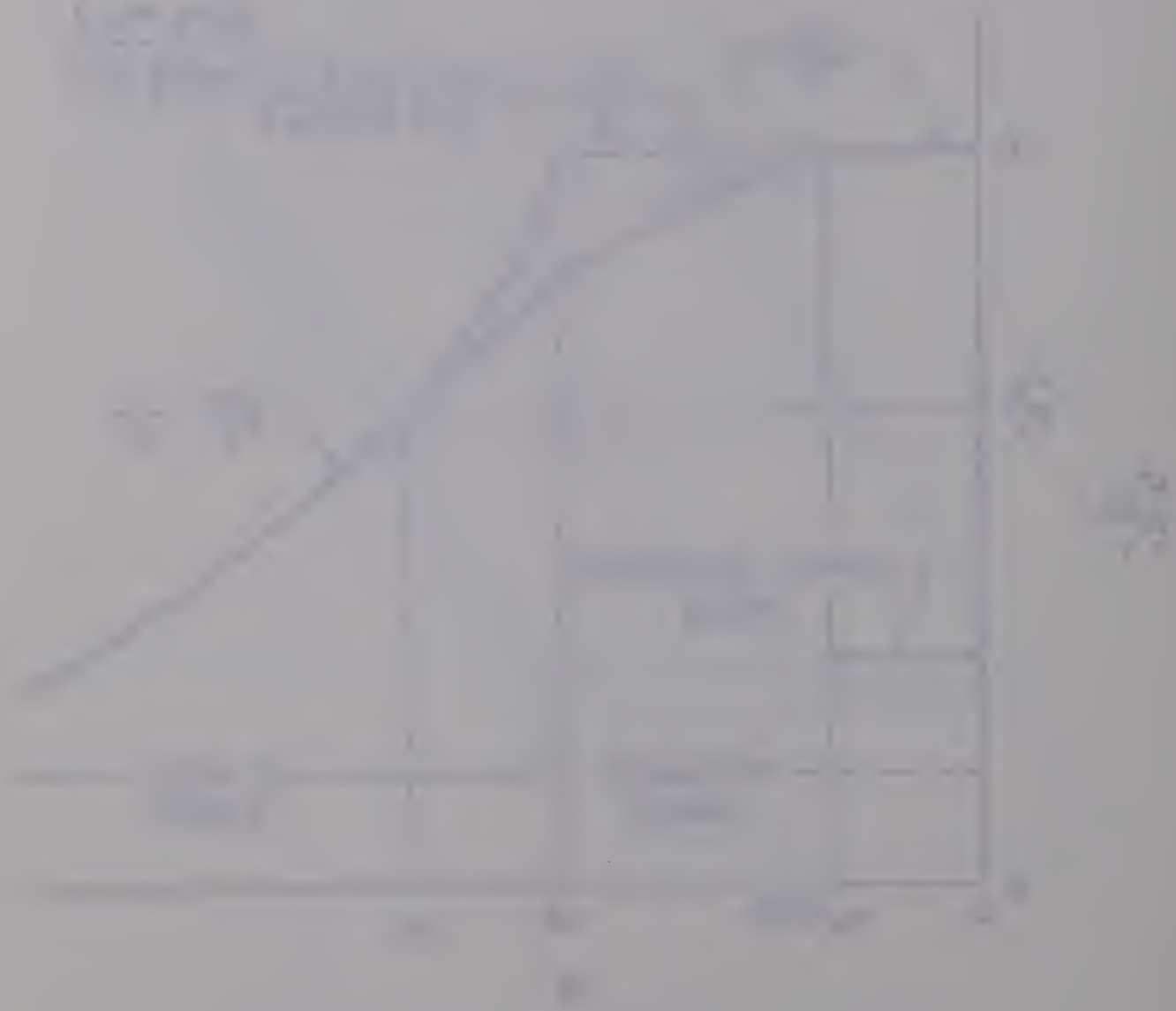

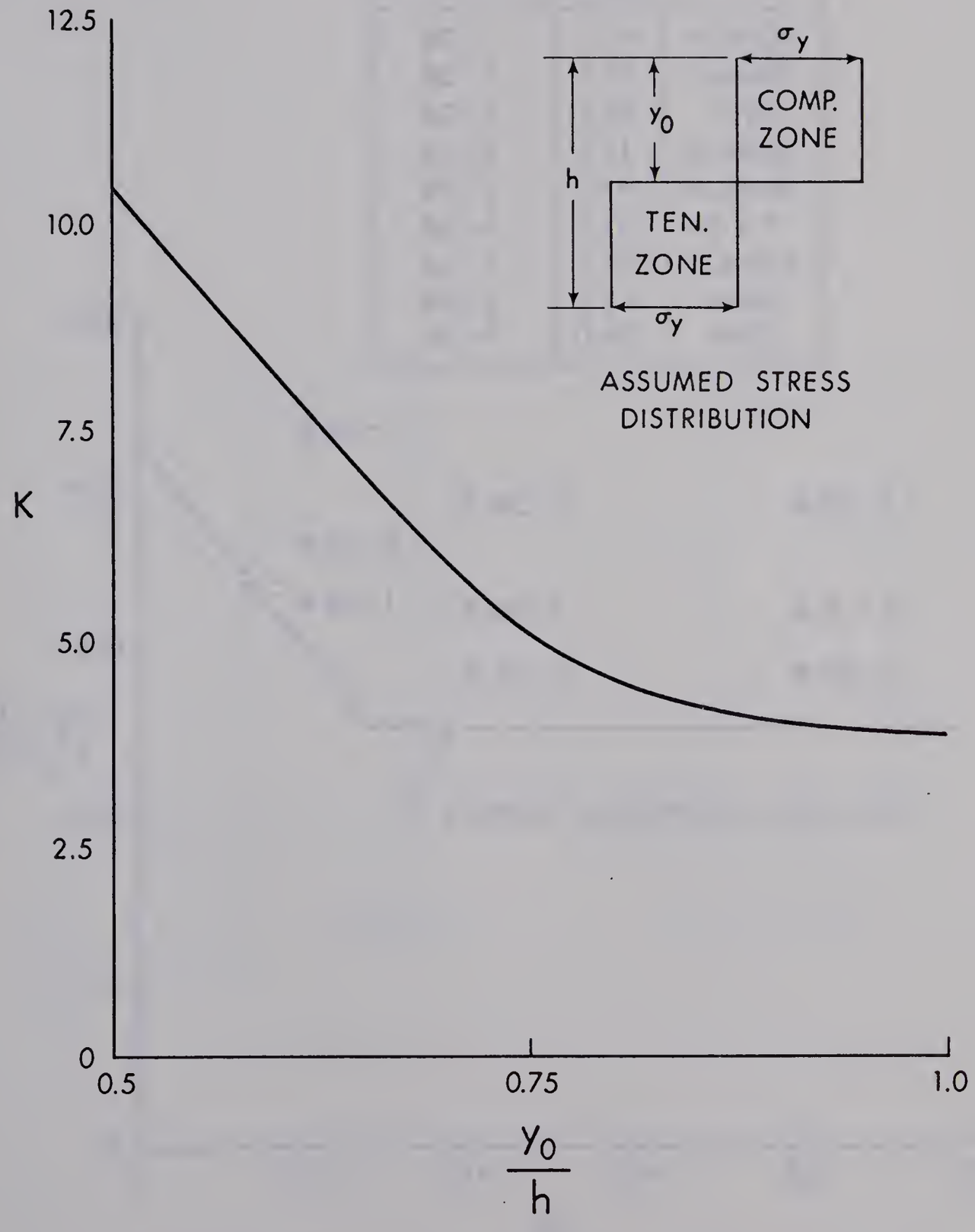

FIGURE 5.4 PLATE COEFFICIENT OF WEBS OF FULLY PLASTIFIED WIDE-FLANGE SECTIONS SUBJECTED TO AXIAL LOAD AND MOMENT

SPECIMEN	$\frac{Mu}{Mpc}$	FAILURE
BC-1	1.18	FLANGE
BC-2	1.18	FLANGE
BC-3	1.04	WEB
BC-4	1.21	FLANGE
BC-5	1.19	FLANGE
BC-6	1.18	W & F
BC-7	1.67	FLANGE
BC-8	1.34	WEB
BC-9	0.90	WEB

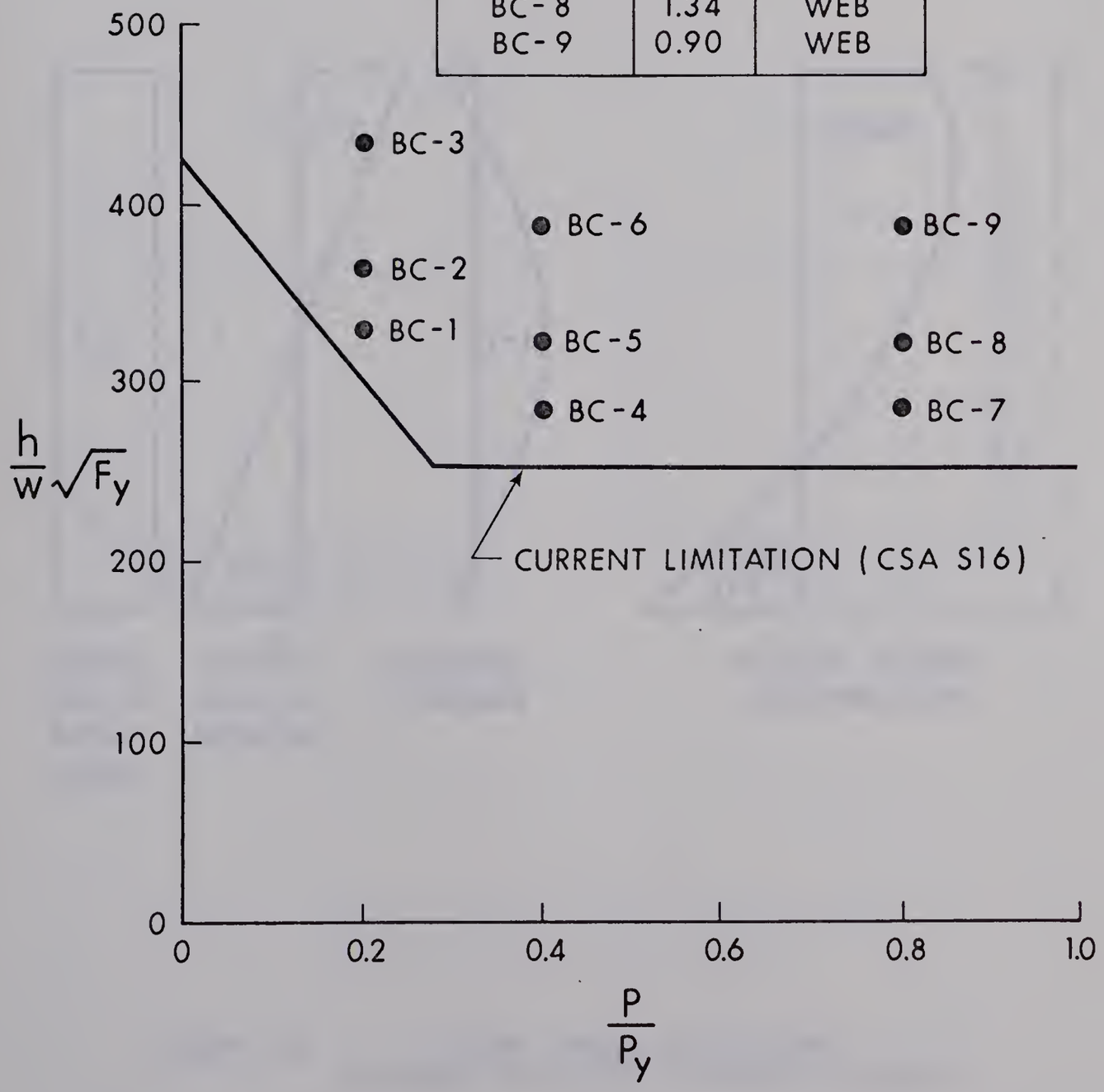

FIGURE 5.5 THE CURRENT WEB SLENDERNESS LIMITS AND THE PRESENT BEAM-COLUMN TESTS

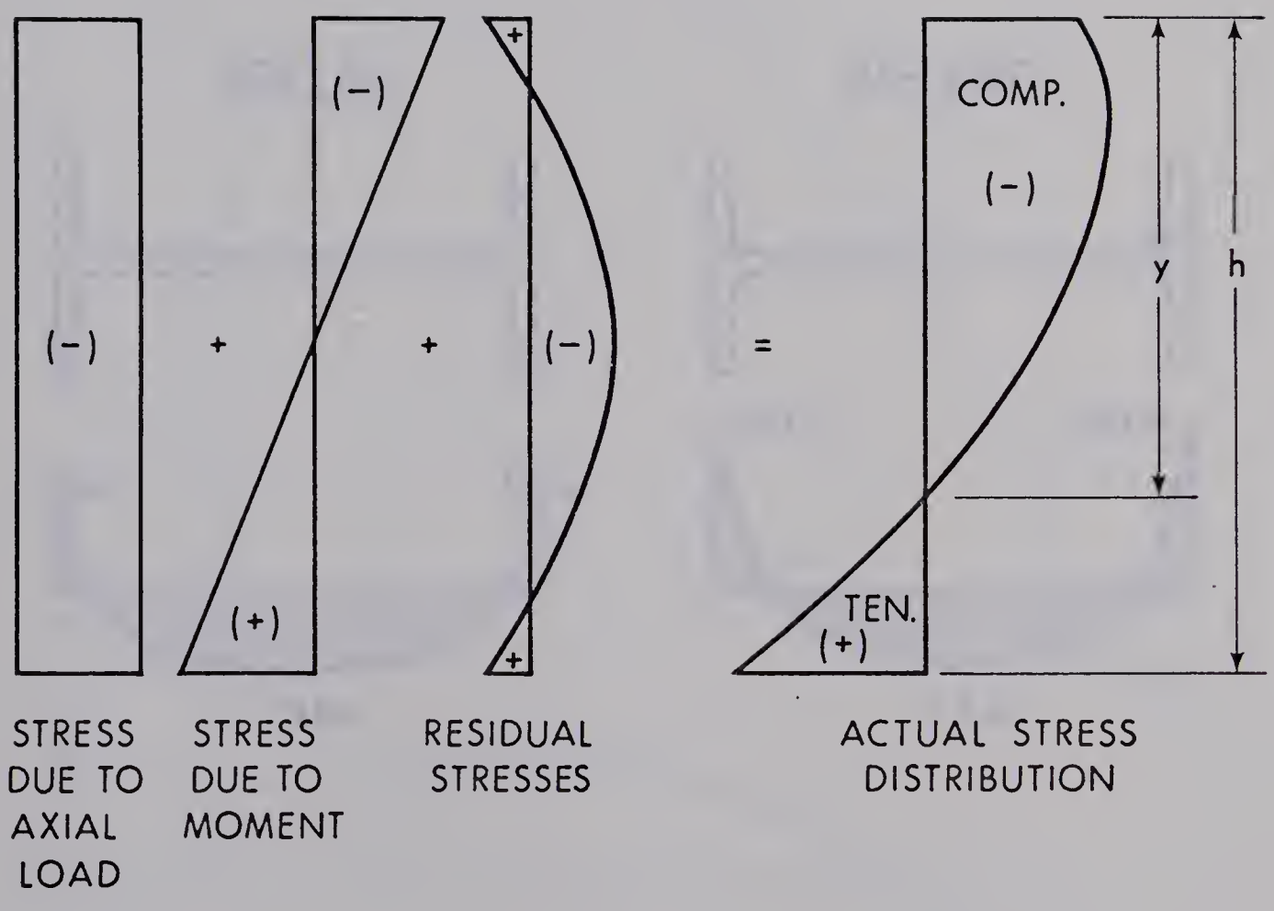

FIGURE 5.6 ACTUAL STRESS DISTRIBUTION INCLUDING THE EFFECT OF RESIDUAL STRESSES

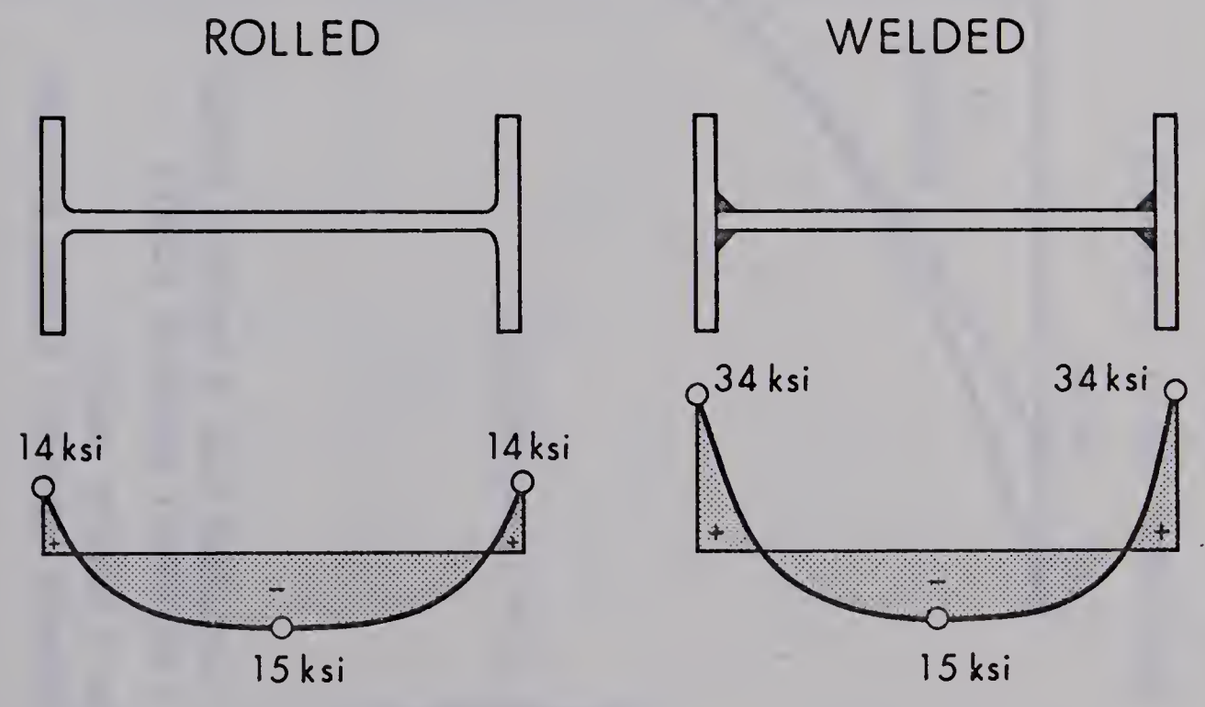

FIGURE 5.7 TYPICAL RESIDUAL STRESS PATTERNS FOR ROLLED AND WELDED STEEL SECTIONS

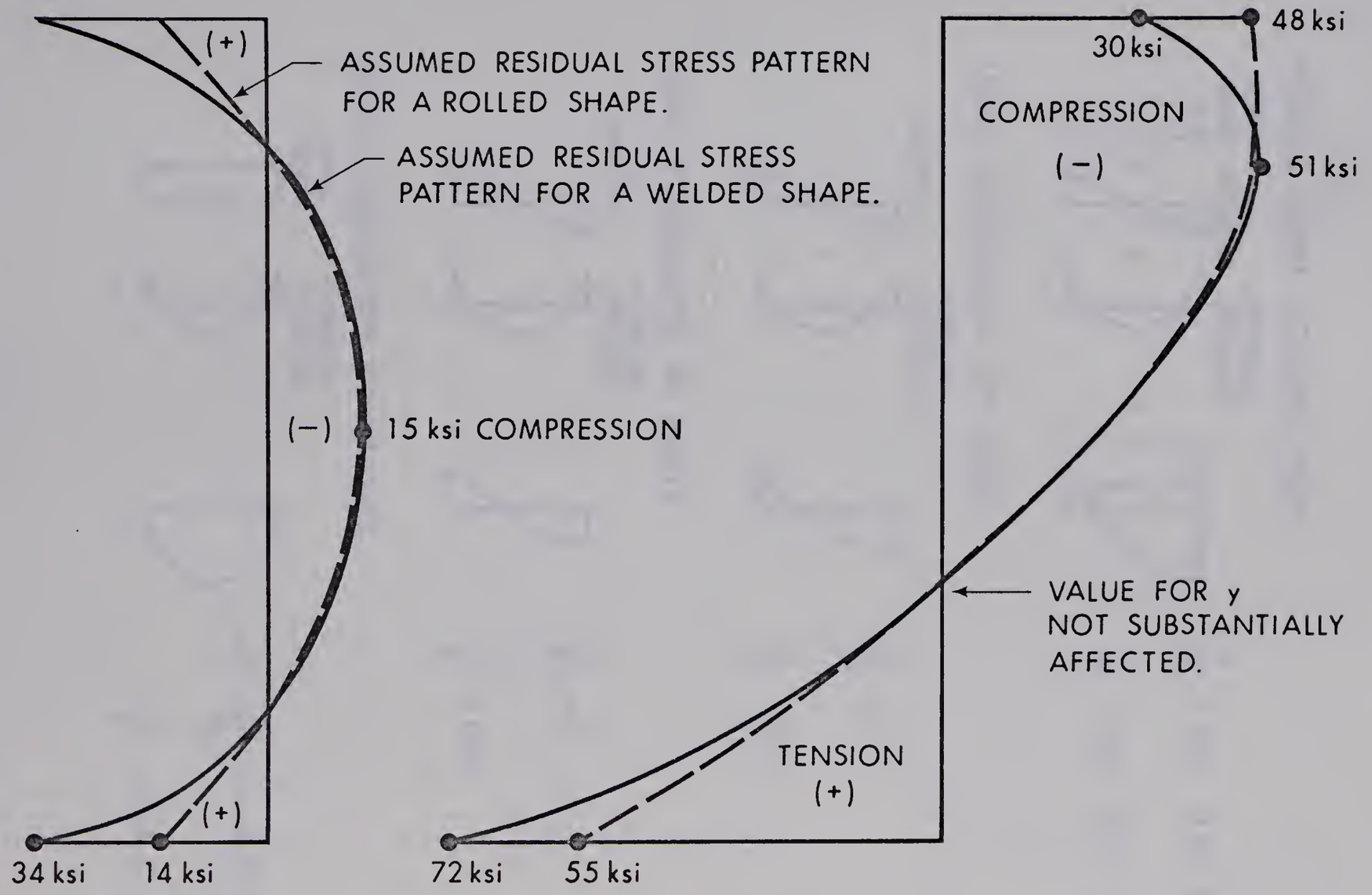

FIGURE 5.8 SYMMETRY AND CONSISTENCY IN RESIDUAL STRESS PATTERNS

PRESENT BEAM - COLUMN TESTS

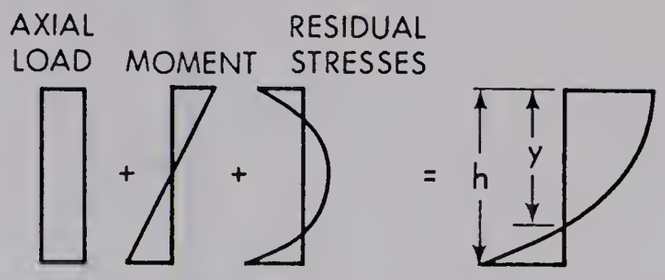

$\frac{P}{P_y}$ = 0.2, 0.4, 0.8,

$\frac{y}{h}$ = 0.70, 0.77, 0.96

TESTS CONDUCTED BY LUKEY

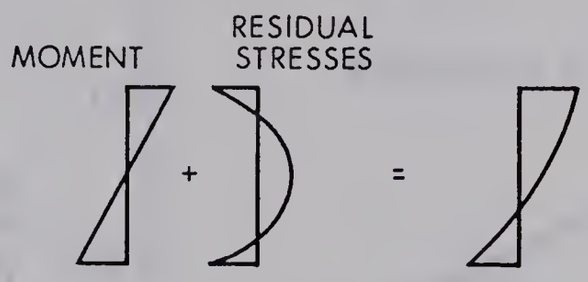

$\frac{P}{P_y}$ = 0

$\frac{y}{h}$ = 0.61

TESTS CONDUCTED BY HOLTZ

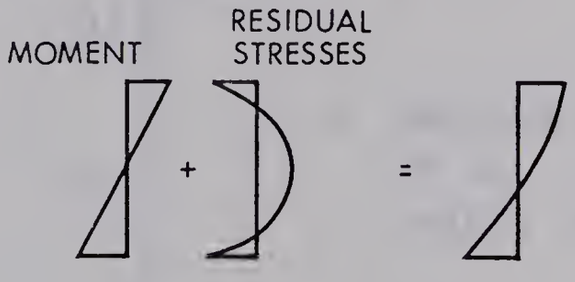

$\frac{P}{P_y}$ = 0

$\frac{y}{h}$ = 0.62

TESTS CONDUCTED BY HAAIJER

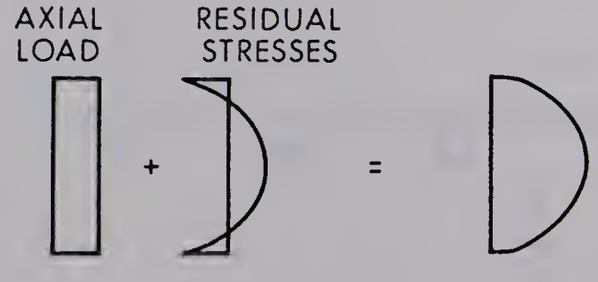

AS $\frac{P}{P_y} \longrightarrow 1.0$

$\frac{y}{h} \longrightarrow \infty$

FIGURE 5.9 SUMMARY OF y/h RATIOS

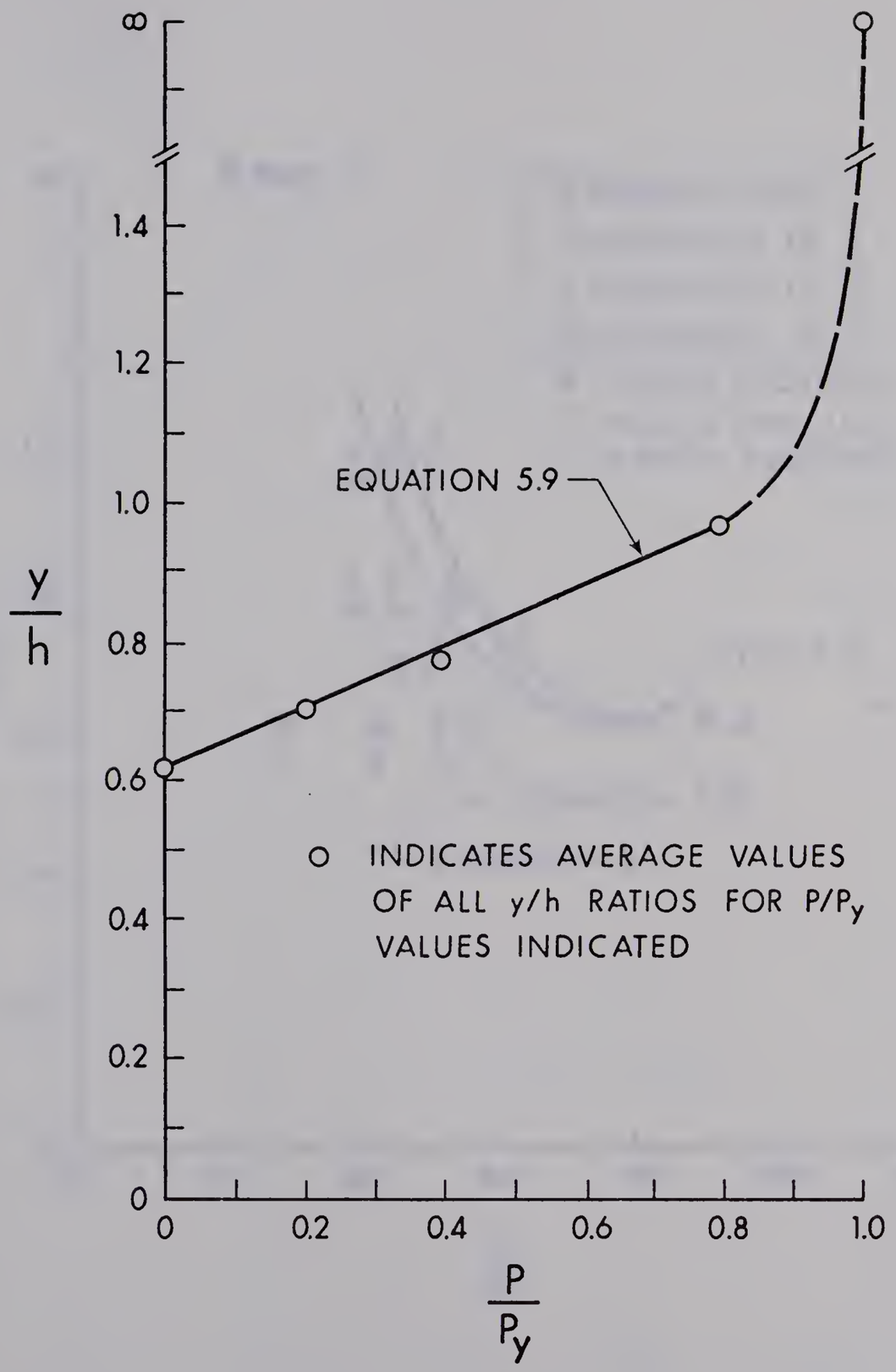

FIGURE 5.10 y/h VERSUS P/P_y

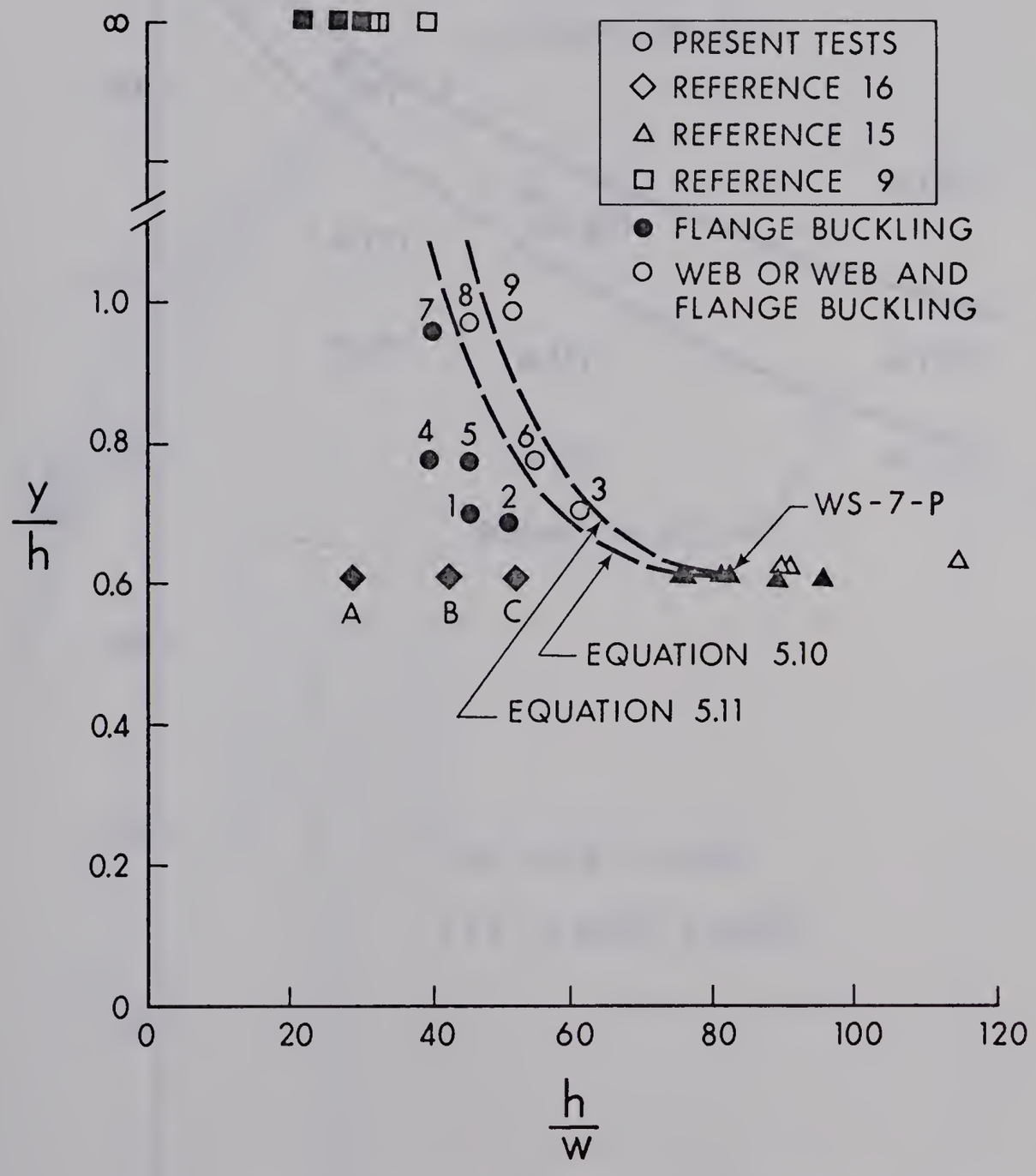

FIGURE 5.11 y/h VERSUS h/w

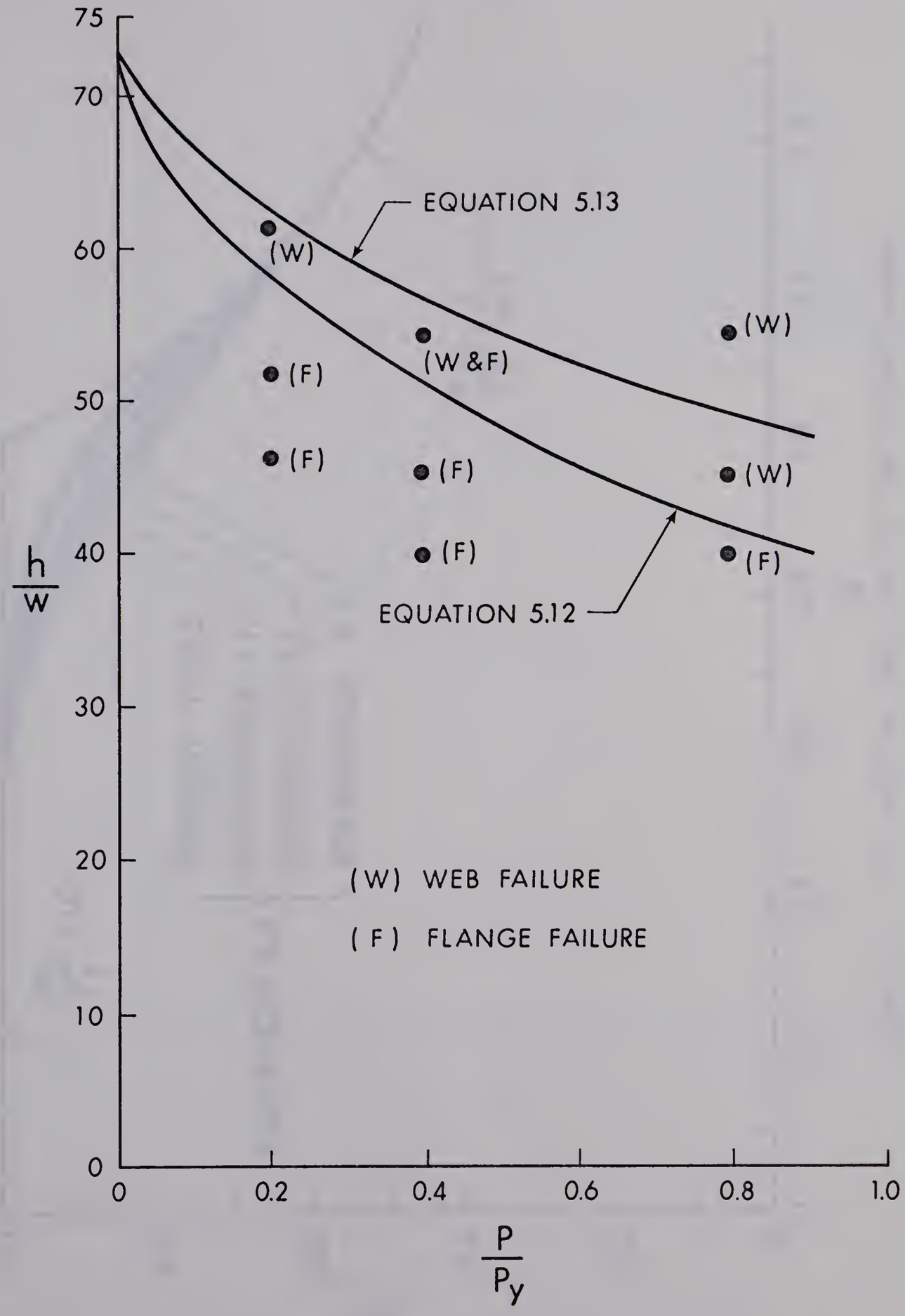

FIGURE 5.12 P/P_y AS A FUNCTION OF h/w

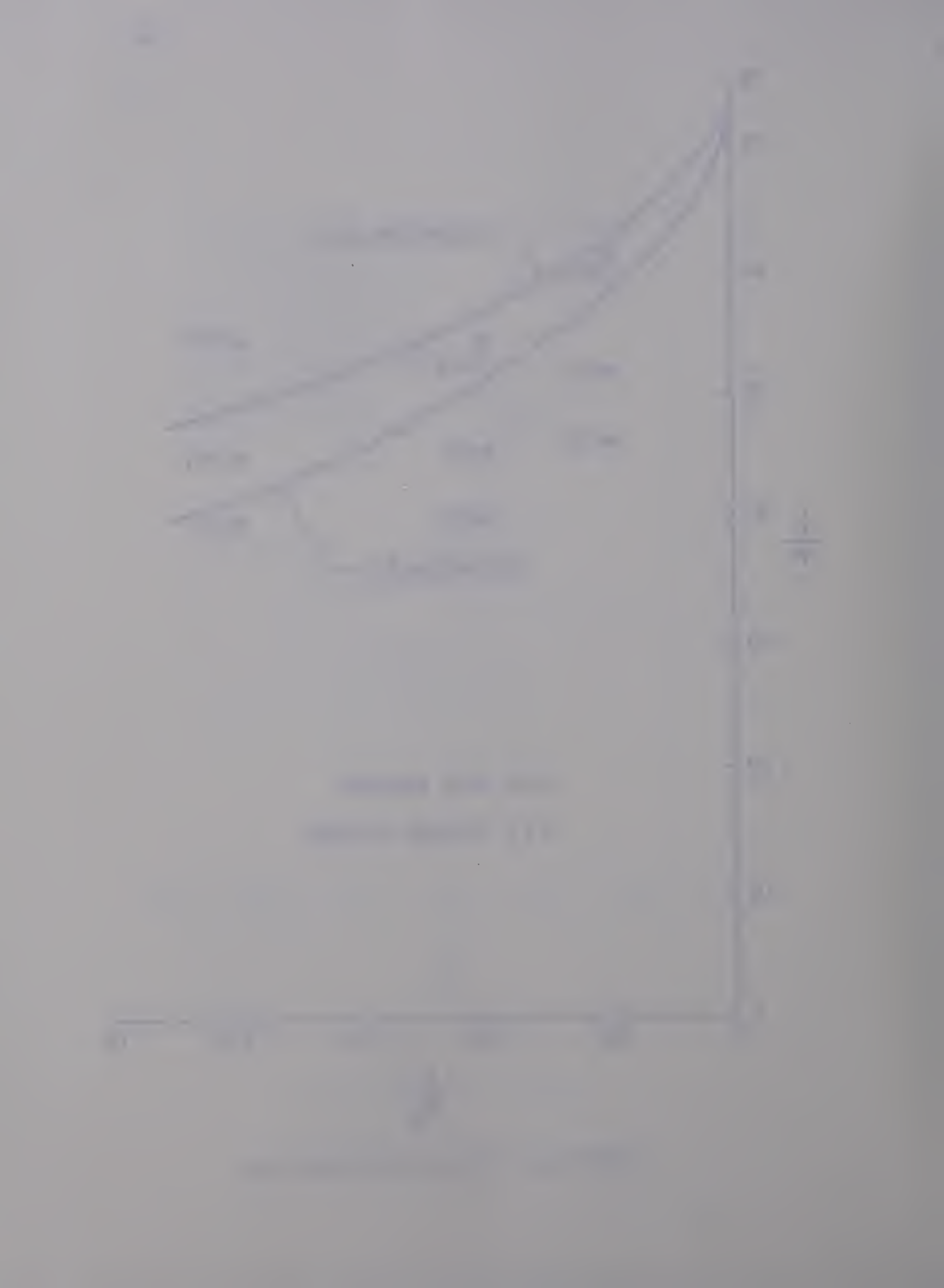

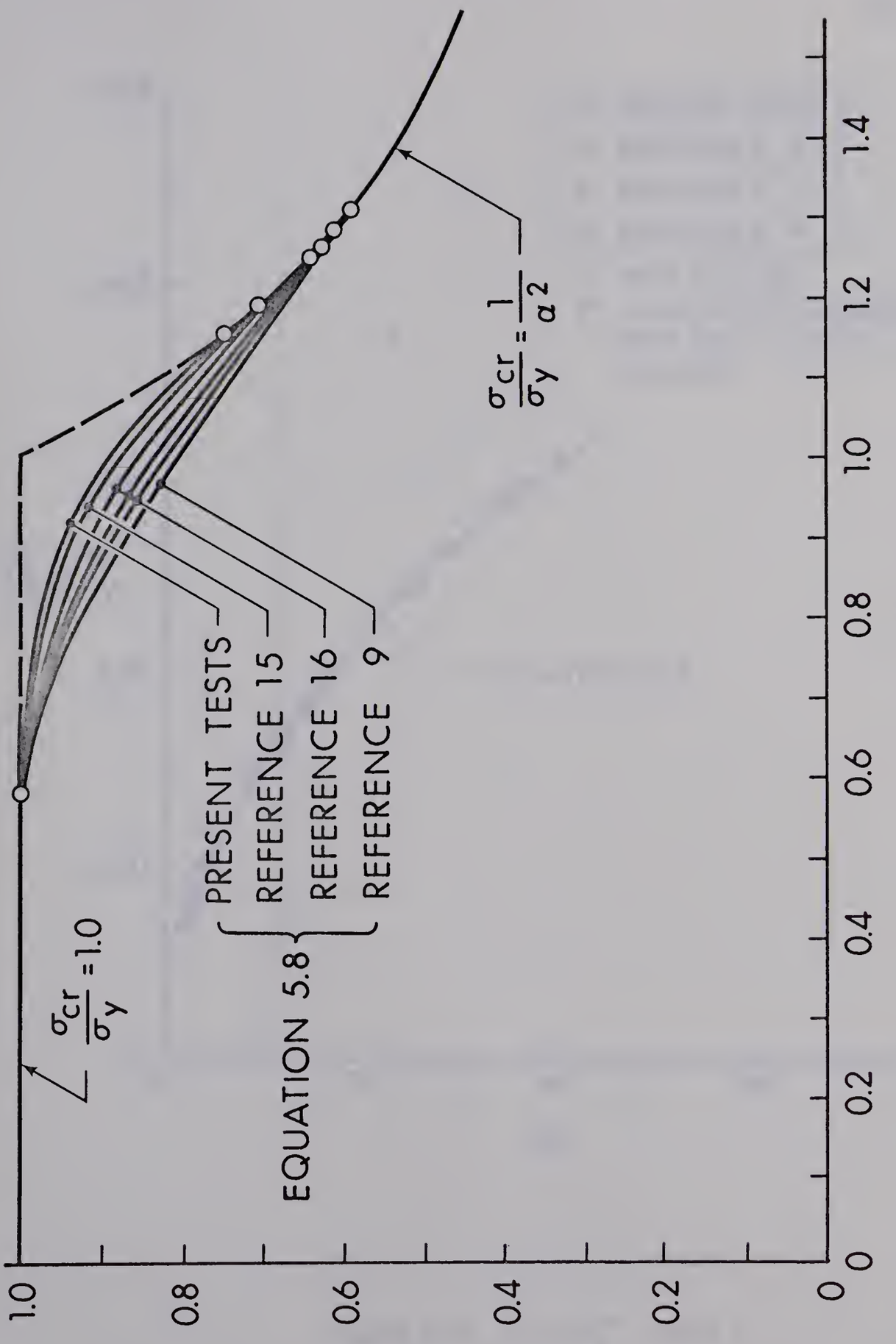

FIGURE 5.13 PLATE BUCKLING CURVES FOR THE FOUR TESTING PROGRAMS

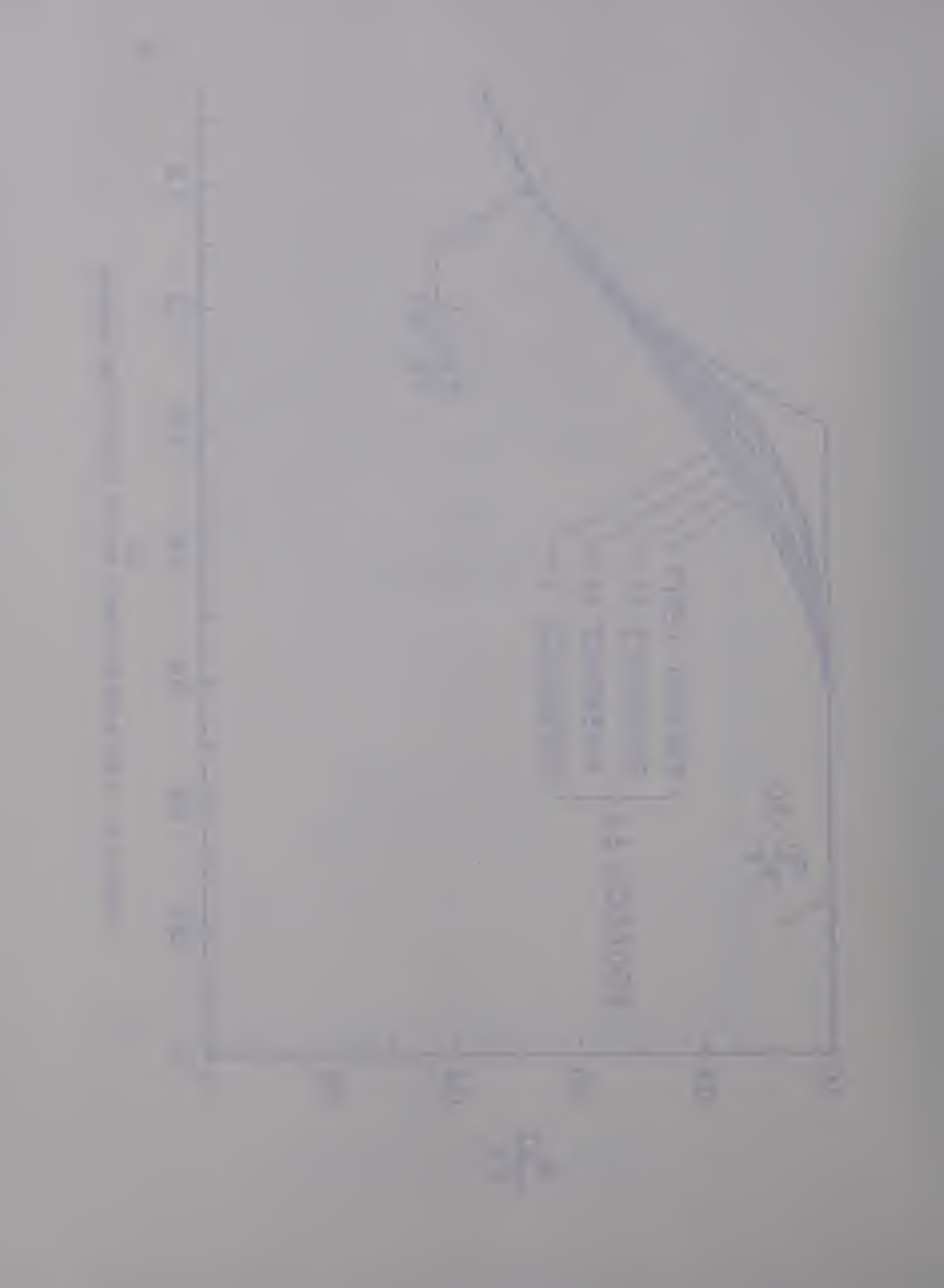

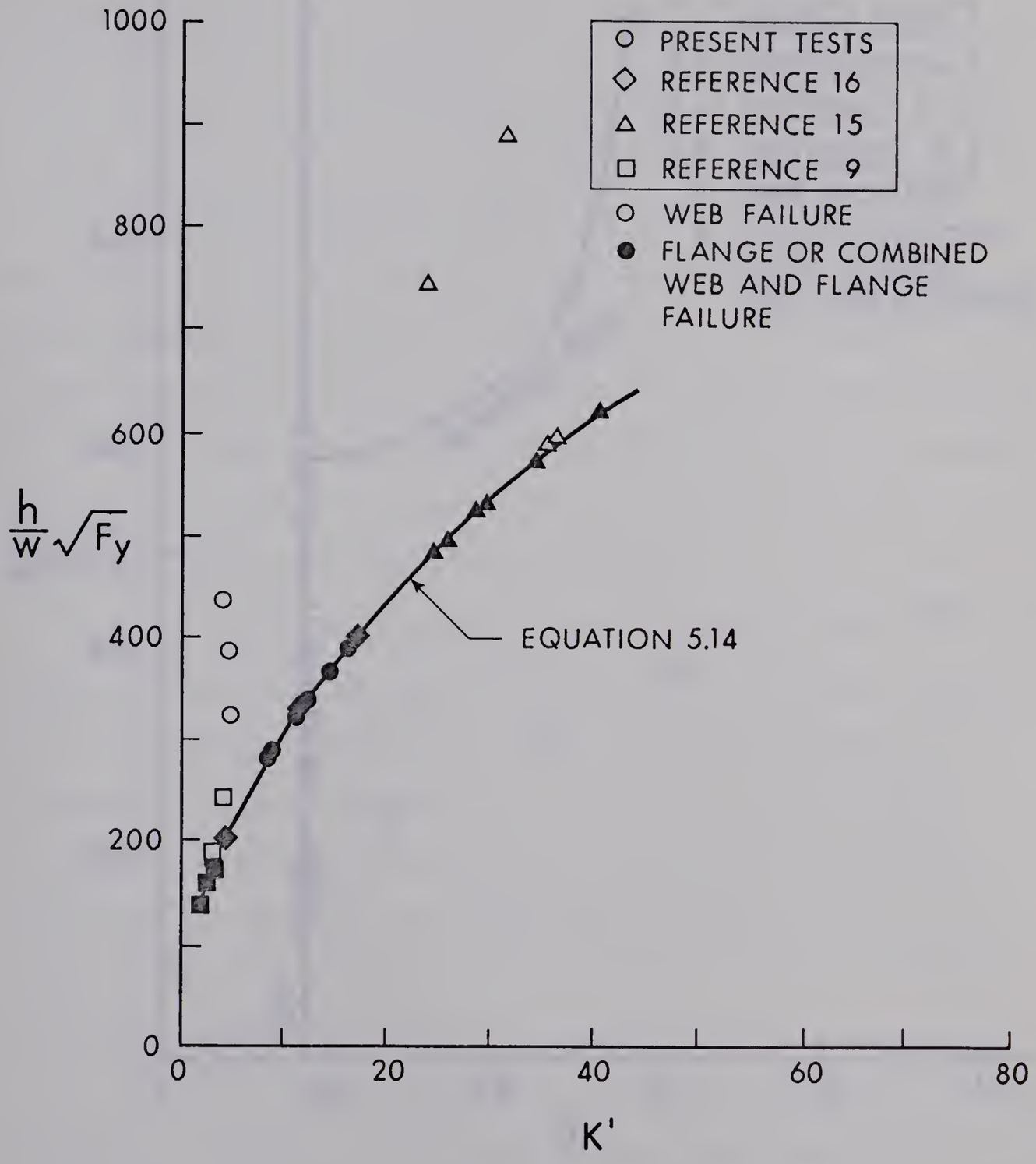

FIGURE 5.14 $(h/w)\sqrt{F_y}$ VERSUS K'

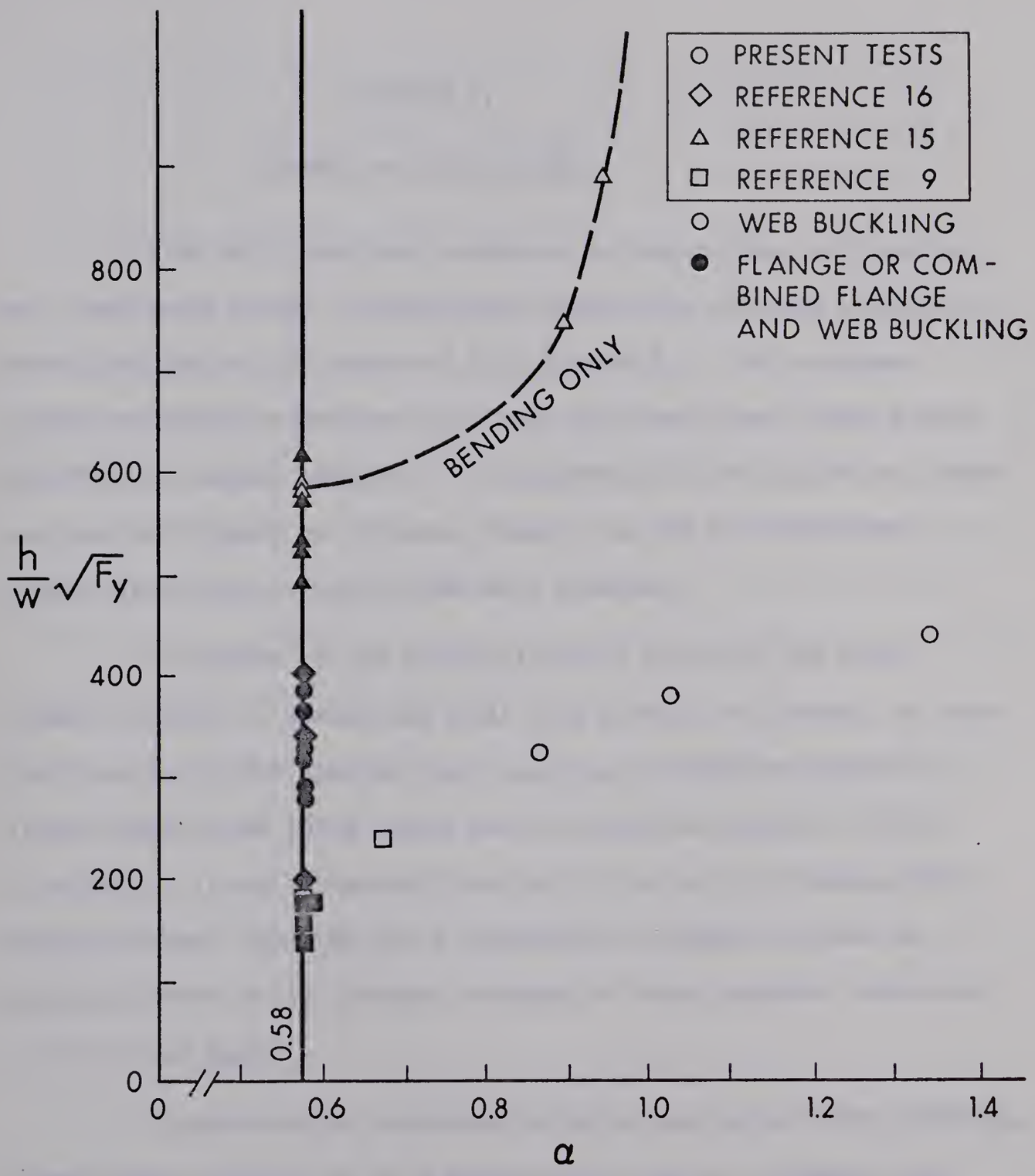

FIGURE 5.15 $(h/w)\sqrt{F_y}$ VERSUS α

CHAPTER VI

SUMMARY AND CONCLUSIONS

Nine tests have been conducted on beam-columns with various web slenderness ratios. Three series, consisting of three tests each, were conducted at P/P_y ratios of 0.2, 0.4 and 0.8. All specimens tested had flange proportions such that the beam-column flange plates qualified as compact elements. The specimens did not qualify as compact sections with regard to the webs, however, as the web slenderness limits prescribed by CSA-S16-1969 were exceeded.

The manner of the load application subjected the beam-column specimens to moment and axial load without the presence of shear. Test results of each specimen were examined to determine whether a local flange or web plate buckle had initiated the specimen failure. In doing so, it was discovered that the initial out-of-flatness of a beam-column web, although not a fundamental variable, did have an apparent effect on the ultimate strength of those specimens subjected to high axial loads.

The beam-column specimens failed either by web plate buckling, flange plate buckling, or by a combination of both. Although local web and flange plate failures have traditionally been treated as independent influences, it is to be expected that there is some inter-relationship between these two buckling phenomena. Nevertheless, since the failure of one plate element usually results in the failure of the

adjoining plate element, specimen failure is classed by the first plate element that deflects substantially. Of the nine beam-column tests, one specimen did exhibit apparent simultaneous buckling of the web and flange plates.

In each of the series, specimens that failed by flange plate buckling ultimately had higher M/M_{pc} ratios than those failures initiated by web buckling. In essence, if web plate buckling would have occurred first, the specimen would not have been able to reach its potential ultimate capacity. Therefore, it would be advantageous from the point of both economics and the strength of the member to raise the web slenderness limits to the level at which web and flange plate buckling would simultaneously become critical.

Along with the beam-column tests reported herein, results from three other testing programs were employed to develop an analysis to predict when simultaneous web and flange plate buckling might occur. The result was two equations, Equations 5.12 and 5.16, both of which can adequately predict this type of member behavior.

Based on the results of this present investigation, it is suggested that the web slenderness limits be raised to those displayed in Figure 6.1. The curve shown in Figure 6.1 could also be expressed by a less refined form of Equation 5.16 (and substituting $\alpha = 0.58$). This is:

$$\frac{h}{w}\sqrt{F_y} = 520\sqrt{1-0.695\ (P/P_y)^{0.3846}} \qquad 6.1$$

For simplicity in use, a bilinear approximation to the curve described by Equation 5.18 is given. The equation of this is:

$$\text{for } P/P_y \leq 0.125, \quad \frac{h}{w}\sqrt{F_y} = 520 \quad (1-1.54\,\frac{P}{P_y}) \qquad 6.2$$

$$\text{for } P/P_y > 0.125, \quad \frac{h}{w}\sqrt{F_y} = 152 \quad (2.89 - \frac{P}{P_y}) \qquad 6.3$$

This bilinear approximation is also shown in Figure 6.1.

In summary, tests were conducted on beam-column specimens with varying web slenderness ratios to determine whether the present CSA-S16-1969 web slenderness limits were conservative or not. From the test results it was found that the present CSA limits were too conservative and more realistic limits were prescribed above the present web slenderness ratios. In doing so, two methods were developed for predicting web buckling. Since both methods give identical results, the position of the new proposed limits was validated.

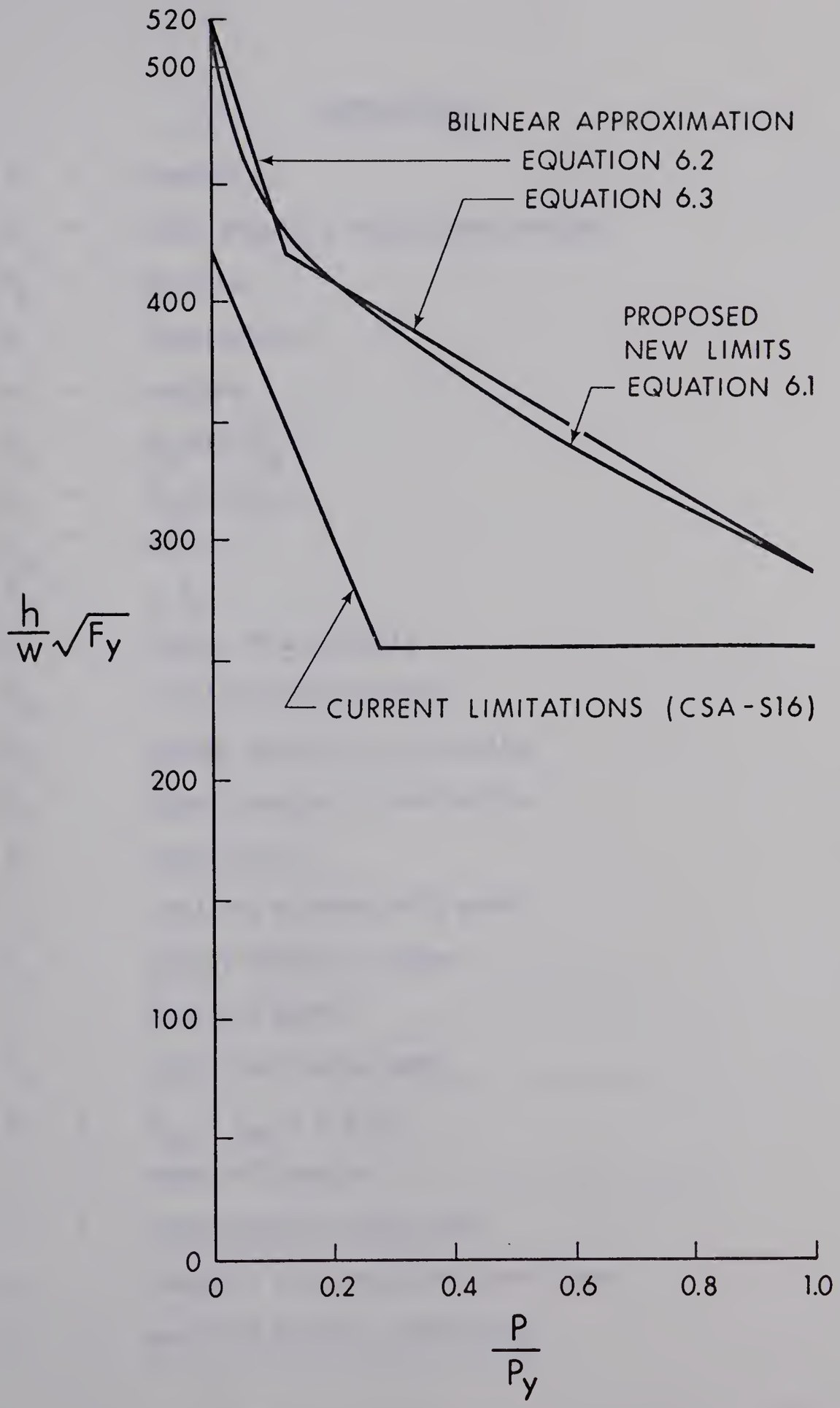

FIGURE 6.1 PROPOSED NEW WEB SLENDERNESS LIMITS

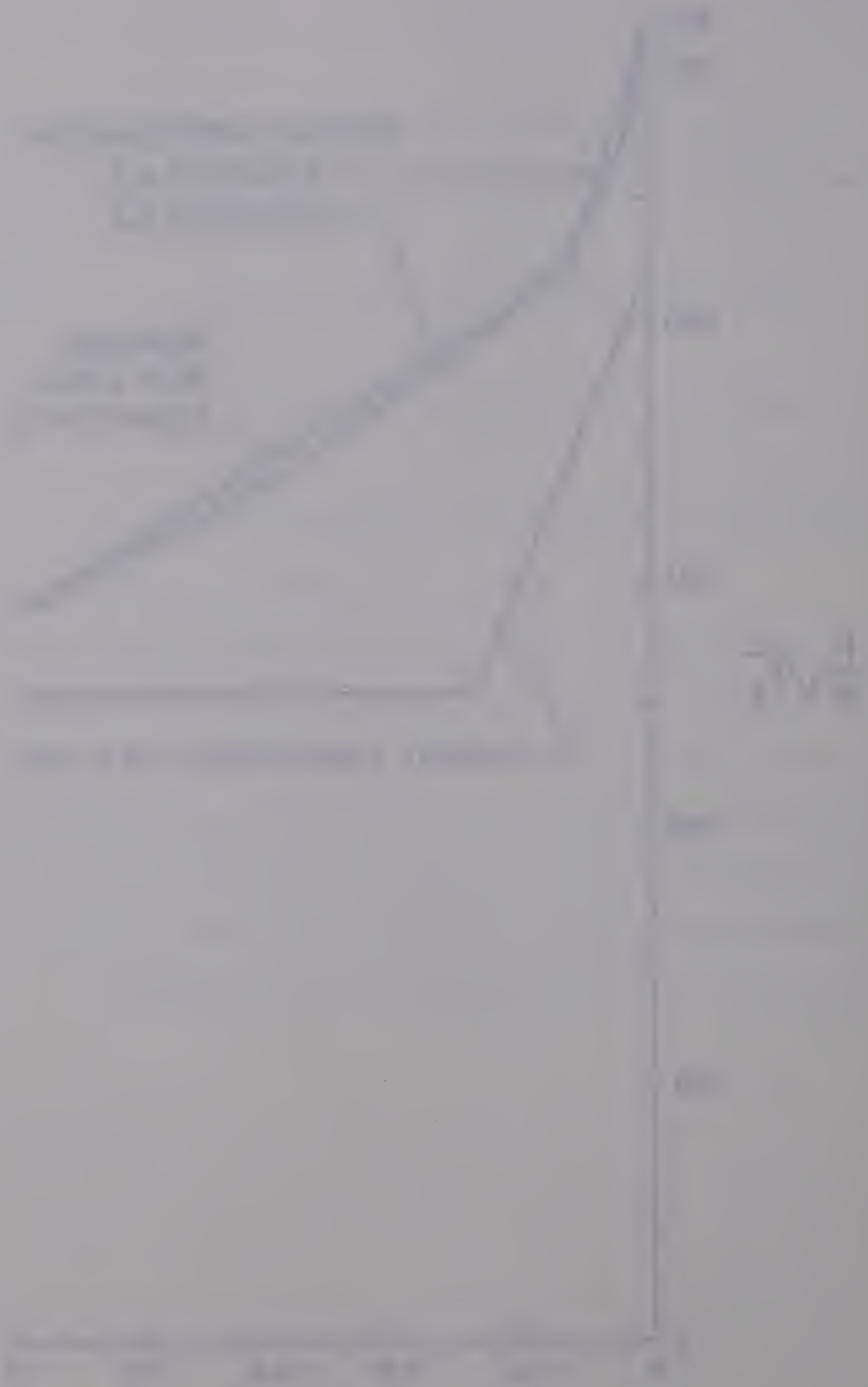

NOMENCLATURE

A = constant

A = total area of a wide-flange section

A_w = web area

b = flange width

B = constant

$D_x = (E_x)/(1-\nu_{xy}^2)$

$D_y = (E_y)/(1-\nu_{xy}^2)$

$D_{xy} = \nu_y D_x$

$D_{yx} = \nu_x D_y$

E = modulus of elasticity

E_{st} = strain-hardening modulus

E_x = tangent modulus in x-direction

E_y = tangent modulus in y-direction

e = eccentricity

F_y = specified minimum yield point

G_t = tangent modulus in shear

h = clear web depth

h_t = total wide-flange depth

$H = (D_{xy} + D_{yx} + 4\ G_t)/2$

I = moment of inertia

K = plate buckling coefficient

K = Haaijer's plate buckling coefficient

K' = new plate buckling coefficient

L = length of plate or column

M = moment

M_{pc} = plastic moment reduced by axial load

M_y = yield moment

M_u = ultimate moment

n = $2(\alpha_p - \alpha_o)/\alpha_p(\alpha_p^2 - 1)$

P = applied axial load

P_y = yield load

P_1 = concentric load

P_2 = eccentric load

r = radius of gyration

t = flange thickness

u = deflection of a plate at center

w = web thickness

x = coordinate axis

y = coordinate axis

y_o = Haaijer's depth of web in compression

y = distance from the compression flange-to-web junction to the position of the neutral axis

α = plate buckling modulus

α_o = value of plate buckling modulus upon first occurrence of yielding

α_p = $\sqrt{\sigma_y/\sigma_p}$

β = B/A = coefficient of restraint

δ = out-of-plane web deflection

Δ = lateral mid-height beam-column deflection about strong axis

Δ_{pc} = Δ at a moment of M_{pc}

ε = strain

ε_m = maximum strain in compression flange

ε_{st} = strain at initiation of strain-hardening

ε_y = yield strain

θ = rotation

θ_{pc} = θ at a moment of M_{pc}

ν = Poisson's ratio

ν_x = coefficient of dilation for stress increment in x-direction

ν_y = coefficient of dilation for stress increment in y-direction

σ = stress

σ_{cr} = critical buckling stress

σ_p = $\sigma_y - \sigma_r$ = proportional limit

σ_r = maximum compressive residual stress

σ_y = yield stress

χ = moment per unit length required for a unit of rotation

LIST OF REFERENCES

1. "CSA S16-1969 Steel Structures for Buildings", Canadian Standards Association, Rexdale, Ontario, 1969.

2. "Specification for the Design, Fabrication and Erection of Structural Steel for Buildings", American Institute of Steel Construction, New York, N.Y. 1969.

3. Haaijer, G., and Thurliman, B., "On Inelastic Buckling in Steel", Proceedings, ASCE, Vol. 84, No. EM2, April 1958.

4. Adams, P.F., "Plastic Design in High Strength Steel", Fritz Engineering Laboratory Report No. 297.19, Lehigh University, Bethlehem, Pa. 1966.

5. Timoshenko, S. and Gere, J., "Theory of Elastic Stability", McGraw-Hill Book Co., Inc., New York, N.Y., 1961.

6. Bleich, F., "Buckling Strength of Metal Structures" McGraw-Hill Book Co., Inc., New York, N.Y., 1952.

7. Noel, Robert, G., "Elastic Stability of Simply Supported Flat Rectangular Plates Under Critical Combinations of Longitudinal Bending, Longitudinal Compression, and Lateral Compression", Journal of Aeronautical Sciences, Vol. 19, May 26, 1952.

8. Johnson, J.H., and Noel, R.G., "Critical Bending Stress for Flat Rectangular Plates Supported Along All Edges and Elastically Restrained Against Rotation Along the Unloaded Compression Edge", Journal of Aeronautical Sciences, Vol. 20, July 15, 1952.

9. Haaijer, G., "Plate Buckling in the Strain-Hardening Range", Journal of the Engineering Mechanics Division, Volume 83, No. EM2, April 1957.

10. "CSA G40.12-1964 General Purpose Structural Steel", Canadian Standards Association, Rexdale, Ontario, 1964.

11. Yarimici, E., Yura, J.A. and Lu, L.W., "Techniques for Testing Structures Permitted to Sway", Fritz Engineering Lab Report No. 273.40, Lehigh University, Bethlehem, Pa., 1966.

12. American Society of Testing and Materials, "Test Methods for Compression Members", ASTM Special Technical Publication No. 419, August, 1967.

13. CSA W59.1-1970 General Specifications for Welding of Steel Structures (Metal-Arc Welding), Canadian Standards Association, Rexdale, Ontario, 1969.

14. Handelman, G.H. and Prager, W., "Plastic Buckling of a Rectangular Plate Under Edge Thrusts", NACA TN-1530, August, 1948.

15. Holtz, N. and Kulak, G., "Web Slenderness Limits for Compact Beams", Dept. of Civil Engineering, University of Alberta, Report No. 43, March 1973.

16. Lukey, A.F. and Adams, P.F., "Rotation Capacity of Wide-Flange Beams Under Moment Gradient", Dept. of Civil Engineering, University of Alberta, Report No. 1, May 1967.

17. McGuire, W. "Steel Structures", Prentice-Hall Inc., Englewood Cliffs, N.J., 1968.

18. Brockenbrough, R.L. and Johnston, B.G., "United States Steel Design Manual", United States Steel Corporation, ADUSS 27-3400-02, November 1968.